Electronic Thesis and Dissertation Repository

10-4-2012 12:00 AM

Dynamic Model Construction and Control System Design for Canadian Supercritical Water-cooled Reactors

Peiwei Sun
The University of Western Ontario

Supervisor
Dr. Jin Jiang
The University of Western Ontario

Graduate Program in Electrical and Computer Engineering
A thesis submitted in partial fulfillment of the requirements for the degree in Doctor of Philosophy
© Peiwei Sun 2012

Follow this and additional works at: https://ir.lib.uwo.ca/etd

Part of the Power and Energy Commons

Recommended Citation

Dynamic Model Construction and Control System Design for Canadian Supercritical Water-cooled Reactors

(Thesis format: Monograph)

By

Peiwei <u>Sun</u>

**Graduate Program in Electrical
and Computer Engineering**

**A thesis submitted in partial fulfillment
of the requirements for the degree of
Doctor of Philosophy**

**The School of Graduate and Postdoctoral Studies
The University of Western Ontario
London, Ontario**

THE UNIVERSITY OF WESTERN ONTARIO
SCHOOL OF GRADUATE AND POSTDOCTORAL STUDIES

CERTIFICATE OF EXAMINATION

Chief Advisor   Examining Board

_____   _____

Dr. Jin Jiang   Dr. Laurence Leung

Advisory Committee   _____

_____   Dr. Sohrab Rohani

                                                   _____

_____   Dr. Ilia Polushin

                                                   _____

                                                   Dr. Lyndon J. Brown

The thesis by

Peiwei Sun

Entitled

Dynamic Model Construction and Control System Design

for Canadian Supercritical Water-cooled Reactors

is accepted in partial fulfillment of the

requirements for the degree of

Doctor of Philosophy

Date: _____   _____

                                        Chair of Examining Board

ABSTRACT

The dynamic characteristics of Canadian Supercritical Water-cooled Reactor (SCWR) are significantly different from those of CANDU reactors due to the supercritical water coolant and the once-through direct cycle coolant system. Therefore, it is necessary to study its dynamic behaviour and further design adequate control system.

An accurate dynamic model is needed to describe the dynamic behaviour. Moving boundary method is applied to improve numerical accuracy and stability. In the model construction process, three regions have been considered depending on bulk and wall temperatures being higher or lower than the pseudo-critical temperature. Benefits of adopting moving boundary method are illustrated in comparison with the fixed boundary method. The model is validated with both steady-state and transient simulations and can predict the dynamic behaviour of the Canadian SCWR.

A linear dynamic model, for dynamic analysis and control system design, is obtained through linearization of the nonlinear dynamic model derived from conservation equations. The linearized dynamic model is validated against the full order nonlinear model in both time domain and frequency domain. The open-loop dynamics are also investigated through extensive simulations.

A cross-coupling analysis among inputs and outputs is examined using Relative Gain Array (RGA) and Nyquist array, from which adequate input-output pairings are identified. Cross-couplings at different operating conditions are also evaluated to illustrate the nonlinearities. It is concluded that the Canadian SCWR is a Multiple Input and Multiple Output (MIMO) system with strong cross-coupling and a high degree of nonlinearity.

Due to the existence of strong cross-coupling, the Direct Nyquist Array (DNA) method is used to decouple the system into a diagonal dominance form via a pre-compensator. Three Single Input and Single Output (SISO) compensators are synthesized to the pre-compensated system in the frequency domain. The temperature variation induced by the disturbances at the reactor power and pressure has been significantly reduced. To deal with the nonlinearities, a gain scheduling control strategy is adopted. Different sets of controllers are used at different load conditions. The control strategy is evaluated under various operating scenarios. It is shown that the gain scheduling control can successfully achieve satisfactory performance for different operating conditions.

Keywords: SCWR, dynamic modeling, moving boundary method, dynamic analysis, decoupling control, gain scheduling control.

ACKNOWLEDGEMENTS

I would like to express my appreciation to my supervisor Dr. Jin Jiang. Without his guide and support, I cannot achieve so much. Throughout my thesis work, he provided me with many constructive ideas and insight.

I would like to thank Dr. Chao Zhang, Department of Mechanical Engineering at the University of Western Ontario, and Dr. Jianqiang Shan, at Xi'an Jiaotong University, for their advices and suggestions on dynamic modelling. Gratitude is also given for the help and support from Prof. Jianmin Zhang of School of Nuclear Science and Technology at Xi'an Jiaotong University.

The support and help from all members of Control, Instrumentation and Electrical Systems group is appreciated.

Finally, my deepest gratitude goes to my parents and my wife Haijun Zhang, for their unconditional love and encouragement. This thesis is also a gift for upcoming birth of my baby Neil Sun.

TABLE OF CONTENTS

LIST OF TABLES

LIST OF FIGURES

ABBREVIATIONS

1D   One-dimensional

3D   Three-dimensional

ACR   Advanced CANDU Reactor

AECL   Atomic Energy of Canada Limited

AGR   Advanced Gas-cooled Reactor

BNL   Brookhaven National Laboratory

BWR   Boiling Water Reactor

CANDU   CANada Deuterium Uranium reactor

CANFLEX   CANDU FLEXible fuelling, an advanced fuel bundle design

CFD   Computational Fluid Dynamics

DNA   Direct Nyquist Array

DM   Detailed Model of the Canadian SCWR

DNB   Departure from Nucleate Boiling

DOE   Department Of Energy

FP   Full Power

FR   Fast Reactor

FUELPIN   FUEL PIN model

GIF   Generation IV International Forum

HPLWR   High Performance Light Water Reactor

I&C   Instrumentation & Control

LOCA   Loss of Coolant Accident

LOFA   Loss of Flow Accident

LPV   Linear Parameter Varying

LQR   Linear Quadratic Regulator

LTI   Linear Time Invariant

LWR   Light Water Reactor

MDNBR   Minimum Departure from Nucleate Boiling Ratio

MIMO   Multiple Input and Multiple Output

OTSG   Once-Through Steam Generator

P/D   Pitch-to-Diameter

PWR   Pressurized Water Reactor

RBMK   Reaktor Bolshoy Mooshchnosti Kanalniy, a class of graphite moderated nuclear

             reactors built in the former Soviet Union

RGA   Relative Gain Array

R&D   Research & Development

RM   RETRAN Model

SCFPP   Supercritical Fossil Power Plant

SCFR   Supercritical Fast Reactor

SCLWR   Supercritical Light Water Reactor

SCLWR-H   High temperature SCLWR

SCWR   Supercritical Water-cooled Reactor

SCWR-M   Mixed spectrum SCWR

SISO   Single Input and Single Output

SM   linearized Simplified Model of the Canadian SCWR

SVD   Singular Value Decomposition

USSR   the Union of Soviet Socialist Republics

UTSG   U-Tube Steam Generator

VVER   Vodo-Vodyanoi Energetichesky Reactor, a series of PWRs developed in the

             former Soviet Union

NOMENCLATURE

A area (m^2)

A_{CV} control valve opening

C precursor concentration (m^{-3})

c_p specific heat at constant pressure (J/(kg K))

D mass velocity (kg/(s m^2))

D_e hydraulic diameter (m)

E Eckert number

E_{CV} control valve coefficient

f friction factor

F correction factor

g gravitational acceleration (m/s^2)

h specific enthalpy (J/kg)

H heat transfer coefficient (W/(m^2 K))

k thermal conductivity (W/(m K))

k_g friction coefficient at the spacer grid

m mass (kg)

M mass flow rate (kg/s)

n neutron flux ($1/m^3$)

N Laplace transform of neutron flux n

Nu Nusselt number

P pressure (MPa)

Pr Prandtl numner

Pow reactor power (W)

q''' heat generation rate per unit volume (W/m^3)

Q heat absorption rate (W)

Q''' heat absorption rate per unit volume (W/m^3)

r radius(m)

R radius (m)

Re Reynolds number

s complex variable in Laplace Transform

S flow channel wetted perimeter (m)

t time (s)

T temperature (K)

V volume (m^3)

w weighting coefficient

W work (J/s)

Z distance (m)

Greek letters

α, β, γ node length (m)

λ delayed neutron precursor delay constant (s^{-1})

ξ pressure loss coefficient

δ perturbation

κ reactivity

K Laplace transform of reactivity κ

ρ density (kg/m^3)

τ time constant (s)

φ delayed neutron fraction

Λ the average neutron life time (s)

Subscripts

b bulk fluid

c cladding

CR control rod

CV control valve

f fuel pin

FP feed-water pump

gap gas gap

i   node number

IP   inlet plenum

in   entering a control volume

j   delayed neutron group number

m   pseudo-critical conditions

OF   outlet feeder

OH   outlet header

out   leaving a control volume

R   reactor

w   wall conditions

1 INTRODUCTION

1.1 Background

Energy crisis is a bottleneck of sustainable development of the world for the increasing energy demand. It is also important to fight global warming and avert damage to the environment while dealing with energy demand. Fossil fuels are not renewable and can do harm to the environment. Solar, wind and tidal energies are clean, but it is difficult to satisfy the massive demand due to their low power density. Nuclear power is a promising alternative. Its fuel is available for multiple centuries. It can be built in a large scale.

There are 435 nuclear reactors in operation worldwide [1]. Nuclear power has good operation and safety records compared with other energy technologies [2]. However, there are still concerns about safety as always, especially considering Chernobyl, Three Mile Island and Fukushima accidents. The existing nuclear systems also show other disadvantages: high original investment, long construction period and large project scale. Facing these challenges, the Generation IV nuclear systems concepts were brought forward. The objectives of Generation IV are to develop and demonstrate advanced nuclear energy systems that can meet future needs for safe, sustainable, environmentally responsible, economical, and proliferation-resistant and physically secure energy.

The existing nuclear systems are divided into three generations as shown in Fig 1.1. Nuclear reactors of Generation I were the early prototypes of the 1950s and 1960s. Commercial reactors built in the 1970s and later, most of which are still operating today, represent the Generation II. They are the ones well-known, such as the light water reactors (LWRs), the CANDU, the AGR, the VVER and the RBMK. These reactors proved that nuclear power could be used on a

commercial scale. Generation III are present day reactors with evolutionary improvements regarding mostly safety and economics. The greatest departure from Generation II designs is that many incorporate passive or inherent safety features, which require no active controls or operational intervention to mitigate accidents, and may rely on gravity, natural convection or resistance to high temperatures.

Under US DOE leadership, Generation IV International Forum (GIF) was chartered in 2001. In 2002, the GIF agreed to proceed with the development of a technology roadmap for Generation IV nuclear energy systems [3]. The purpose of the roadmap was to identify the most promising nuclear energy systems for improving of safety, economics, waste and proliferation resistance. The GIF agreed on a set of goals for the new systems and selected six most promising nuclear system technologies, among which the only water-cooled reactor is Supercritical Water-cooled Reactor (SCWR).
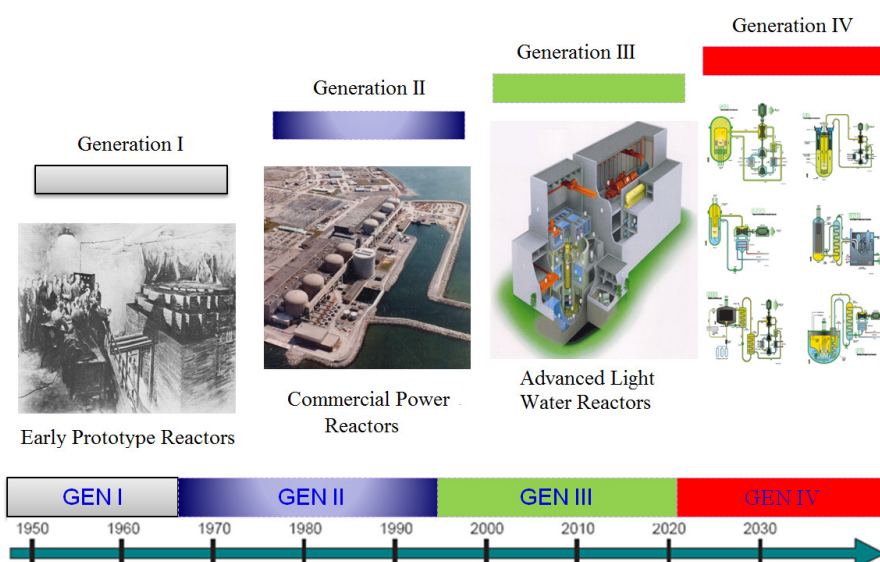
Fig 1.1 Four generations of nuclear reactors

1.1.1 Supercritical Water

A supercritical fluid is a substance at a temperature and pressure above its thermodynamic critical point. The critical point represents the highest temperature and pressure (critical temperature and critical pressure) at which the distinction between the liquid and vapour disappears. At the critical point, specific heat has its maximum value. Supercritical water has both the gaseous property of being able to penetrate and the liquid property of being able to dissolve.

The phase diagram of water is shown in Fig 1.2. The critical point of water is at $374^{o}C$ and 22.1MPa. Above the critical point, the water is called supercritical water and there is no phase transition and no boiling exists. A pseudo-critical point corresponds to the maximum value of the specific heat at the pressure and temperature above the critical point. The pseudo-critical line is the locus of pseudo-critical points. The pseudo-critical temperature increases with pressure. Compressed water is the water at a pressure above the critical pressure, but at a temperature below the critical temperature. The supercritical water in this study includes both terms: a supercritical water and a compressed water. Supercritical water is divided into two states: high density *liquid-like fluid* and low density *vapour-like fluid* by the pseudo-critical line. Below the critical point, the maximum specific heat is located at the saturation line between water and steam. From water state to steam state across the saturation line, boiling occurs.
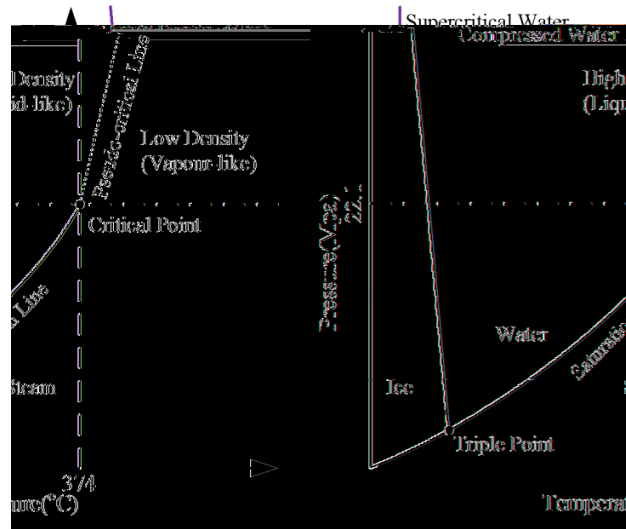
Fig 1.2 Phase diagram of water

Variations of specific heat and density of water with temperature at 25MPa and 10MPa are shown in Fig 1.3. At the pressure of 25MPa, the pseudo-critical temperature is 384°C. The thermal properties are continuously changing with temperature. Around the pseudo-critical point, there is a region where the specific heat is much higher than other part. Before the pseudo-critical point, it is liquid-like fluid, and after that point, it is vapour-like fluid. The thermal properties change abruptly around the pseudo-critical point. When the temperature increases from 374°C to 384°C, the density is decreased by 31.7% and the specific heat is increased by 404.9%; when the temperature increases from 384°C to 394°C, the density is decreased by 46.2% and the specific heat is decreased by 71.2%. At a pressure of 10MPa, the boiling point is at 311°C. From water state to steam state across the boiling point, the density decreases stepwise and the specific heat increases stepwise for the existence of latent heat of vapourization.
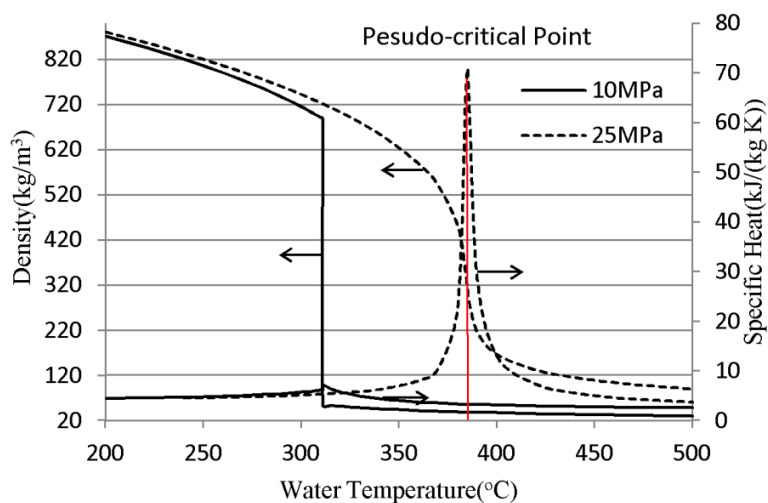
Fig 1.3 Thermal properties of supercritical water

Although there is no boiling at supercritical pressures, the thermal properties show similar trends at the pseudo-critical point with those at the boiling point: the variation of the thermal properties is steep before and after these points. One main difference is that under supercritical conditions the thermal properties are continuously changing while under the subcritical pressure there is a stepped change at the boiling point.

1.1.2 Heat Transfer at Supercritical Pressure

A large variation of thermal physical properties of supercritical water occurs near the pseudo-critical point, and results in high complexity in the heat transfer mechanism. As shown in the survey [4], if taking a single-phase heat transfer correlation Dittus-Boelter equation (1.1.1), to calculate the heat transfer coefficient under supercritical pressures, the heat transfer coefficient varies strongly near the pseudo-critical line due to the variation in thermal physical properties. At low heat fluxes, the real heat transfer coefficient is higher than that predicated using Eq. (1.1.1). At high heat fluxes, the heat transfer coefficient is lower than that calculated by Eq. (1.1.1). Thus,

it was agreed in the open literature that the real heat transfer coefficients deviate from those derived from the Dittus-Boelter equation, especially near the pseudo-critical line.

$$Nu = 0.023 * \mathrm{Re}^{0.8} * \mathrm{Pr}^{1/3} \tag{1.1.1}$$

where Nu is the Nusselt number, Re is the Reynolds number and Pr is the Prandtl Number.

Comprehensive studies including experimental studies and numerical analyses on heat transfer under supercritical conditions have been carried out. The literature review and summary of such works can be found in [4, 5]. Empirical approaches are mainly used in the prediction of heat transfer coefficients of supercritical fluids. Most of the empirical correlations have the general form of a modified Dittus-Boelter equation:

$$Nu_b = C \, \mathrm{Re}_b^n \, \mathrm{Pr}_b^m \, F \tag{1.1.2}$$

where F is a correction factor and subscript b refers to bulk fluid conditions. F takes into account the effects from the property variation between the bulk fluid temperature and the surface temperature. For most correlations, the correction factor mainly depends on the specific heat ratio and the density ratio

$$F = f(\frac{\rho_w}{\rho_b}, \frac{c_{P,A}}{c_{P,b}}) \tag{1.1.3}$$

where ρ is the density, c_P is the specific heat , $c_{P,A}$ is the effective specific heat and subscript w refers to wall conditions. The effective specific heat $c_{P,A}$ is defined as

$$c_{P,A} = \frac{h_w - h_b}{T_w - T_b} \tag{1.1.4}$$

Therefore, the heat transfer coefficient of supercritical water depends on not only the bulk conditions but also the wall conditions. Discontinuity in the heat transfer coefficient may occur due to such dependence.

1.1.3 Supercritical Water-cooled Reactor

The use of supercritical water in power production was firstly applied for the fossil-fired supercritical power plants in the 1950s [6]. At the end of the 1950s and the beginning of the 1960s, studies were conducted to investigate a possibility of using supercritical water in nuclear reactors. Several concepts were proposed in Great Britain, France, US and the former USSR. However, the concepts were found to be feasible in principle, not economically competitive. They were abandoned as commercial pressurized water reactors (PWRs) and boiling water reactors (BWRs) became the industry standard.

In the 1990s, the idea of developing a nuclear reactor using supercritical water as its coolant was reconsidered. The SCWR design is based on the mature technology of water-cooled nuclear reactor and supercritical fossil power plant (SCFPP) and its conceptual design is shown in Fig 1.4. SCWR is normally operated at 25MPa with steam temperature above 500°C, therefore its thermal efficiency can be significantly improved. It adopts a once-through direct cycle coolant system. There is no need for steam generator and pressurizer as in a PWR, or recirculation and steam separation system as in a BWR. Costs are reduced by eliminating those expensive components. This in turn leads to more compact plant and smaller containment building and further reduces the construction cost.
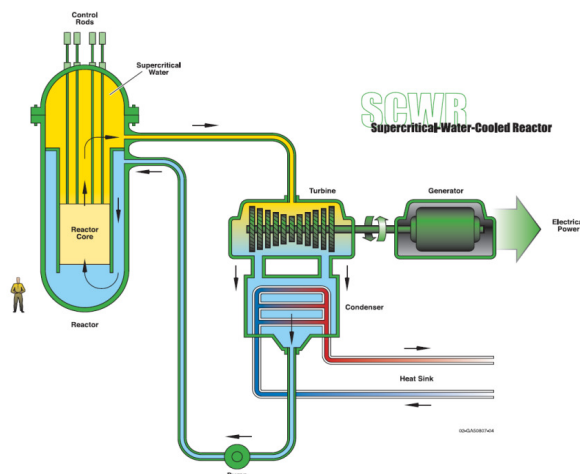
Fig 1.4 Diagram of SCWR [3]

The SCWR concepts are divided into two types: pressure-vessel type and pressure-tube (channel) type. Japan, Europe and China are focusing on pressure-vessel type SCWR concepts. Supercritical light water reactor (SCLWR) and supercritical fast reactor (SCFR) of Japan [7] and high performance light water reactor (HPLWR) of Europe [8] are typical pressure-vessel type SCWR. Canada is developing pressure-tube type SCWR.

CANDU-SCWR [9] is a natural evolution from subcritical CANDU reactors using supercritical water as the coolant. Similar to current CANDU design, CANDU-SCWR is moderated by heavy water and the fuel bundles reside in the horizontal pressure tubes. The once-through direct coolant system is adopted. The CANDU-SCWR is replaced by the concept Canadian SCWR [10], considering the difficulties and challenges of online refueling caused by high pressure and high temperature coolant system and high wall temperatures at elements in the top of the bundle caused by the buoyancy effects of supercritical water.

A diagram of a Canadian SCWR is shown in Fig 1.5 and the design parameters are shown in Table 1.1. The Canadian SCWR is different from the traditional CANDU reactor design. The fuel is thorium mixed with plutonium not natural uranium. Thus, batch refuelling is adopted and

the fuel bundles are located inside vertical pressure tubes. The inlet headers are eliminated and replaced by inlet plenum. The coolant flows downward and is collected at the outlet header after heated and directly sent to the turbine.
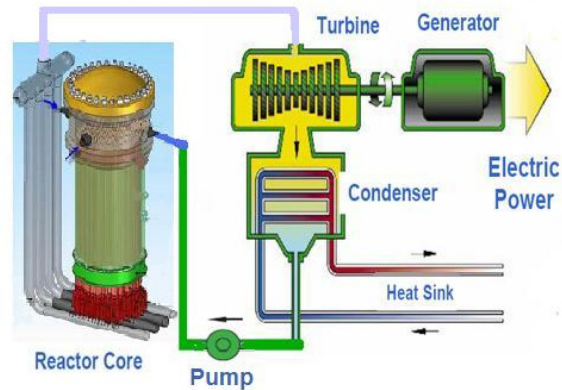
Fig 1.5 Diagram of a Canadian SCWR [10]

Table 1.1 Design Parameters of the Canadian SCWR [10]

Spectrum	Thermal
Moderator	Heavy Water
Coolant	Light Water
Thermal Power	2540 MW
Flow Rate	1320 kg/s
Number of Channels	336
Electric Power	1200 MW
Efficiency	48%
Fuel	UO_2/Th
Enrichment	4%
Inlet Temperature	$350\,^{o}C$
Outlet Temperature	$625\,^{o}C$
Cladding Temperature	$<850^{o}C$

1.2 Motivations and Objectives

Significant efforts have been made to examine relevant issues of the Canadian SCWR, such as, core design [10, 11], fuel channel design [12, 13], safety analysis [14], thermal-hydraulic

analysis [15] and material study [16, 17]. So far, little work has been done on dynamic analysis and Instrumentation & Control (I&C) issues for such reactors.

The dynamic characteristics of the Canadian SCWR are different from those of the CANDU reactor and advanced CANDU reactor (ACR) for the following reasons:

1. The thermal properties of coolant are different. The coolant of the Canadian SCWR is supercritical light water while the coolant in the CANDU reactor and ACR is subcritical heavy water and subcritical light water, respectively. The dynamic responses of supercritical water are different from those of subcritical water under the same disturbance [18].

2. The coolant flow rate of the Canadian SCWR is about one-eighth of that of the CANDU reactor and the ACR with an equivalent amount of thermal power. There is a small water inventory in the reactor core. The ratio of the reactor power over the coolant flow rate (power-to-flow ratio) is relatively high. Therefore, the Canadian SCWR is more susceptible to disturbances. For example, 2% decrease in the reactor power leads to 14°C decrease in the main 'steam' temperature.

3. The coolant density at the reactor core outlet of the Canadian SCWR is about one-ninth of that at the reactor core inlet. In the CANDU reactor and the ACR, the coolant density at the reactor outlet is approximately 80% of that at the reactor inlet. The coolant density reactivity feedback of the Canadian SCWR has larger effects on the reactor kinetics.

4. The Canadian SCWR adopts a once-through direct cycle coolant system while there are steam generators between primary and secondary loops of the CANDU reactor and the ACR. This means that without the steam generator as a buffer, disturbances from the turbine side will

have a direct impact on the reactor. This means that the reactor and the turbine are strongly coupled.

Thus, an accurate dynamic model is necessary to investigate the unique dynamic characteristics of the Canadian SCWR. A suitable dynamic model should be selected due to the thermal properties and heat transfer characteristics of the supercritical water.

The once-through direct cycle adopted in the Canadian SCWR appears to be similar to that of a BWR. The Canadian SCWR is also a Multiple Input and Multiple Output (MIMO) system. In a BWR, there are two phases of water due to the existence of boiling. There is no boiling taken place in the Canadian SCWR to act as a cushion between the reactor and the turbine. The Canadian SCWR has much stronger coupling among different system variables.

Even though an SCFPP also has strong cross-coupling among its variables, the dynamic characteristics of the Canadian SCWR are more complicated than those of an SCFPP. The response time of an SCFPP is longer and the dynamic is slower due to its lower heat flux in the water wall and longer length of heated tube. Furthermore, there is no reactivity feedback issue in an SCFPP.

Therefore, the control strategy for a BWR and an SCFPP cannot be directly applied to the Canadian SCWR. A linearized dynamic model is required to facilitate the dynamic analysis and control system design.

The coolant flow rate in the Canadian SCWR is maintained in a correct proportion to the reactor power output so that the main 'steam' temperature can be kept constant. At a lower power level, the coolant flow rate is lower, which leads to a higher percentage change in the flow rate for a disturbance of the same magnitude. The coolant flow velocity and the heat transfer coefficient

are also low at low power levels, and the time constant is larger. Thus, the gain and the time constant of the system vary as the power level changes. This represents typical behaviour of a nonlinear dynamic system.

Therefore, the Canadian SCWR can be characterised as a MIMO system with high power-to-flow ratio, strong cross-coupling and high degree of nonlinearity. These pose difficulties and challenges for the control system design. Thus, it is necessary to carry out dynamic analysis to determine the appropriate input-output pairing and control strategies.

The Canadian SCWR is operated at high pressure and temperature. Large fluctuations of thermal parameters may speed up corrosion, thermal stress and fatigue of critical components. The variation in the main 'steam' temperature should be limited to reduce damages and improve the lifetime. The power-to-flow ratio is high, as a result the 'steam' temperature is more sensitive to disturbances. Furthermore, the existence of strong cross-coupling makes the 'steam' temperature even harder to regulate, because it is sensitive to change of other parameters, such as, the reactor power and the 'steam' pressure. Thus, it is necessary to select a proper control strategy to decouple the system and ensure that the 'steam' temperature is less affected by other subsystems. In this way, the variation on the 'steam' temperature under different disturbances can be efficiently suppressed.

Because of nonlinearities, the control system designed for lower power levels will not produce satisfactory performance for the same system operating at high power levels. Therefore, the nonlinearity is also an issue to be considered during the control system design.

Based on the analysis of the problems existing in the dynamics and control of the Canadian SCWR, the research objectives are identified as:

1.) To establish a suitable dynamic model of the Canadian SCWR to describe its dynamic characteristics;

2.) To construct a linearized dynamic model of the Canadian SCWR plant system as the platform for the dynamic analysis and control system design;

3.) To perform dynamic analysis and investigate the cross-coupling and nonlinearities of the Canadian SCWR;

4.) To design an adequate control system for the Canadian SCWR to deal with its strong cross-coupling and high degree of nonlinearity.

1.3 Scope and Methodologies

Extensive knowledge has been achieved from the decade's operation of nuclear power plant under subcritical conditions. However, the dynamics of SCWR are relatively less known. The scope of the study in this thesis is focused on the supercritical conditions of SCWR. Fast dynamics related to severe accidents, such as loss of coolant accident (LOCA), are not considered. The dynamics under normal operation or transients due to operator control action or load variation are studied. The dynamic models are developed for dynamic analysis and control system design, not for safety analysis.

The methodologies to deal with different objectives are represented as follows:

1.3.1 Dynamic Model of the Canadian SCWR

To obtain a dynamic model, a suitable tool is the first thing to choose. Computational Fluid Dynamics (CFD) code, such as, FLUENT and system code, such as, RETRAN [19] and CATHENA [20], can simulate behaviour of the system under the supercritical conditions. These

codes are well verified and their results are widely accepted by the nuclear industry. But it is time-consuming to simulate a transient process and impossible to derive a linear dynamic model directly from these codes. Even the simulation data can be used to construct a linear dynamic model through system identification techniques, it is hard to investigate the system dynamics in depth due to lack of inside knowledge. It is not convenient to implement designed control system to test the performance. Thus, the platform of MATLAB/SIMULINK^{TM} is chosen to develop the dynamic model of the Canadian SCWR through first principle modeling. These models can be used to investigate the dynamic characteristics, validate the linear dynamic model and evaluate the performance of designed closed-loop control system. CFD codes and system codes are used to verify the dynamic model developed.

The main and most challenging part of the Canadian SCWR dynamic modeling is the modeling of the reactor core. Since the supercritical water is in a single phase, the modeling methods to deal with single-phase heated tubes problems are investigated: lumped-parameter modeling, linear distributed-parameter modeling, and nonlinear distributed-parameter modeling [21].

Lumped-parameter modeling assumes that the whole medium in the heated tube is uniform and one representative point is chosen as the parameter for the whole medium. The advantages of the lumped-parameter modeling are: simple and suitable for response of large perturbations. But it is difficult to reflect the distributed-parameter nature of the problem. To reflect the distributed-parameter characteristics, the heated tube can be divided into a certain number of nodes depending on the actual conditions. This method is widely adopted in the modeling of steam generators, boilers and nuclear reactors.

The original differential equations based on the fundamental equations are linearized and then transfer functions are obtained by taking Laplace transform in the linear distributed-parameter

modeling method. This method only reflects the distributed-parameter characteristics of the system under small perturbation conditions.

The partial differential equations are solved using approximation method in the nonlinear distributed-parameter modeling method. This method is used for simulation with large perturbations and represents nonlinear distributed-parameter characteristic of the system. But it is more difficult to solve partial differential equations for complex systems and the computation is time-consuming.

The linear distributed-parameter modeling method is only accurate for linear distributed-parameter system or nonlinear distributed-parameter system under small disturbances. It is not suitable for the Canadian SCWR modeling for its strong nonlinear characteristics along the coolant channel. The Canadian SCWR coolant channel is best described by nonlinear distributed-parameter models. But, the thermal-hydraulic of the Canadian SCWR is coupled with neutronics. To simplify the modeling process, the lumped-parameter modeling method with multiple nodes is suitable for nonlinear distributed-parameter system under different magnitude disturbances. Therefore, the lumped parameter method with multiple nodes is adopted in this thesis for the Canadian SCWR dynamic modeling.

The supercritical water shows significant difference in thermal properties before and after the pseudo-critical point. In the modeling process, the thermal properties inside each control volume should be as consistent as possible. Normally, for each thermodynamic state, there are different equations to calculate the related parameters. Large calculation errors will occur if one control volume contains fluid with more than one state. For the unique thermal physical properties of supercritical water, the empirical correlations to predict the heat transfer coefficient are divided into several sub-correlations by the correction factor. The discontinuity is caused by the

correction factor. When the boundary of the control volume is close to the discontinuity, numerical oscillation can occur.

Therefore, the moving boundary method is adopted to deal with possible numerical convergence and instability problems. The boundary positions are set at the pseudo-critical point and also at the location where the discontinuity in the heat transfer correlation may happen. In every control volume, there is only one thermodynamic state. Thus, the calculation errors can be reduced. Under the requirement of the same accuracy, the number of control volume can be reduced and the computational time can be shortened as compared with using a fixed boundary method. Furthermore, numerical oscillations can be potentially avoided.

The dynamic model development is based on the fundamental conservation equations of mass, energy and momentum. Since the boundary of control volume is moving, the conservation equations are in the form of partial differential equations. All the partial differential equations have to be converted into ordinary differential equations and these ordinary differential equations are much easier to solve.

1.3.2 Linear Dynamic Model of the Canadian SCWR Plant System

There are two main approaches to construct a dynamic model of a plant: white-box modeling based on first principles and black-box modelling based on the input and output data of the plant. The former is referred to as first principle modeling and the latter is termed as system identification.

System identification techniques use statistical methods to build mathematical models of dynamical systems from measured input and output data. The mathematical relation is determined without going into details of physics of what is actually happening inside the system.

The advantages of this method are no time consuming model development and no need for analyzing the internal behaviour of the system.

The first principle modeling is based on the physical laws of a plant. This approach needs comprehensive knowledge of the plant system. The advantage of first principle modeling is that it can supply extrapolation in addition to the interpolation provided by system identification.

The first principle modeling is adopted for the linearized dynamic model development of the Canadian SCWR plant system. In such a way, the internal knowledge is better understood and the linearized dynamic model obtained at one operating point can be easily extended to other operating points by changing corresponding parameters.

Since the thermal parameters of the Canadian SCWR are implicitly coupled with one another, it is difficult and complex to linearize such a model directly using traditional methods. An empirical correlation is introduced to evaluate the coolant flow rate to decouple it from the reactor power and pressure. The reactor model is simplified to two regions by means of the moving boundary to reduce the order of the system. For other system components in the plant, lower order models are used in the modeling process. System identification technique is also adopted to assist the linear dynamic model development.

For the linear dynamic model verification, comparisons on the time domain responses with the nonlinear dynamic model to the same disturbance are an obvious choice. But different transfer functions may produce similar responses for certain inputs. Thus, the verification is also carried out in frequency domain. The differences from the nonlinear dynamic model can be derived and used to evaluate the accuracy of the linear dynamic model.

1.3.3 Dynamic Analysis of the Canadian SCWR

The Canadian SCWR plant system is a MIMO system and the input-output relationship is shown in Fig 1.6. There are mainly three inputs to the plant: feed-water flow rate, control rod reactivity and control valve opening. There are three output variables: reactor power, 'steam' temperature and main 'steam' pressure.
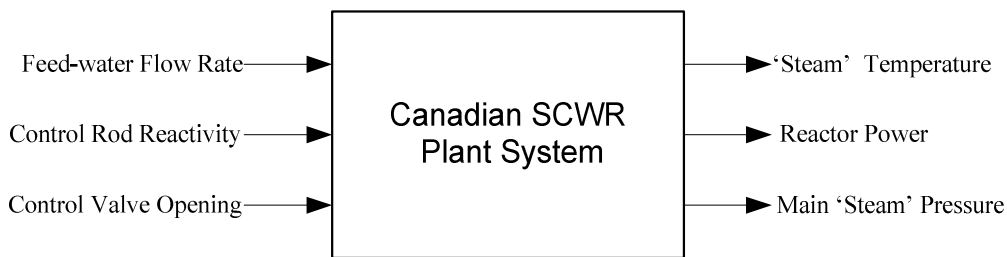
Fig 1.6 Input-output relationship of the Canadian SCWR plant system

A change in any input will result in all changes in three outputs. The multivariable dynamic analysis techniques are applied to carry out the dynamic studies. The dynamic analysis of the Canadian SCWR is performed in both steady-state and dynamic states.

The Relative Gain Array (RGA) method [22] is an effective and widely used method to describe the cross-coupling among different inputs and outputs of a MIMO system. The RGA is a normalized form of the gain matrix that measures the impact of a control input on an output, relative to its impact on the other outputs. It is an analytical tool to determine the input-output pairing.

The Nyquist array can provide a basis for estimating the cross-coupling among system inputs and outputs as a function of frequency, and is adopted since the open-loop transfer function matrix is already obtained from the linear dynamic model development. The Nyquist array consists of a set of standard polar plots of the magnitude and the phase angle for each element in the transfer function matrix of the system. It is a graphical representation of the open-loop relationship

among inputs and outputs. The degree of the interactions at different frequencies is evaluated so that the most appropriate input-output pairing is determined.

Multiple linear dynamic models at different operating points are necessary to study the nonlinearity of the Canadian SCWR. The RGA and Nyquist array analyses are carried out at the 100% full power (FP) operating point as well as other operating points. In such a way, the cross-coupling at different operating points is analyzed. At the same time, the dynamics at different operating points are obtained and nonlinearities can be evaluated.

1.3.4 Control System Design of the Canadian SCWR

The Canadian SCWR is a MIMO system with strong cross-coupling. There are mainly three approaches to control a multivariable plant: decentralized control, decoupling control and multivariable optimal control.

The decentralized control is only valid when the multivariable plant is weakly coupled. The decoupling control can be realized by introducing of a decoupling compensator to reduce the interactions among inputs and outputs and then a diagonal loop compensator is designed to obtain the desired performances. The multivariable optimal control can synthesize a multivariable controller directly to minimize or maximize certain objective functions.

The weakly-coupled requirements for decentralized control are not met for the Canadian SCWR. It is difficult to implement and intervene during operation for operators in a case of optimal control. Therefore, decoupling control is chosen for the control system design. A decoupling pre-compensator is employed such that the pre-compensated system satisfies the weakly-coupled requirements. The purpose of a pre-compensator is to maximize the diagonal dominance, ideally diagonal if possible. In such a way, the 'steam' temperature will be less sensitive to changes in the reactor power and the 'steam' pressure. Then, the pre-compensated system is treated as

several SISO systems to obtain the overall desired responses. The key performances are achieved by specifying the gain and the phase margins. The combination of the decoupling pre-compensator and the loop compensator forms the multivariable controller for the Canadian SCWR.

The Direct Nyquist Array (DNA) method [23] is a powerful tool for the analysis and design of a pre-compensator in frequency domain. The open-loop transfer function matrix of the Canadian SCWR is available for the pre-compensator design. The DNA method is suitable to achieve diagonal dominance. Bode plots are applied to design the loop compensator and to meet the requirements on the gain and the phase margins.

Dynamics of a nonlinear system depend strongly on one or more system parameters characterizing its operating point. The common approach to dealing with strongly parameter-dependent dynamic system is gain scheduling. In gain scheduling control schemes, a typical approach is to develop a linearized dynamic model of the control object in the sufficiently dense grid of fixed operating points. Then a control law is obtained by combining the information together, which is capable of accommodating for the changing dynamics. Two general approaches to achieving such a control law are: controller parameter scheduling and controller output scheduling.

In the controller parameter scheduling approach, a curve fitting technique is chosen to combine the linearized models into a single parameter dependent model description. For fitting a function to the different values of the model parameter, an optimization scheme is applied to each model parameter. An estimate of the nonlinear system at a given operating point is obtained by interpolating between different values of model parameters according to the function used in the curve fitting. Then a single controller is designed to generate the control signal.

In the controller output scheduling approach, the model is chosen to be a linear combination of all the linear dynamic models. A linear time invariant (LTI) controller is designed for each of the linear models and the output of the controllers are weighted using exactly the same weights as for the models. This linear combination of outputs is used as the final control signal.

The linear parameter varying (LPV) method is a different method to deal with parameter-dependent dynamics from the conventional gain scheduling approach. It involves the direct synthesis of a controller rather than construction from a collection of local linear controllers designed by LTI methods. The LPV method typically utilizes norm based performance measures. It is nearly impossible to find a suitable parameter to describe the dynamics of the Canadian SCWR as a LPV system due to strong cross-coupling and nonlinearity.

The controller output scheduling approach is selected for the gain scheduling control strategy of the Canadian SCWR. Multiple linear dynamic models at different operating points are developed. The pre-compensator and the loop compensator are designed and verified at selected operating conditions. The control performance is optimized for each fixed operating point. Finally, the compensators are combined together to obtain an overall controller that covers the desired operating range of the Canadian SCWR.

1.4 Contributions of the Thesis

Main contributions of this study are summarized as follows:

   a.) Dynamic Model of the Canadian SCWR with Moving Boundary Method.

The moving boundary method is successfully applied to model the Canadian SCWR and proven to be suitable to overcome numerical difficulties under supercritical conditions. It is the first

application of the moving boundary method to the dynamic modeling of an SCWR. The dynamic model provides not only unique dynamic characteristics, but also a verification tool for linear dynamic model development and a useful platform for evaluating the control performance of the designed control system.

   b.) Linear Dynamic Model of the Canadian SCWR Plant System.

A linearized dynamic model of the Canadian SCWR plant system is obtained in the form of transfer function matrix. It is verified comprehensively with nonlinear dynamic model in both time and frequency domains. The linear dynamic model is the first one for an SCWR in the open literature and establish a foundation for dynamic analysis and control system design.

   c.) Dynamic Analysis of the Canadian SCWR.

The degree of interaction among inputs and outputs at steady-state and dynamic conditions is evaluated and the appropriate input-output pairing is determined. Multiple linear dynamic models at different operating points are developed and the nonlinearity is derived and investigated. It is the first time to systematically study the degree of cross-coupling and nonlinearities of an SCWR.

   d.) Control of the Canadian SCWR.

The high power-to-flow ratio of the Canadian SCWR makes the plant vulnerable to disturbances. It is difficult to suppress the 'steam' temperature variation due to the existence of the strong cross-coupling. A decoupling pre-compensator is designed to reduce the interaction from the reactor power and 'steam' pressure. The variation on the 'steam' temperature under the decoupling control system has been efficiently suppressed. It is the first control system of an SCWR with cross-coupling explicitly considered. The nonlinearity is dealt with gain scheduling

control. Wide range operation is carried out smoothly without exceeding the limit on the variation of the 'steam' temperature. The study of the nonlinear behaviour of an SCWR is not available in the open literature yet.

1.5   Organization of the Thesis

The rest of the thesis is organized as follows: in Chapter 2, the modeling methods of SCWR are briefly reviewed. Applications of the moving boundary method and control of SCWR are introduced. A dynamic model for the Canadian SCWR is constructed with moving boundary method in the Chapter 3. The model is verified with a CFD code. Advantages of adopting the moving boundary method are derived by comparing with the fixed boundary method. In Chapter 4, a simplified dynamic model of the Canadian SCWR plant system is developed based on first principle modeling and its linear dynamic model is obtained through linearization and Laplace transformation. The linear dynamic model is validated against its nonlinear counter-part both in time and frequency domains. The dynamic analysis is carried out in Chapter 5. The interactions among inputs and outputs at steady-state and dynamic conditions are analyzed and the input-output pairing is determined. The nonlinearity is evaluated based on multiple linear dynamic models at different operating points. In Chapter 6, the decoupling control is designed to handle the cross-coupling and gain scheduling control is applied to deal with nonlinearities. The conclusions are drawn in the last chapter and future work is also suggested.

2   LITERATURE REVIEW

A literature review related to modeling and control of SCWR is performed in this chapter. Different modeling techniques and relevant work on SCWR are introduced in the first section. Among the transient analysis methods, the moving boundary method is comprehensively studied under both subcritical and supercritical conditions in the second section. In the last part, the preliminary work on the control of SCWR is presented. As background information, the control of BWR and SCFPP is also included.

2.1   Modeling of SCWR

Since SCWR was selected as one of six Generation IV nuclear systems, different modeling techniques have been applied to investigate issues related to the Research and Development (R&D) of SCWR. The main purposes of the investigation are to assist the SCWR reactor design and demonstrate adequate safety margins under normal operating conditions and the effectiveness of the safety systems in preventing core melt in the event of design basis accidents. Three major types of modeling techniques are being used: full three-dimensional (3D) CFD analysis, quasi-3D sub-channel analysis and one-dimensional (1D) transient analysis.

2.1.1   CFD Analysis

The CFD uses numerical methods and algorithms to solve the governing laws of fluid dynamics. The conservation equations for mass, energy and momentum within a complex geometry are represented by a complex set of partial differential equations. These differential equations are solved in a discrete form by dividing the complex geometry into discrete meshes. Therefore, CFD analysis can provide solutions to modeling general 3D thermal-hydraulic situations, which

are not modelled adequately by other system codes. They are particularly useful to model flows where 3D effects and turbulent mixing phenomena are of importance.

Due to high cost and limitation in the measurement techniques of experiments at supercritical pressure, numerical simulation using CFD codes becomes a practical and efficient approach to investigate thermal-hydraulic behaviour of supercritical water flows in an SCWR. Examples of such codes are CFX, FLUENT, STAR-CD. Extensive efforts have been made to assess the applicability of existing CFD codes for heat transfer simulation at supercritical pressure conditions.

Yang *et al.* [24] studied turbulence models for upward flows of supercritical water in circular tubes using STAR-CD. The results of numerical simulation were compared with experimental data and correlations. Through comparisons in both low and high bulk temperature regions, they concluded that the two-layer model gives a better prediction to the heat transfer and the standard k-ε high Re model with the standard wall function also shows an acceptable predicting capability.

Cheng *et al.* [25] investigated turbulence models for supercritical water flows in circular tube vertically oriented by CFX. Four ε-type and two ω-type turbulence models were applied in the simulation. Through comparisons, the ω-type turbulence models were not recommended for heat transfer in supercritical fluid. A good agreement has been found between all the ε-type turbulence models except where bulk fluid temperature is close to the pseudo-critical point.

Zhang *et al.* [26] evaluated turbulence models for supercritical water flows in vertical and horizontal circular tubes using FLUENT code. Six turbulence models were used in the numerical simulation. The numerical results were compared against the experimental data to investigate the accuracy and applicability of the turbulence models. Through comparisons, it was concluded that the Reynolds stress model gives better agreement with the experimental data.

Similar work can also be found in [27, 28]. In spite of quantitative deviation between the numerical results and the experimental data, CFD is proven to be a suitable approach for the analysis of the thermal-hydraulic behaviour of supercritical fluids.

Some numerical studies were carried out to investigate the heat transfer phenomena of supercritical water using CFD [29-36]. These studies are helpful to interpret the mechanisms of unique heat transfer characteristics of supercritical water. But they are mostly limited to simple flow channel geometries, such as circular tube. The conclusions achieved in circular tubes cannot be directly applied to non-circular flow channel. Therefore, CFD analyses have also been performed to investigate the thermal-hydraulic behaviour of supercritical water in sub-channel and fuel bundles.

Shang [37] investigated the thermal-hydraulic behaviour of 3D vertical rod bundles of an SCWR using STAR-CD. It was found that the wall temperature distributions were non-uniform along the wall and their values depended on the geometry frame. The pitch-to-diameter (P/D) ratio around 1.25 has been recommended considering the effects of the flow direction, the maximum value of the wall temperature and the wall temperature differences.

Gu *et al.* [38] studied the thermal-hydraulic behaviour of supercritical water flows in sub-channels of an SCWR using CFX. Three types of sub-channel were analyzed. Effects of various parameters, such as boundary conditions and P/D ratio, on the mixing phenomenon in sub-channels and heat transfer were investigated.

Similar studies are found in [25, 39-47]. The knowledge of SCWR on the thermal-hydraulic behaviour, including flow pattern, turbulence mixing and heat transfer were obtained through these studies. The results of these studies supplied useful data and guideline for the

improvements of SCWR design. Furthermore, these studies provided inputs to sub-channel codes (for example, turbulent mixing coefficient) and models for benchmarking system codes.

CFD codes are also useful in modeling complex geometries with arbitrary boundary shapes and internal structures. For example, Wank *et al.* [48] studied different measures to enhance mixing with CFD analysis to minimize hot spots in the core of HPLWR.

2.1.2 Sub-channel Analysis

In sub-channel analysis, the fluid temperature, pressure and velocity in a sub-channel is averaged and each sub-channel is considered as a unit. Empirical correlations are employed to reference the flow and heat transfer in each sub-channel to those in circular tubes. Therefore, the fluid flow is treated as a quasi-3D model. In a nuclear reactor, the fluid flow model is coupled with 1D model of fuel rod with different ratings. The heat transfer between the surface of the cladding and the coolant is considered. Detailed flow and temperature distributions in the reactor core, which are important for safe and reliable operation, can be calculated with relative low computational resources as compared to CFD. Correlations for heat transfer coefficient and turbulent mixing coefficient are derived from experimental or CFD numerical results. A well-known example of sub-channel code is COBRA.

Yoo *et al.* [49] performed a sub-channel analysis for supercritical water-cooled fast reactor fuel assembly using the sub-channel code STARS. Several suggestions were made to reduce the peak cladding temperature arising from channel heterogeneity. The limiting thermal condition of peak cladding temperature was determined.

Li *et al.* [50] developed a sub-channel code ATHAS for the analysis of flow and cladding temperature in CANDU fuel at supercritical pressure. The peak cladding temperature of a CANFLEX bundle was found to be below the limit of design. It was concluded that it is

appropriate for the CANFLEX bundle to be used in the CANDU-SCWR based on the heat transfer analysis.

Similar studies are found in [51-57]. Most of the sub-channel analyses are carried out to facilitate the fuel channel design and determine the operation margin at normal operating conditions. It is also extended to investigate the start-up process of SCWR [58]. These studies are based on the thermal-hydraulic sub-channel codes only. Due to sharp variation of supercritical water density across the pseudo-critical point, it is necessary to perform coupled analysis between neutronics code and sub-channel thermal-hydraulic code.

Shan *et al.* [59] studied the design characteristics of a pressure-tube type SCWR fuel channel by coupling the neutronics code MCNP with the sub-channel code ATHAS. Based on the analyses, the coolant and cladding temperature distributions could be optimized to satisfy the design criteria by improving the radial fuel enrichment profile and smaller pressure tube pitch would result in more flatten the axial power distribution and more uniform radial power distribution.

More works on fuel channel design of SCWR based on coupling of neutronics and sub-channel codes can be found in [60-67].

2.1.3 Transient Analysis

In transient analysis, large system codes are developed for analysis of various fault conditions and initiating events. They are derived based on a lumped parameter approach. The components of a nuclear power system are represented as 1D model. The flow, temperature and pressure in the primary and secondary loops are calculated. System codes include modeling of the reactor vessel (or tube), hot and cold legs, pressurizer, steam generator and safety systems using fundamental components of pipes, vessels, and valve etc. A point reactor kinetics model to calculate the reactor power and a fuel rod model to compute the heat transfer between the fuel

and coolant are also included in such codes. Examples of such codes include RELAP5, CATHENA and RETRAN.

Lee *et al.* [68] developed a LOCA analysis code SCRELA for SCWR. SCRELA was validated with REFLA-TRAC code. A large break LOCA of an SCLWR was analyzed using SCRELA. The code showed that the SCLWR under a large break LOCA is safe and the peak cladding temperature is sufficiently lower than the limiting temperature of stainless steel cladding, and could be applied to LOCA analysis of other types of SCWR.

Xu *et al.* [69] constructed a model of mixed spectrum SCWR (SCWR-M) system using a revised version RELAP5. Parametric analyses were performed to investigate the transient behaviour of an SCWR-M and develop mitigation measures during a loss of flow accident (LOFA). Three important mitigation measures for LOFA were derived from the analyses.

Some other system codes (newly developed or revised based on the old version) were developed and applied to analyze the transient behaviour and safety issues of SCWR [70-82]. Transient analysis system codes of SCWR were also constructed and applied to design control system of SCWR [83-85] and the detailed information will be given in the Section 2.3.

2.2 Moving Boundary Modeling Method

The fixed boundary method is the most commonly used technique in thermal-hydraulic modeling. Some existing system codes, such as RELAP5, also adopt this method. In the fixed boundary method, the position and the length of each node or control volume do not change. It is impossible to distinguish the boundaries. Taking the boiling boundary as an example, the position of the boiling point generally does not coincide with the boundary of one node in the

fixed boundary method, because it is not tracked in this method. Thus, one node must contain both water and steam, which have different thermal properties. One requirement for this method is that the thermal properties in each node should be kept as consistent as possible. If this requirement cannot be met, serious numerical consequences can follow. The problem is that due to an abrupt change in water/steam properties at the boiling boundary under subcritical pressure or water properties at the pseudo-critical boundary under supercritical pressure, significant errors can be introduced into the computation. Furthermore, a discontinuity in heat transfer correlation due to abrupt changes in thermal properties of water may result in numerical convergence and stability problem. The moving boundary method can track such points and overcome these drawbacks.

The moving boundary method was compared against the fixed boundary in the modeling of an once-through steam generator (OTSG) under subcritical conditions [86]. Ten nodes were applied in the moving boundary method, and 10 and 25 nodes were adopted in the fixed boundary method. The simulation results were compared with the experimental results. It was found that the model using moving boundary method is more accurate than that of the fixed boundary method with the same number of nodes, and the computational time is less. Large errors could happen and misleading results were given to some disturbances using the fixed boundary method. It is concluded that the moving boundary method is suitable for dynamic modeling of OTSG.

The moving boundary method has been successfully applied to the modeling of U-tube steam generator (UTSG), OTSG and LWRs. Most of the following references are relevant to different boiling modes at subcritical pressure. The boiling heat transfer mechanism is well understood now and can be found in open literatures. Interested readers are referred to [87].

A dynamic model of an integral economizer UTSG was developed using moving boundary method [88]. The moving boundary was set at the saturation conditions in the secondary side of the UTSG. It was assumed that there was a distinct boundary between a sub-cooled region and a boiling region. The assumption ignored the complicated sub-cooled boiling process in the sub-cooled region and variations in the boiling mechanism in the boiling region. The model was obtained by applying the time-dependent mass and energy conservation equations and time-independent momentum equation. A linear model was obtained through linearization. For this reason, the linear model is restricted to simulate the conditions around the original steady-state conditions.

Gal *et al.* [89] constructed a UTSG module for a dynamic simulator for nuclear power plants using the moving boundary method. The boundary position was determined by the location of the fluid saturation enthalpy. There were two moving boundaries on the secondary side. One is placed between the steam dome and the downcomer separating the steam from the sub-cooled water. The other boundary was located between the boiling and sub-cooled regions on the UTSG shell side. The model was derived from the mass and energy balance questions. Two integral momentum equations were developed for the primary and secondary flow paths.

An OTSG dynamic model with moving boundaries and variable nodes was developed for a liquid-metal fast breeder reactor [90]. The OTSG model consisted of four regions: sub-cooled region, nucleate boiling region, film boiling region and superheated steam region. The boundaries between regions were determined by the points where the fluid reached liquid saturation point, departure from nucleate boiling (DNB) point and dry saturation steam point, respectively. The node number in each region could be changed to assess its effect on the results. The model was derived from the mass and energy conservation equations. The momentum

equation was decoupled and included in the overall system via the external pipe model. A similar model was also developed for a helical-coil OTSG [91].

Tzanos [92] developed an OTSG model with multiple nodes using the moving boundary method. The OTSG model was divided into four regions: sub-cooled region, nucleate boiling region, film boiling region and superheated steam region. The boundaries of these regions were determined by the water/steam specific enthalpy and steam quality: specific enthalpy of saturated liquid, steam quality at the point of DNB and the unit steam quality. In the model, the pressure of the secondary side was allowed to vary with time, but not with space. An accurate description of the DNB boundary could be obtained by the developed model.

Yoon *et al.* [93] developed a thermal-hydraulic design and performance analysis code for an OTSG with helically coiled tubes using the moving boundary method. A minimum of three control volumes were used: economizer region, evaporator region and superheated region. These regions were separated by the specific enthalpy of saturated liquid and dry saturated steam. When the fully developed nucleate boiling and mist heat transfer regions were modelled, the additional region boundaries were located using empirical correlations within the economizer and evaporator regions, respectively. These two boundaries were placed at the net vapour generation point and the dryout point. Two integral momentum equations were developed for the primary and secondary flow paths.

A dynamic model of once-through boiler using moving boundary method was developed [94]. The working fluid inside the evaporator pipes was characterized by three regions: sub-cooled liquid, two-phase mixture, and superheated steam. The boundaries were determined by the specific enthalpy of the saturated liquid and the dry saturated steam. The time dependence of the momentum equation was neglected.

A dynamic model of an OTSG with concentric annuli tubes using the moving boundary method was developed [95]. The secondary side was divided into three regions: sub-cooled liquid region, nucleate boiling region, and superheated steam region according to the phase change and different heat transfer characteristics. The boundary positions were determined by the specific enthalpy of the saturated liquid and dry saturated steam. The time dependence of momentum equation was neglected.

Li *et al.* [96] developed a lumped parameter mathematical model of the helical coiled OTSG of a 10MW high-temperature gas-cooled reactor based on the fundamental conservation equations of mass, energy and momentum. The OTSG model was divided into three regions: sub-cooled region, boiling region, and superheated region. The boundary positions were placed at the specific enthalpy of the saturated liquid and the dry saturated steam. The time dependence of momentum equation was considered in this model.

Han and Stanley [97] constructed a fuel pin model (FUELPIN) with moving boundaries to accommodate the core thermal-hydraulic model of LWRs with detailed thermal conduction in fuel elements. The model was divided into five regions: sub-cooled liquid convective region, sub-cooled nucleate boiling region, saturated nucleate boiling (pre-DNB) region, saturated film boiling (post-DNB) region, and superheated steam region. The boundary positions were determined by the bulk water/steam specific enthalpy or steam quality: specific enthalpy at the bubble detachment, specific enthalpy of saturated liquid, steam quality at DNB, and specific enthalpy of dry saturated steam. A single mixture momentum equation is used over the entire channel of the reactor core. An accurate minimum departure from nucleate boiling ratio (MDNBR) and its boundary position versus time within the fuel channel were predicted during transients. The FUELFIN obtained higher MDNBR values than those calculated by sub-channel

code COBRA. Therefore, the FUELPIN transient MDNBR methodology predicted a greater thermal margin than the COBRA methodology. The studies showed that the moving boundary formulation could provide an efficient and suitable tool for thermal transient analysis of LWRs. Similar results are also reported in [98].

A nodal model with moving boundary of a heated boiling channel was derived for the dynamic stability analysis [99]. The boiling channel model was divided into two regions: single-phase and two-phase regions by the net vapour generation point. The derivation was based on the integration of the conservation equations in space. The resulted model was used to evaluate the linear dynamic stability of a vertical boiling channel. The results obtained using moving boundary method with a relatively small number of nodes, compared favourably with experimental results and those with distributed parameter and fixed node models, which required many axial nodes.

The moving boundary method is also applied in the modeling of supercritical once-through boiler and SCWR.

A nonlinear lumped parameter dynamic model of a supercritical once-through 600MW boiler with the moving boundary method was developed for a large load change or large scale disturbance simulation [100, 101]. The model was divided into water region and steam region by the pseudo-critical point at the supercritical pressure. At the subcritical pressure, the model was constructed similar to those of an OTSG using moving boundary method. The simulation results showed that the model developed can predict the dynamics of supercritical boiler adequately.

Li and Ren [102] developed a dynamic model for a supercritical once-through boiler steam generator. Considering the heat transfer coefficient influenced by the specific enthalpy of the working fluid, the model was divided into three regions at the pressure above 21MPa: sub-cooled

region, large heat transfer coefficient region and superheated region. The regions were separated by the specific enthalpy of saturated liquid and saturated vapour at 21MPa. When the pressure is less than 21MPa, the model is divided into sub-cooled region, two-phase region and superheated region at the subcritical conditions. Therefore, the model developed could be used for both supercritical and subcritical conditions.

A single-channel thermal-hydraulic model of the US reference SCWR was constructed for stability analysis at both steady-state and sliding pressure start-up conditions [103]. The supercritical water flow in the reactor core was simulated using a three-region model: a heavy fluid, a mixture of heavy fluid and light fluid, and a light fluid. The heavy fluid was assumed to be an incompressible liquid with constant density. The mixture of heavy fluid and light fluid was similar to a homogeneous-equilibrium two-phase mixture. The light fluid behaved like an ideal gas or superheated steam. These regions were separated by the respective boundaries as follows:

1) Fluid temperature at 350°C, where the density starts to drops drastically as fluid temperature increases;

2) Fluid temperature at the pseudo-saturation vapour state calculated by the following

$$T = n_2 + (\frac{P - n_3}{n_1})^{0.5}$$

where

T is the fluid temperature (K);

$$n_1 = 0.101930 * 10^{-2}$$

$$n_2 = 0.572545 * 10^{3}$$

$$n_3 = 0.139189*10^2$$

P is the system pressure (MPa).

It was found that the US reference SCWR design could operate in a stable region with a large margin.

A lumped parameter dynamic model of an SCWR was developed for analysis of coupled neutronics/thermal-hydraulic instability [104]. The coolant channel was divided into two nodes with a moving boundary between them. The boundary position was placed at the pseudo-critical point. A thermal-hydraulic stability analysis was carried out for various values of parameters such as reactor power, coolant mass flow rate, and inlet temperature. It was found that the analysis with neutronics was more conservative and showed that the system became unstable for large perturbations, even if it was stable for small disturbances.

2.3 Control of Supercritical Water-cooled Power Plants

BWR adopts once-through coolant system, which is similar to that of the SCWR power plant. Light water coolant is also worked as the moderator in a BWR. The coolant absorbs the heat generated by fission reaction in the fuel rods and produces steam through boiling. The steam is directly used to drive the turbine. Then it is condensed back into water in a condenser. The water is preheated and sent back to the reactor core to complete the cycle.

In a BWR, there are three main parameters to be controlled: pressure, reactor power, and water level.

The reactor pressure is controlled by regulating the opening of the turbine control valve. The turbine control valve is adjusted to maintain relatively constant reactor pressure in the BWR. The

temperature of the saturated steam is a function of the pressure only. Therefore, the steam temperature is kept constant by maintaining the constant reactor pressure.

The reactor power in a BWR is controlled by changes in the recirculation flow rate or by moving of the control rods. When an increase in the recirculation flow happens, the volume of the steam in the reactor core will be temporarily reduced for a faster rate in removing the steam voids. This results in higher coolant density and further leads to an increase in the reactivity and reactor power level. Withdrawing a control rod reduces the neutron absorption and increases the reactivity, which leads to an increase in the reactor power. Control rod movement is the normal method of making large adjustments in the reactor power.

The water inventory in a BWR can be evaluated by the water level in the reactor core. The feed-water flow rate is controlled to maintain the water level within a predetermined range. The feed-water control system utilizes signals from reactor vessel water level, steam flow, and feed-water flow, and is called three-element control. In a BWR, the coolant also acts as the moderator, and the disturbances in the coolant flow affects the neutronics and the change in the reactor power also influences the dynamics of the coolant. The feed-water flow can be adjusted to achieve the required water level. At the same time, the reactivity is also changed due to the reactivity feedback caused by the change in the feed-water flow. The recirculation flow is independent from the feed-water flow and has negligible effects on the water level directly. The reactivity caused by the change in the feed-water flow rate can be compensated by the recirculation flow rate.

Among the three control systems above, dynamics of the pressure are fastest and those of the water level are slowest. The control of the water level is the most complex and the changes in the reactor power and pressure can affect the dynamics of the water level.

In a BWR, there is no steam generator as a cushion between the reactor and the turbine. The disturbances from the reactor (or turbine) directly affect the behaviour of the turbine (or reactor). Thus, the reactor and the turbine is directly coupled. But the level of the coupling between them is low due to the existence of boiling process. The dynamic process of the reactor is slow compared to that of the turbine. The turbine-following-reactor operation mode is used in BWR. When the load is increased, the opening of the turbine governor valve is increased and more steam is drawn from the reactor. The recirculation flow rate is increased to raise the power level to meet the desired load demand. The loss of the steam can be recovered by boiling of the coolant. The water level can be adjusted to the desired level by increasing the feed-water flow rate. The feed-water flow rate is regulated to be proportional to the load level at steady-state conditions.

In an SCFPP, an once-through cycle coolant system is also applied. The feed-water is pumped to the boiler. In the boiler, the water is heated and superheated steam is generated. Then the steam is sent to the steam turbine, which is coupled to a generator to produce electricity. The steam out of the turbine is cooled by the condenser and sent back to the boiler. There are mainly four parts in the boiler of an SCFPP: economizer, evaporator, superheaters and reheaters. In the economizer, the feed-water is preheated. The evaporator contains water wall area. In a subcritical once-through power plant, boiling takes place and the steam is produced in the evaporator. In an SCFPP, the evaporator is the most important part. The heat flux is the highest and more than half of the temperature increase happens in the evaporator. The large specific heat region of supercritical water also locates in the evaporator. The steam is superheated in the superheaters and reheated in the reheaters using the flue gas, before it is sent to the turbine.

The load, the steam temperature and steam pressure of an SCFPP are all affected by the turbine control valve, fuel/air flow and feed-water flow rate. The SCFPP boiler can be modelled as a three-input and three-output system. The control strategy can be different depending on the operation mode selected.

In the turbine-following-boiler operation mode, the steam pressure is mainly regulated by the opening of the turbine control valve. The power is generated by a combustion process and determined by the fuel/air flow. The fuel/air flow is an index for the power output and used to follow the load demand. The water inventory of an SCFPP is evaluated by the intermediate temperature, which is measured at the outlet of the evaporator. The intermediate temperature is required to be slightly higher than the pseudo-critical temperature of the corresponding pressure to ensure the cooling capacity of the boiler. The main steam temperature is controlled by the fuel to feed-water flow ratio and superheater sprayer. The fuel to feed-water flow ratio is the main manipulate variable to regulate the main steam temperature. The superheater sprayer is a supplement and only used to reduce steam temperature at emergence conditions. The fuel to feed-water flow ratio is the most critical variable for the operation of an SCFPP. It is used not only to meet the steam requirement of the turbine but also to regulate the main steam temperature. Because of the presence of large time constants in the boiler due to the large metal mass and delays in the combustion system, the feed-forward control is introduced to maintain the fuel to feed-water flow ratio when it is required to operate the plant at large load gradients or to stress the plant as little as possible.

In the boiler-following-turbine mode, the turbine governor as a fast-acting load controller is used. Opening the governor valves releases the stored energy in the boiler and meets short-term

increases in the electrical demand. These actions alter the main steam pressure, and the pressure controller adjusts the fuel-firing rate to maintain the main steam pressure.

The sliding pressure mode is an evolutionary extension from the constant pressure mode. When the load is varying, the steam pressure also varies. At a low load output, the reduced throttling-back action by the governor control valves leads to improved unit efficiency. Sliding pressure operation also provides fast unit loading, and enables stable operation of the turbine at lower temperature and pressure conditions.

The once-through cycle adopted in the SCFPP leads to a strong coupling between the boiler and the turbine. It is necessary to integrate the boiler and turbine as a whole and consider the balance of energy supply and demand. A coordinated control strategy is applied to coordinate the activities of various subsystems of an SCFPP so as to minimize the influence of both plant-wide interactions and disturbances and to avoid violating thermal constraints during large load changes and system disturbances. The coordinated control system, which unites the boiler and turbine controls, generates and regulates the setpoint of unit load. The demand signals are sent out to the Boiler Master and Turbine Master in parallel. The Boiler Master demand is used to regulate the feed-water flow and firing rate to improve the unit response to a load change. The Turbine Master demand controls the turbine control valves.

Although lots of efforts have been made in the development of SCWR, there are limited reports in the open literature on the control of SCWR.

Several similarities between SCWR and BWR or PWR were identified to determine the control strategy [105]. The similarities for BWR are associated with the direct cycle with feed-water flow entering directly into the reactor vessel and steam flow going directly to the turbine. A balance between feed-water and steam is required to maintain the water inventory in the vessel.

The similarities for PWR are associated with the high operating pressure, the single-phase conditions at the core outlet and a core outlet temperature that is a function of power and coolant flow. Unique aspects of the SCWR that influences the control concept include the elimination of the recirculation pumps, the low water inventory in the reactor pressure vessel, the large change in the coolant density across the core, and the absence of a coolant level under supercritical conditions.

Considering the characteristics of SCWR, two recommendations were made for the SCWR control system based on the base load operation assumption:

a)   Control of the main reactor variables. The control rods are used to control the thermal power. The turbine control valve provides the control of the pressure, and the feed-water flow performs the control of the outlet temperature. The coolant inventory in the vessel is controlled by assuring that the steam and the feed-water flow are balanced at the same time maintaining the correct core outlet temperature.

b)   Integrated control system approach. The relatively small vessel water inventory, the neutronic/thermal-hydraulic coupling, the lack of level indication under supercritical conditions and the absence of recirculation flow make control more challenging. Thus, the use of an integrated control would allow the system to anticipate changes and react accordingly.

Nakatsuka *et al.* [83] studied the control system design for an SCFR plant. A computer code was developed for transient behaviour analysis of the SCFR plant. Lumped parameter and nodal methods have been used to the thermal-hydraulic modeling. The reactor core was represented as a single channel. Dittus-Boelter's formula was adopted for the heat transfer coefficient calculation. Point reactor kinetics with six delayed neutron groups were used to calculate the core power.

The dynamic behaviours of the SCFR were analyzed through introducing different perturbations of feed-water flow rate, control rods and turbine control valves. Based on the observation of the dynamic responses, the input-output pairings are determined: the pressure is controlled by the turbine control valves, the main steam temperature is controlled by the feed-water flow rate, and the core power is controlled by the control rods.

The similar control strategy of a BWR was applied to control system design of the SCFR. Sequential loop closing approach and trial and error method were carried out to tune the parameters of the control system. The chosen tuning criteria were damping ratio larger than 0.75 and overshoot less than 15%.

Typical disturbances were introduced to investigate the reactor behaviour with the designed control system. It was concluded that the designed control system could keep the SCFR plant stable against different disturbances, such as setpoint changes and feed-water temperature changes.

The work in the control system design for the SCFR plant [83] was extended to the control system design of high temperature SCLWR (SCLWR-H) [84]. The similar design procedure was adopted in the control system design of SCLWR-H.

Ishiwatari *et al*. [85] improved the feed-water controller for a Super Fast Reactor (FR) to suppress the variation of the main steam temperature. The plant system code SPART-F was used to model the Super FR. The original feed-water controller was designed only considering the deviation of the main steam temperature. The variation of the main steam temperature of the Super FR to different disturbances is large due to its high power-to-flow ratio. To reduce the variation, three parameters are considered in the modified feed-water controller design: the deviation of the power-to-flow ratio (A), the deviation of the power (B), and the time derivative

of the power (C). The trial and error method was applied in the controller design. Five typical perturbations were analyzed to confirm the performance of the new feed-water controllers. It was observed that the feed-water controller (B) gave a smaller or at least not larger variation of the main steam temperature compared with the original one under all the perturbations, while the feed-water controllers (A) and (C) resulted in a larger variation in particular cases. It was concluded that the original feed-water controller was successfully improved by the feed-water controller (B).

These control systems designed are in decentralized structure. Decentralized control is only valid when the weakly-coupled requirement is satisfied. SCWR is a MIMO system with strong interactions among inputs and outputs. Decentralized control can only achieve limited control performance and may even cause dynamic stability issue. Decoupling control is an efficient approach to deal with cross-coupling and has been applied in different industries.

A multivariable controller was designed for CANDU 600 MWe nuclear power plant using the inverse Nqyusit array method [106]. A decoupling compensator was selected to improve the diagonal dominance. Then analysis of the closed-loop system was performed and a feedback matrix was chosen to meet the design specifications. The controller was implemented on a reference nonlinear model to assess its overall performance. The results showed that the multivariable controller achieves better overall regulation than the conventional controller.

A decoupling compensator of a boiler-turbine unit was designed by DNA method [107]. Diagonal dominance was achieved so that the decoupled MIMO system was transformed into several SISO systems. Then PID controllers were obtained based on the gain and phase margin specifications. Simulation results showed that the designed controller for the boiler-turbine unit has much better dynamics performance than the one designed by Tan's method [108].

3 CONSTRUCTION OF A DYNAMIC MODEL USING MOVING BOUNDARY METHOD

3.1 Introduction

The dynamic characteristics of the Canadian SCWR are different from those of the CANDU reactor or ACR. To examine its unique dynamics, it is necessary to have a dynamic model. The dynamics of the Canadian SCWR depend on the reactor core, and require coupling of the reactor kinetics with the feedback reactivity. The dynamic model of the Canadian SCWR can be divided into a thermal-hydraulic model and a reactor kinetics model. The thermal-hydraulic model is focused on the hydraulic flow influenced by the external heating. The reactor kinetics model is to calculate the reactor power, that is, the heat generation rate in the fuel rods. The reactor kinetics model supplies the reactor power to the thermal-hydraulic model as the heat source, while the thermal-hydraulic model provides the reactivity feedback, which is related to the thermal parameters of the reactor, to the reactor kinetics model.

The Canadian SCWR is still at the conceptual development stage. There is no real plant built yet. CFD method has been extensively adopted as an effective and powerful approach for thermal-hydraulic behaviour analysis at the supercritical conditions. The results obtained by the CFD simulation are widely accepted. Therefore, CFD numerical simulation is adopted here as a verification tool for the thermal-hydraulic model.

The modeling process consists of several steps. Firstly, the thermal-hydraulic model of the reactor is constructed based on the fundamental conservation equations of mass, energy and momentum. Secondly, the transient behaviour of the Canadian SCWR is obtained with the thermal-hydraulic model coupled with the reactor kinetics model. Based on the results of the

transient simulation of the thermal-hydraulic model, a set of linear dynamic models are obtained using a least-square system identification method. The development of the thermal-hydraulic model is performed separately for the following reasons:

a) The thermal-hydraulic model can be separated from the reactor kinetics model. The reactor power is considered as an input to the thermal-hydraulic model.

b) It is convenient to use the CFD method to verify the thermal-hydraulic model. The CFD method is mainly focused on the thermal-hydraulic analysis. User defined function will be needed and computational time may be increased if the reactor kinetics model is included in the CFD simulation.

c) It is convenient for the linear dynamic model development using system identification techniques. The system identification is carried out on the thermal-hydraulic model only. If the system identification is applied to the dynamic model with the coupling of the thermal-hydraulic and reactor kinetics, the existence of the internal feedback will cause difficulties during the system identification process.

For the thermal-hydraulic modeling, a moving boundary method is adopted to solve the problems due to the unique characteristics of thermal properties and heat transfer of supercritical water. The supercritical water exhibits significant difference in its thermal properties before and after the pseudo-critical point as shown in Section 1.1.1. In the modeling process, the thermal properties inside each control volume should be as consistent as possible. If the boundary of a control volume is constant, that is, the length of the control volume does not change, it is possible that there are two thermodynamic states in one single control volume. Normally, for each thermodynamic state, there are different equations to calculate the related parameters. In this control volume, no matter which state is adopted, large errors will occur.

For the unique thermal physical properties of supercritical water, the empirical correlations to predict heat transfer coefficient are divided into several sub-correlations by the correction factor. As shown in Section 1.1.2, the correction factor F usually depends on the specific heat ratio and the density ratio. The discontinuity on the heat transfer coefficient can be caused by the correction factor F. When the boundary of a control volume is close where the discontinuity may happen, numerical oscillation can occur. Therefore, the moving boundary method is adopted. The boundary positions are set at the pseudo-critical point and where the discontinuity in the heat transfer function may happen. In every control volume, there is only one thermodynamic state. Thus, the calculation errors are reduced. Under the same accuracy requirement, the amount of control volume can be reduced and the computational burden can be reduced. The numerical oscillation can be avoided.

The rest of this chapter is organized as follows: in Section 3.2, a detailed thermal-hydraulic model of the Canadian SCWR using moving boundary method is developed. In Section 3.3, the thermal-hydraulic model is validated using commercial CFD code: FLUENT 6.1. In Section 3.4, the benefits of adopting the moving boundary method are illustrated by comparisons with the fixed boundary method. In Section 3.5, the dynamic model of the Canadian SCWR is obtained by coupling the thermal-hydraulic model with its reactor kinetics model, and the steady-state and transient simulation results are also presented. To illustrate the uniqueness of Canadian SCWR, the dynamics of the Canadian SCWR are compared with those of ACR-700. In Section 3.6, a set of linear dynamic models around the full power operating point are developed using system identification techniques and validated with the nonlinear dynamic model.

3.2 Thermal-hydraulic Model Development for the Canadian SCWR

The fuel bundle geometry of the Canadian SCWR has not yet been established. Previous studies

showed that the CANFLEX fuel bundle is applicable to the Canadian SCWR [53]. The cross-

section of a CANFLEX fuel bundle is shown in Fig 3.1. The parameters are listed in Table 3.1.
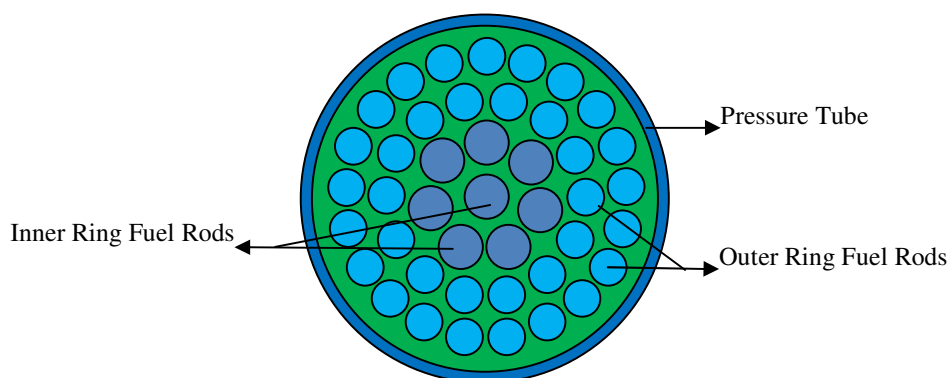
Fig 3.1 Cross-section of CANFLEX

Table 3.1 Parameters of CANFLEX

Channel Length	5.944 m	Pressure Tube Diameter	104.0 mm
Fuel Rod Diameter (Inner Ring)	13.5 mm	Pellet Diameter (Inner Ring)	12.6 mm
Fuel Rod Diameter (Outer Ring)	11.5 mm	Pellet Diameter (Outer Ring)	10.7 mm
Cladding Thickness (Inner Ring)	0.36 mm	Cladding Thickness (Outer Ring)	0.33 mm

It is shown in surveys [109-111] that a lot of experimental works on heat transfer of supercritical

fluids have been done and different empirical correlations have been developed. In this thesis,

Yamagata's correlation is chosen because its experimental conditions are close to those of the

Canadian SCWR. There are some discrepancies in the heat transfer coefficients for downward

and upward flows around the pseudo-critical point. But little influences will occur on the

dynamics because most the fuel channel in the Canadian SCWR is occupied by the vapour-like

fluid, which has a large time constant.

The Yamagata correlation is described [112]:

$$Nu_b = 0.0135 * \text{Re}_b^{0.85} * \text{Pr}_b^{0.8} * F_c \qquad (3.2.1)$$

where

$$F_c = 1.0, \ E > 1$$

$$F_c = 0.67 * \text{Pr}_m^{-0.05} * (\overline{c}_P / c_{P_b})^{n_1}, \ 0 \le E \le 1$$

$$F_c = (\overline{c}_P / c_{P_b})^{n_2}, \ E < 0$$

$$n_1 = -0.77 * (1 + \frac{1}{\text{Pr}_m}) + 1.49$$

$$n_2 = 1.44 * (1 + \frac{1}{\text{Pr}_m}) - 0.53$$

E is Eckert number defined by $\dfrac{T_m - T_b}{T_w - T_b}$, where T_b is the bulk fluid temperature, T_w is the wall

temperature, and T_m is the pseudo-critical temperature.

$\overline{c}_P$ is an average specific heat defined by $\dfrac{h_w - h_b}{T_w - T_b}$, where h_w is the specific enthalpy of bulk fluid

according to the wall conditions, and h_b is the specific enthalpy of the bulk fluid.

Yamagata's correlation is divided into three sub-correlations by the parameter E as shown in Eq.

(3.2.1). The two boundary points are where E equals to 0, that is, $T_b = T_m$, and where E equals to 1,

that is, $T_w = T_m$.

It is assumed that the reactor core is approximated by 1D single-channel. The thermal-hydraulic

model includes a coolant model and a fuel rod model. The coolant is simplified as a single

channel 1D flow. In the single channel model, the radial distribution of the reactor is not considered, and the flows in all fuel channels are assumed to be the same and averaged. When the coolant flow rate is controlled for fuel assemblies depending on their power, the flow velocities are different in the fuel assemblies. This will affect the system responses. Although the single channel model can only obtain the average effect of different channels, it reflects a good approximation of the overall dynamic behaviour. The hydraulic diameter is calculated as 7.7mm by four times of the total coolant flow area over the total wetted perimeter. The nodalization of the coolant model is shown in Fig 3.2. In the model construction process, three regions have been considered: Liquid Region I, Liquid Region II and Vapour Region. The pseudo-critical point lies in the boundary between Liquid Region and Vapour Region. From the thermal properties of the supercritical water, it is known that before the pseudo-critical point is reached, the water is liquid-like fluid and after this point is passed, it becomes vapour-like fluid. For simplicity, before the pseudo-critical point, it is called Liquid Region and after this point, it is referred to as Vapour Region. Within the Liquid Region, the fluid can further be divided into two sub-regions, Liquid Region I and Liquid Region II, separated by the point where the cladding temperature equals to the pseudo-critical temperature. In the Liquid Region I and II, different correlations are used to calculate the heat transfer coefficient as shown in Eq. (3.2.1).

As shown in Fig 3.2, the length of the Liquid Region I is Z_L. There are L nodes and the distance between adjacent nodes is α. The length of the Liquid Region II is $(Z_M\text{-}Z_L)$. There are $(M\text{-}L)$ nodes and the distance between adjacent nodes is β. The length of the Vapour Region is $(Z_N\text{-}Z_M)$. There are $(N\text{-}M)$ nodes and the distance between adjacent nodes is γ.
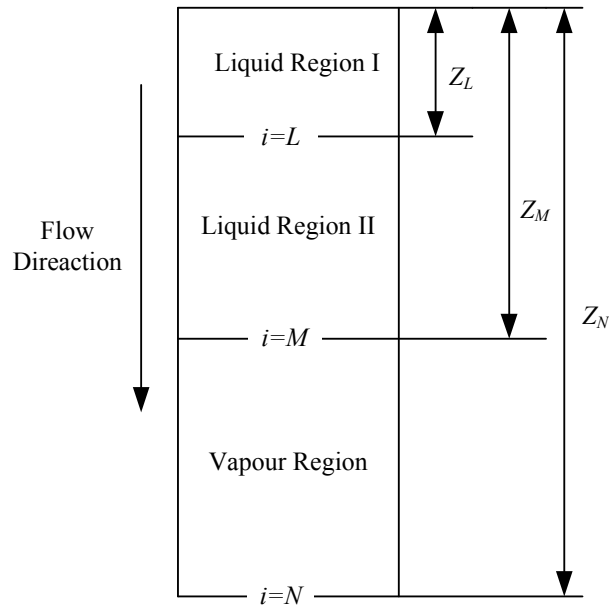
Fig 3.2 Nodalization of the Canadian SCWR coolant model

3.2.1 Fuel Rod Model

The following assumptions are made in the fuel rod model:

a. The heat transfer in the fuel element is only considered in the radial direction;

b. Fuel thermal conductivity and specific heat are a function of temperature;

c. Fuel density is assumed to be constant;

d. Heat storage in the gas gap and the fuel cladding is negligible.

Based on these assumptions, the thermal conduction in the fuel rod can be described by the Fourier heat conduction equation in cylindrical coordinates:

$$\rho \frac{\partial}{\partial t}\left(c_P(T)T(r,t)\right) = \frac{1}{r}\frac{\partial}{\partial r}\left[k(T)r\frac{\partial T(r,t)}{\partial r}\right] + q'''(r,t) \tag{3.2.2}$$

where k is the thermal conductivity, and q''' is the heat generation rate per unit volume and depends on the reactor power. The thermal parameters of the fuel can be found in [113]. The axial power distribution is determined by the reactor kinetics model and assumed to be a cosine function. In the radial direction, the power distribution is uniform.

The boundaries of the fuel rod model are the same as those of the coolant model as shown in Fig 3.2. Since the boundaries are a function of time, the integral of Eq. (3.2.2) can be treated using the Leibnitz theorem:

$$\int_{A(t)}^{B(t)} \frac{\partial f(Z,t)}{\partial t} dZ = \frac{d}{dt} \int_{A(t)}^{B(t)} f(Z,t) dZ - f(B(t),t) \frac{dB(t)}{dt} + f(A(t),t) \frac{dA(t)}{dt}$$

For simplicity, (r, t) is eliminated in the subsequent equations for the integration of Eq. (3.2.2). The term with time derivative is integrated and expressed as

$$\begin{aligned}
\int_{Z_{i-1}}^{Z_i} \frac{\partial}{\partial t} \left(c_P(T)T \right) dZ &= \frac{d}{dt} \left(c_P(T_i)T_i(Z_i - Z_{i-1}) \right) - c_P(\frac{T_i + T_{i+1}}{2}) \frac{T_i + T_{i+1}}{2} \dot{Z}_i + c_P(\frac{T_{i-1} + T_i}{2}) \frac{T_{i-1} + T_i}{2} \dot{Z}_{i-1} \\
&= \frac{d}{dt}(c_P(T_i)T_i)(Z_i - Z_{i-1}) + c_P(T_i)T_i(\dot{Z}_i - \dot{Z}_{i-1}) - c_P(\frac{T_i + T_{i+1}}{2}) \frac{T_i + T_{i+1}}{2} \dot{Z}_i + c_P(\frac{T_{i-1} + T_i}{2}) \frac{T_{i-1} + T_i}{2} \dot{Z}_{i-1}
\end{aligned} \quad (3.2.3)$$

where, Z_{i-1} and Z_i are the lower and the upper distances of the ith node from the reactor inlet. The temperature at the boundary is approximated as the average temperature of the adjacent nodes.

The integration of the remaining terms of Eq. (3.2.2) leads to

$$\int_{Z_{i-1}}^{Z_i} \left(\frac{1}{r} \frac{\partial}{\partial r} \left[k(T) r \frac{\partial T}{\partial r} + q''' \right] \right) dZ = \left(\frac{1}{r} \frac{\partial}{\partial r} \left[k(T_i) r \frac{\partial T_i}{\partial r} + q_i''' \right] \right) (Z_i - Z_{i-1})$$

Thus, Eq. (3.2.2) for the ith node is represented as

$$\rho\frac{\partial}{\partial t}(c_P(T_i)T_i) = \frac{1}{r}\frac{\partial}{\partial r}\left[k(T_i)r\frac{\partial T_i}{\partial r}\right] + q_i''' - \rho c_P(T_i)T_i\frac{\dot{Z}_i - \dot{Z}_{i-1}}{Z_i - Z_{i-1}} + \rho c_P(\frac{T_i + T_{i+1}}{2})\frac{T_i + T_{i+1}}{2}\frac{\dot{Z}_i}{Z_i - Z_{i-1}}$$

$$-\rho c_P(\frac{T_{i-1} + T_i}{2})\frac{T_{i-1} + T_i}{2}\frac{\dot{Z}_{i-1}}{Z_i - Z_{i-1}} \tag{3.2.4}$$

A lumped dynamic model developed at Brookhaven National Laboratory (BNL) [114] is applied to Eq. (3.2.4) to calculate the thermal conduction with convection boundary conditions in a fuel rod. In this model, the radial temperature distribution in the fuel pin is assumed to be a second order polynomial, while in the gas gap and cladding, they are assumed to be linear. The radial temperature distribution in the fuel pin, gas gap and cladding is illustrated in Fig 3.3.
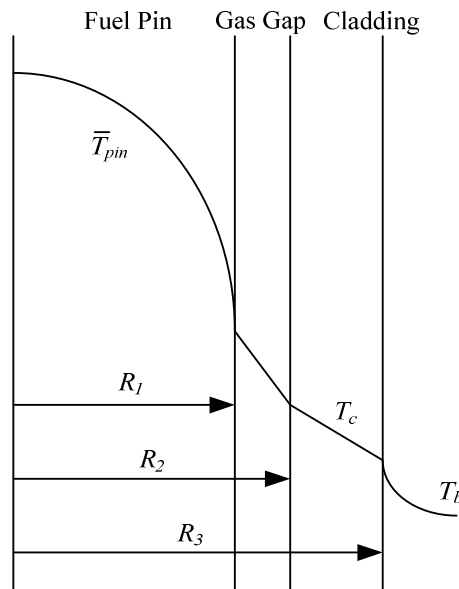
Fig 3.3 Temperature distribution in a fuel rod

According to the assumptions on the temperature distribution, the average temperature of the fuel pin can be described by [114]

$$\frac{d\overline{T}_{pin_i}}{dt} = \frac{2}{(R_3 - R_2)R_3} \frac{k_c}{(\rho c_P(\overline{T}_{pin_i}))_f} \frac{N_{Bi,c}}{\left[1 + (C_{gm} + F_{pr})N_{Bi,c}\right]} (T_b - \overline{T}_{pin_i})$$

$$+ (\frac{R_1}{R_3})^2 \frac{q_i'''}{(\rho c_P(\overline{T}_{pin_i}))_f} - \overline{T}_{pin_i} \frac{\dot{Z}_i - \dot{Z}_{i-1}}{Z_i - Z_{i-1}} + \frac{(c_P(\frac{\overline{T}_{pin_i} + \overline{T}_{pin_{i+1}}}{2}))_f}{(\rho c_P(\overline{T}_{pin_i}))_f} \frac{\overline{T}_{pin_i} + \overline{T}_{pin_{i+1}}}{2} \frac{\dot{Z}_i}{Z_i - Z_{i-1}} \qquad (3.2.5)$$

$$- \frac{(c_P(\frac{\overline{T}_{pin_{i-1}} + \overline{T}_{pin_i}}{2}))_f}{(\rho c_P(\overline{T}_{pin_i}))_f} \frac{\overline{T}_{pin_{i-1}} + \overline{T}_{pin_i}}{2} \frac{\dot{Z}_{i-1}}{Z_i - Z_{i-1}}$$

where,

$\overline{T}_{pin}$: Average temperature of the fuel pin;

$N_{Bi,C}$: Biot number $= H(R_3 - R_2)/k_c$, where H is the heat transfer coefficient and k_c is the thermal conductivity of the cladding;

C_{gm}: Geometric constant $= \left(\frac{R_1}{R_3}\right)^2 + \left[1 - \left(\frac{R_2}{R_3}\right)^2\right]\left[\frac{3(R_2 + R_3) - (R_3 - R_2)}{6(R_2 + R_3)}\right]$;

F_{pr}: Property function $= \frac{R_1^3}{(R_3 - R_2)R_3^2}(\frac{k_c}{4k_f} + \frac{k_c}{R_1}\frac{1}{H_{gap}})$.

The cladding surface temperature, the average temperature of the fuel pin and the coolant bulk temperature are related as [114]

$$T_c - T_b = \frac{\overline{T}_{pin} - T_b}{1 + (C_{gm} + F_{pr})N_{Bi,C}} \qquad (3.2.6)$$

where, T_c is the cladding surface temperature.

3.2.2 Coolant Model

The coolant model is developed under the assumption that it is a 1D flow. The nodalization of the coolant model has been shown in Fig 3.2. The location of the ith node is denoted by the index

i. Generally, the index notation *i-1/2* is used to indicate the boundary position between node *i-1* and *i*. Here, the 1/2 is not used and integer values are used by shifting the index by -1/2, that is, the node *i* is surrounded by node boundaries *i-1* and *i*. The conservation of fluid mass, energy, and momentum in the flow channel can be represented as the following set of partial differential equations:

$$\frac{\partial \rho}{\partial t} = -\frac{\partial D}{\partial Z} \tag{3.2.7}$$

$$\frac{\partial (\rho h)}{\partial t} = -\frac{\partial (Dh)}{\partial Z} + Q''' + \frac{\partial P}{\partial t} \tag{3.2.8}$$

$$\frac{\partial D}{\partial t} = -\frac{\partial}{\partial Z}(\frac{D^2}{\rho}) - \frac{\partial P}{\partial Z} - \frac{1}{2}\frac{D^2}{\rho}f_r\frac{S}{A} - \rho g \tag{3.2.9}$$

where, D is the mass velocity; Q''' is the heat absorption rate per unit volume; f_r is the friction factor; S is the flow channel wetted perimeter; and A is the flow area.

In the Canadian SCWR reactor core, the pressure drop is only a small fraction of the absolute pressure. The pressure in the coolant model is considered as a function of time only and the momentum equation is not considered.

To solve Eqs. (3.2.7) and (3.2.8), the integrals that involve time derivatives are evaluated using Leibnitz theorem:

$$\int_{Z_{i-1}}^{Z_i} \frac{\partial f}{\partial t}dZ = \frac{d}{dt}\int_{Z_{i-1}}^{Z_i} f dZ - f_i\frac{dZ_i}{dt} + f_{i-1}\frac{dZ_{i-1}}{dt} \tag{3.2.10}$$

where,

$$f = \rho, \rho h, P$$

$$f_i = f(Z_i, t)$$

$$f_{i-1} = f(Z_{i-1}, t)$$

$Z_{i-1}, Z_i =$ the distance of ith node lower and upper boundary from the reactor inlet.

The first term on the right hand side of Eq. (3.2.10) can be rewritten as:

$$\frac{d}{dt} \int_{Z_{i-1}}^{Z_i} f dZ = \frac{d(\overline{f_i}(Z_i - Z_{i-1}))}{dt} = \dot{f_i}(Z_i - Z_{i-1}) + f_i(\dot{Z_i} - \dot{Z_{i-1}}) \qquad (3.2.11)$$

where, $\overline{f_i}$ is the average value of f in the ith node and can be defined as $\overline{f_i} = \theta f_{i-1} + (1-\theta) f_i$, θ is the weighting coefficient.

Generally it can be assumed that f varies linearly within each node and $\theta = 0.5$ is adopted. For larger nodes, $\theta = 0.5$ can lead to unstable and physically unmeaningful solutions. To avoid this problem, in this study , the upwind approximation is adopted for the average value $\overline{f_i}$ and θ is set to be 0. Eq. (3.2.10) yields

$$\int_{Z_{i-1}}^{Z_i} \frac{\partial f}{\partial t} dZ = \dot{f_i}(Z_i - Z_{i-1}) + f_i(\dot{Z_i} - \dot{Z_{i-1}}) - f_i \dot{Z_i} + f_{i-1} \dot{Z_{i-1}} \qquad (3.2.12)$$

Thus,

$$\int_{Z_{i-1}}^{Z_i} \frac{\partial f}{\partial t} dZ = \dot{f_i}(Z_i - Z_{i-1}) + (f_{i-1} - f_i) \dot{Z_{i-1}} \qquad (3.2.13)$$

The integration of the remaining terms in Eqs. (3.2.7) and (3.2.8) lead to:

$$\int_{Z_{i-1}}^{Z_i} \frac{\partial D}{\partial Z} dZ = D_i - D_{i-1} \qquad (3.2.14)$$

$$\int_{Z_{i-1}}^{Z_i} \left[-\frac{\partial(Dh)}{\partial Z} + q''' \right] dZ = D_{i-1} h_{i-1} - D_i h_i + Q_i''(Z_i - Z_{i-1}) \qquad (3.2.15)$$

From Eqs. (3.2.13), (3.2.14) and (3.2.15), Eqs. (3.2.16) and (3.2.17) are obtained

$$\dot{\rho}(Z_i - Z_{i-1}) - \dot{Z}_{i-1}(\rho_i - \rho_{i-1}) + D_i - D_{i-1} = 0 \qquad (3.2.16)$$

$$\frac{d(\rho h)_i}{dt}(Z_i - Z_{i-1}) - \dot{Z}_{i-1}((\rho h)_i - (\rho h)_{i-1}) + D_i h_i - D_{i-1} h_{i-1} = Q_i'''(Z_i - Z_{i-1}) + \dot{P}(Z_i - Z_{i-1}) \quad (3.2.17)$$

The density of the supercritical water is considered as a function of its pressure and specific enthalpy:

$$\rho = f(P, h) \qquad (3.2.18)$$

Therefore, the derivative of the density can be represented as

$$\dot{\rho} = \frac{\partial \rho}{\partial P}\dot{P} + \frac{\partial \rho}{\partial h}\dot{h} \qquad (3.2.19)$$

Substituting Eq. (3.2.19) into Eq. (3.2.16), one can obtain:

$$\dot{h}_i = \frac{\dot{Z}_{i-1}(\rho_i - \rho_{i-1}) - (D_i - D_{i-1}) - \frac{\partial \rho_i}{\partial P}\dot{P}(Z_i - Z_{i-1})}{\frac{\partial \rho_i}{\partial h_i}(Z_i - Z_{i-1})} \qquad (3.2.20)$$

Substitute Eq. (3.2.20) into Eq. (3.2.17), and the following relationship is obtained:

$$D_i = [-\dot{Z}_{i-1}\left(\frac{\partial \rho_i}{\partial h_i}\rho_{i-1}(h_i - h_{i-1}) - \rho_i(\rho_i - \rho_{i-1})\right) - \dot{P}(Z_i - Z_{i-1})(\frac{\partial \rho_i}{\partial h_i} + \frac{\partial \rho_i}{\partial P}\rho_i)$$
$$- \frac{\partial \rho_i}{\partial h_i}Q_i'''(Z_i - Z_{i-1}) + D_{i-1}(\frac{\partial \rho_i}{\partial h_i}(h_i - h_{i-1}) + \rho_i)] / \rho_i \qquad (3.2.21)$$

The specific enthalpy and the coolant flow rate for each node are determined by Eqs. (3.2.20) and (3.2.21). The boundary position Z_i is unknown and will be solved in the subsequent sections.

As mentioned earlier, the boundary between Liquid Region I and Liquid Region II is the point where the cladding surface temperature equals to the pseudo-critical temperature. Taking derivative of Eq. (3.2.6) for the Lth node of the fuel model, the following equation is obtained

$$\dot{T}_{c_L} - \dot{T}_L = \frac{\dot{T}_{pin_L} - \dot{T}_L}{1 + (C_{gm} + F_{pr})B_{Bi,C}}$$

(3.2.22)

Eq. (3.2.22) is reorganized as

$$\dot{T}_L = \frac{\dot{T}_{c_L}[1 + (C_{gm} + F_{pr})N_{Bi,C}] - \dot{T}_{pin_L}}{(C_{gm} + F_{pr})N_{Bi,C}}$$

(3.2.23)

The temperature of the supercritical water is considered as a function of pressure and specific enthalpy,

$$T = f(P, h)$$

(3.2.24)

Therefore, the derivative of the temperature can be expressed as

$$\dot{T} = \frac{\partial T}{\partial P}\dot{P} + \frac{\partial T}{\partial h}\dot{h}$$

(3.2.25)

Substituting Eq. (3.2.25) into Eq. (3.2.23) leads to

$$\dot{h}_L = \left(\frac{\dot{T}_{c_L}[1 + (C_{gm} + F_{pr})N_{Bi,C}] - \dot{T}_{pin_L}}{(C_{gm} + F_{pr})N_{Bi,C}} - \frac{\partial T_L}{\partial P}\dot{P} \right)\frac{\partial h_L}{\partial T_L}$$

(3.2.26)

From Eq. (3.2.20), for the Lth node of the coolant model, one can obtain

$$\dot{h}_L = \frac{\dot{Z}_{L-1}(\rho_L - \rho_{L-1}) - (D_L - D_{L-1}) - \frac{\partial \rho_L}{\partial P}\dot{P}(Z_L - Z_{L-1})}{\frac{\partial \rho_L}{\partial h_L}(Z_L - Z_{L-1})}$$

(3.2.27)

The following equation is obtained from Eqs. (3.2.26) and (3.2.27)

$$\dot{Z}_{L-1} = \left(\frac{\dot{T}_{c_L}[1+(C_{gm}+F_{pr})N_{Bi,C}] - \dot{\bar{T}}_{pin_L}}{(C_{gm}+F_{pr})N_{Bi,C}} - \frac{\partial T_L}{\partial P}\dot{P} \right) \frac{\partial h_L}{\partial T_L}\frac{\partial \rho_L}{\partial h_L}(Z_L - Z_{L-1})/(\rho_L - \rho_{L-1})$$

$$+ \frac{(D_L - D_{L-1}) - \frac{\partial \rho_L}{\partial P}\dot{P}(Z_L - Z_{L-1})}{\rho_L - \rho_{L-1}}$$

(3.2.28)

The node length in the Liquid Region I is

$$\dot{\alpha} = \frac{\dot{Z}_{L-1}}{L-1}$$

(3.2.29)

The boundary between Liquid Region II and Vapour Region is the pseudo-critical point. At the pseudo-critical points, the relationship between the pressure and the temperature can be described by the following equation under the supercritical pressure:

$$T_m = 294.13 + 3.63 * P$$

(3.2.30)

The comparisons of the pseudo-critical temperatures under different pressures with those calculated from Eq. (3.2.30), and the densities [115] at the pseudo-critical points are shown in Table 3.2.

Table 3.2 Pseudo-critical Point Parameters

Pressure (MPa)	Pseudo-critical Temperature (^{o}C)	Temperature Calculated (^{o}C)	Density (kg/m^3)
23	377.5	377.6	311.6
24	381.2	381.2	315.8
25	384.9	384.8	316.1
26	388.5	388.5	318.4
27	392.0	392.1	321.4

From Table 3.2, it is shown that Eq. (3.2.30) predicts the pseudo-critical points accurately. The densities at the pseudo-critical points under different pressures are slightly different and can be considered as a constant. Thus, for the Mth node,

$$\dot{\rho}_M = 0 \tag{3.2.31}$$

Substituting Eq. (3.2.31) into Eq. (3.2.17), one can obtain

$$\dot{Z}_{M-1} = \frac{\dot{h}_M \rho_M (Z_M - Z_{M-1}) + D_M h_M - D_{M-1} h_{M-1} - \dot{P}(Z_M - Z_{M-1}) - Q'''_M (Z_M - Z_{M-1})}{\rho_M h_M - \rho_{M-1} h_{M-1}} \tag{3.2.32}$$

The node length in the Liquid Region II is

$$\dot{\beta} = \frac{\dot{Z}_{M-1} - \dot{\alpha} L}{M - L - 1} \tag{3.2.33}$$

The total length of the channel does not change with time. Thus,

$$L\dot{\alpha} + (M - L)\dot{\beta} + (N - M)\dot{\gamma} = 0 \tag{3.2.34}$$

Eq. (3.2.34) can be reorganized and the node length in the Vapour Region is

$$\dot{\gamma} = \frac{-\dot{\alpha} L - \dot{\beta}(M - L)}{N - M} \tag{3.2.35}$$

The boundary positions of the coolant model are determined by Eq. (3.2.36)

$$\dot{Z}_i = \begin{cases} i\dot{\alpha}, 1 \le i \le L \\ \dot{\alpha} L + (i - L)\dot{\beta}, L < i \le M \\ \dot{\alpha} L + (M - L)\dot{\beta} + (i - M)\dot{\gamma}, M < i \le N \end{cases} \tag{3.2.36}$$

Subsequently, the dynamic behaviours of the coolant can be described by Eqs. (3.2.20), (3.2.21), (3.2.28), (3.2.32), (3.2.35) and (3.2.36).

The thermal-hydraulic model of the Canadian SCWR has been completed. The boundary conditions for the thermal-hydraulic model are the feed-water flow rate and the outlet pressure. The input for the fuel model is the heat source dependent on the reactor power. The input for the coolant model is the feed-water flow rate and the outlet pressure. The fuel rod model and the coolant model are interacted by the heat convection between the coolant and cladding. The feed-water temperature is kept constant at $350^{o}C$. The input-output relationship of the thermal-hydraulic model of the Canadian SCWR is described in Fig 3.4. There are three inputs: feed-water flow rate, reactor power and outlet pressure and four outputs: outlet temperature, outlet flow rate, average coolant density and average fuel rod temperature. The boundary positions are also recorded to understand the dynamics of the Canadian SCWR. The flowchart of the thermal-hydraulic model is shown in Fig 3.5.
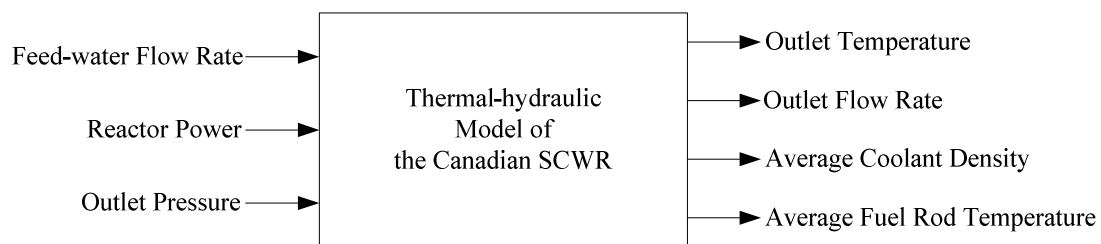
Fig 3.4 Input-output relationship of the thermal-hydraulic model of the Canadian SCWR
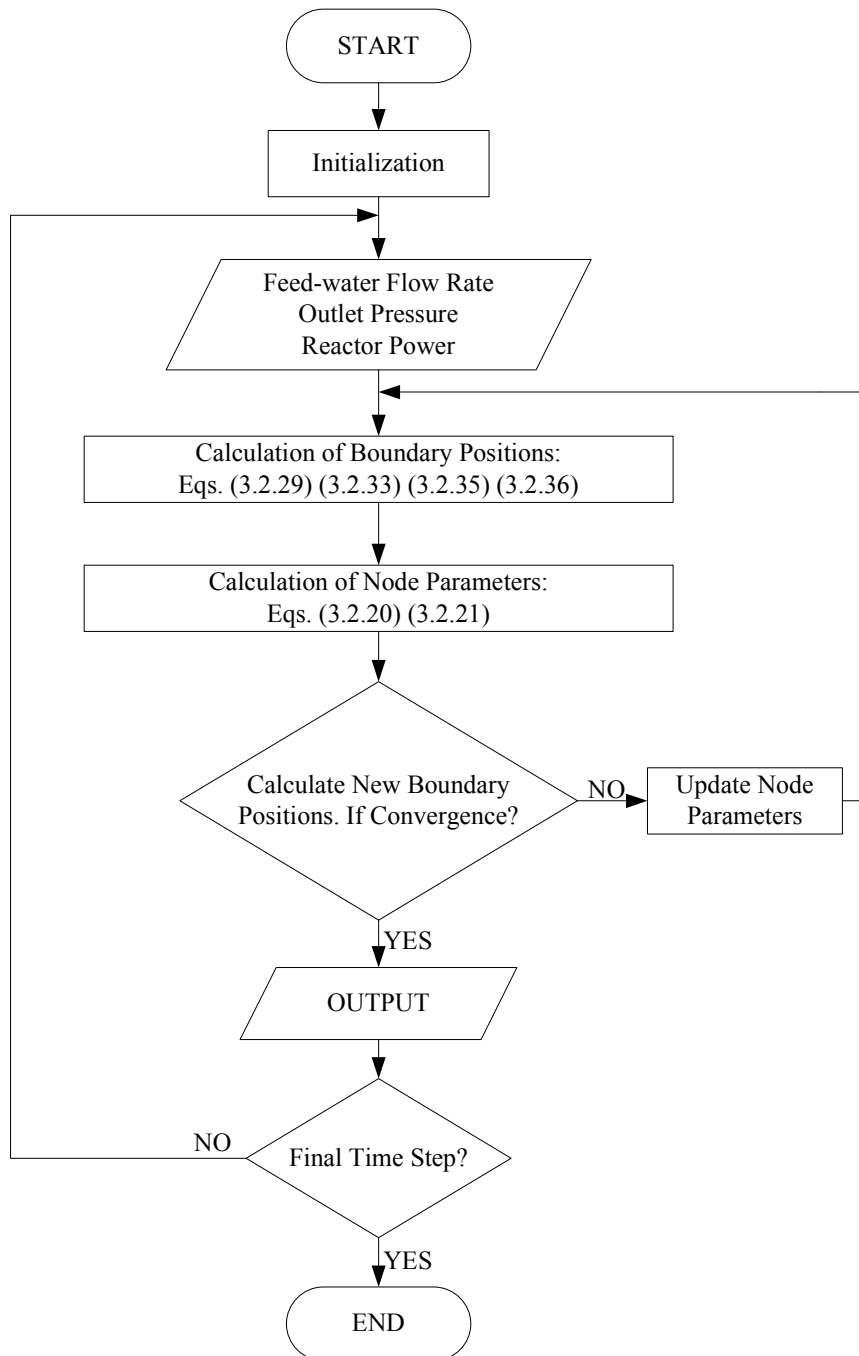
Fig 3.5 A flowchart of the thermal-hydraulic model of the Canadian SCWR

3.3 Thermal-hydraulic Model Validation

The CFD method has been adopted for thermal-hydraulic analysis under supercritical conditions. The commercial CFD software FLUENT 6.1 is adopted as the verification tool for the thermal-hydraulic model of the Canadian SCWR. The diagram for the CFD model of the Canadian SCWR is shown in Fig 3.6. For the symmetric reason, only one quarter of a single-pin model is selected. The model includes the fuel pin, gas gap, cladding and coolant. The reference pressure is 25MPa. The thermal physical properties of the supercritical water are given at the 25MPa. 2% disturbances are introduced to the inputs except the outlet pressure. The simulation results are shown in Figs 3.7 and 3.8.
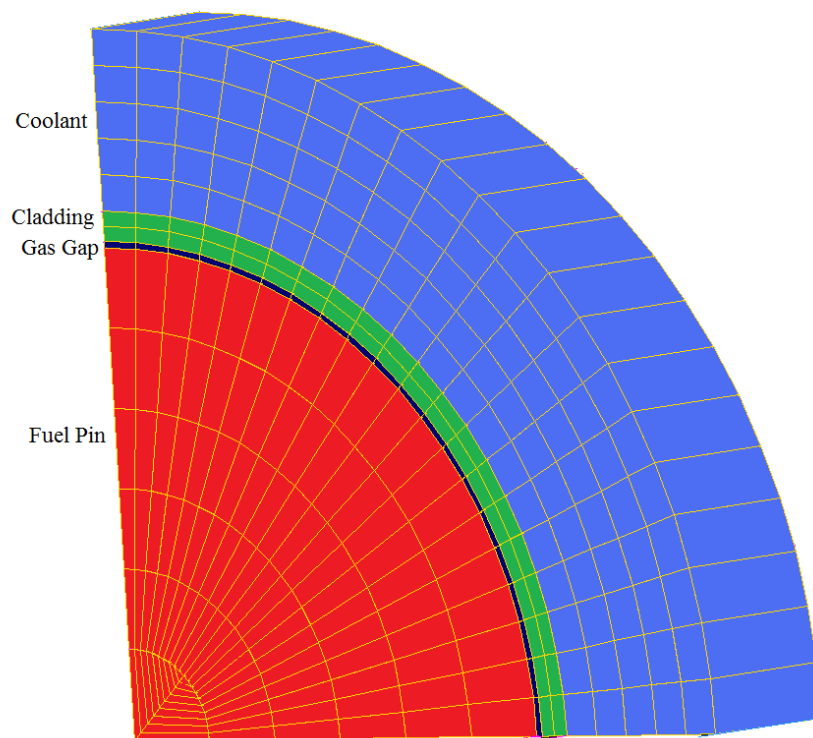
Fig 3.6 Diagram for CFD model of the fuel pin in a Canadian SCWR

The responses to a 2% step increase in the reactor power are shown in Fig 3.7. The outlet temperature increases with increasing reactor power and reaches 638.3^{o}C at 70.0s. The outlet

flow rate increases because of the decrease in the density and returns to its original value to balance the inlet flow rate. As shown in Fig 3.7, the responses of the thermal-hydraulic model agree well with those of the FLUENT model. The average difference of the outlet temperature is -0.3^{o}C and the standard difference is 0.3^{o}C.

The responses to a 2% step decrease in the feed-water flow rate are shown in Fig 3.8. The outlet temperature increases for the decrease in the inlet flow rate and settles at 638.3^{o}C. The outlet flow rate promptly follows the decrease in the inlet flow rate and stabilizes. As shown in Fig 3.8, the responses of the thermal-hydraulic model are consistent with those predicted by the FLUENT simulations. The average difference of the outlet temperature is 0.1^{o}C and the standard difference is 0.5^{o}C.

Through the analysis of the dynamic responses, the simulation results of the thermal-hydraulic model are consistent with those predicted by the FLUENT model. Therefore, the thermal-hydraulic model of the Canadian SCWR with moving boundary can capture the main dynamics of the Canadian SCWR and it is accurate enough for dynamic analysis.
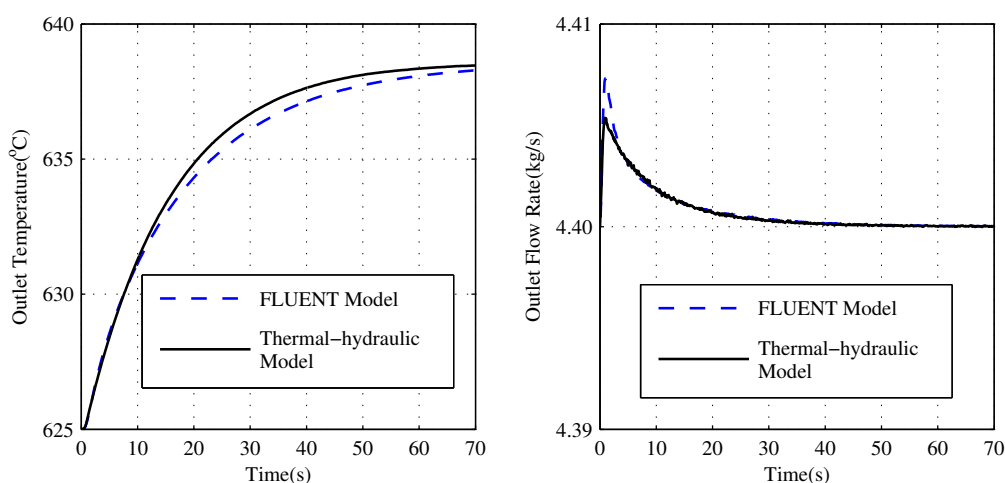
Fig 3.7 Responses to a 2% step increase in the reactor power
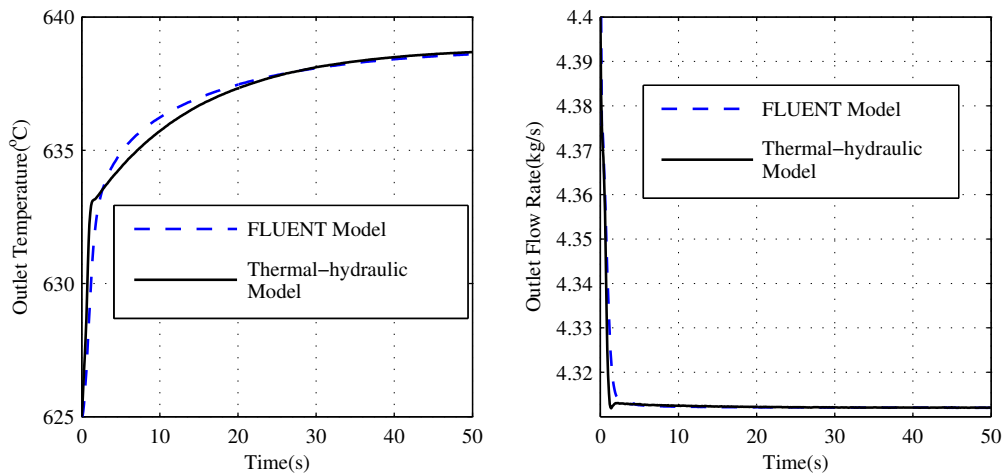
Fig 3.8 Responses to a 2% step decrease in the feed-water flow rate

3.4 Comparisons with the Fixed Boundary Method

To show the benefits of the moving boundary method, comparisons are made with the fixed boundary method. For the fixed boundary method with 29 nodes adopted, the temperature of 10th node of the coolant model is close to the pseudo-critical temperature at 25MPa. The temperature at the 3rd node of the fuel rod model is close to the pseudo-critical temperature at 25MPa when 21 nodes are adopted. The steady-state simulation does not converge. When there are 27 nodes, a step change in the feed-water flow rate from 4.4kg/s to 4.05kg/s is introduced and the simulation results are shown in Fig 3.9. The oscillations in the outlet temperature can be seen from 5 to 12 seconds in Fig 3.9(a). There are no such problems with the moving boundary method. This is due to the 9th node temperature of the coolant model close to the pseudo-critical temperature during this time interval as shown in Fig 3.9(b). When the moving boundary method is used, such problems are not observed. Thus, one benefit of the moving boundary method is the improvement on numerical stability.

(a) The outlet temperature   (b) 9th node temperature of the coolant model
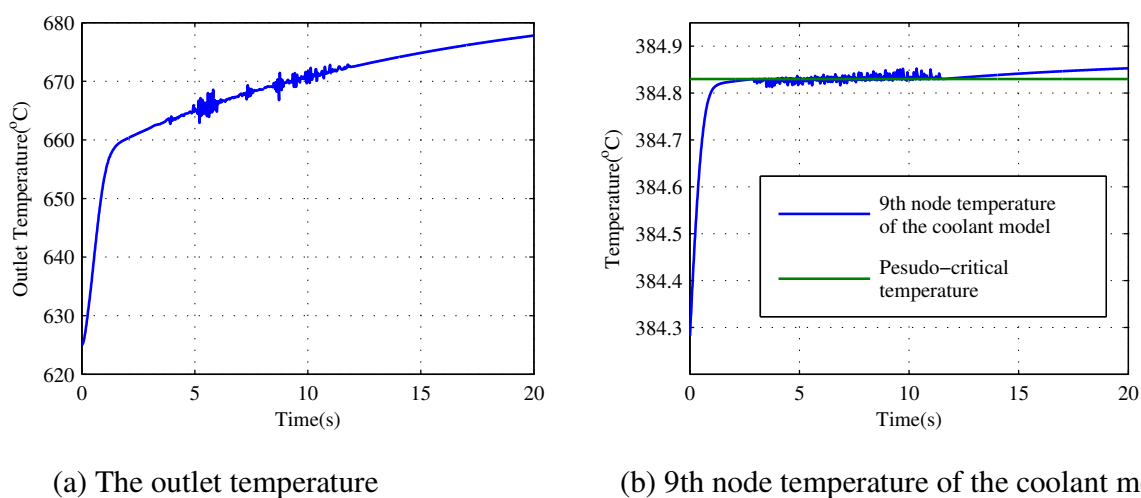
Fig 3.9 Responses to a step change in the feed-water flow rate using the fixed boundary method

Next, a step change in the feed-water flow rate from 4.4 kg/s to 4.2 kg/s and 10 nodes are adopted to investigate the sensitivity with respect to the change in the time step. With the fixed boundary method, when the time step is increased from 0.01 to 0.02 seconds, the calculation can proceed properly without any convergence issues. However, when the time step is further increased to 0.05 seconds, the computation fails to converge. On the other hand, using the moving boundary method, when the time step ranges from 0.01 to 1.0 second, the calculation can proceed properly. The time step of the moving boundary method can be over 20 times larger than that of the fixed boundary method, for the same level of simulation accuracy.

With the same time step, the moving boundary method is capable of dealing with severe disturbances. For example, the moving boundary method can adapt a step change in the feed-water flow rate from 4.4kg/s to 3.7kg/s while the fixed boundary method cannot.

Therefore, there are several advantages of using the moving boundary method for the Canadian SCWR modeling. Firstly, the oscillation and divergence of the numerical simulations can be potentially avoided. Secondly, the incremental time step in the computation can be increased. In

addition, the simulation is more robust against severe conditions, for example, large and fast disturbances.

3.5 Dynamic Model of the Canadian SCWR with Reactor Kinetics

For the reactor kinetics modeling, point reactor kinetics equations with six groups of delayed neutrons are adopted [116].

$$\frac{d}{dt} n(t) = \frac{\Delta \kappa_N - \varphi}{\Lambda} n(t) + \sum_{j=1}^{6} \lambda_j C_j(t) \tag{3.5.1}$$

$$\frac{d}{dt} C_j(t) = \frac{\varphi_j}{\Lambda} n(t) - \lambda_j C_j(t), j = 1...6 \tag{3.5.2}$$

where, n is the neutron flux, $\Delta \kappa_N$ is the net reactivity, φ is the total delayed neutron fraction, Λ is the average neutron life time, φ_j is the delayed neutron fraction of the jth group delayed neutron, λ_j is the delayed neutron precursor delay constant of the jth group delayed neutron, C_j is the precursor concentration of the jth group delayed neutron.

The shape of the axial power distribution is assumed to be a cosine function. In the radial direction, the power distribution is uniform. The reactivity is calculated from the reactivity feedbacks of the fuel rod temperature and the coolant density, as well as the reactivity changes induced by movements of control rods:

$$\Delta \kappa_N = \alpha_d \Delta \overline{d} + \alpha_T \Delta \overline{T} + \Delta \kappa_{CR} \tag{3.5.3}$$

where,

$\Delta \overline{d}$ is the difference between the current and initial average coolant density,

$\Delta \bar{T}$ is the difference between the current and initial average fuel temperature,

α_d is the coolant density reactivity coefficient,

α_T is the fuel temperature reactivity coefficient, and

$\Delta \kappa_{CR}$ is the reactivity change caused by the control rods.

The dynamic model of the Canadian SCWR has been completed. The dynamic model structure is shown in Fig 3.10. The three inputs are feed-water flow rate, control rod reactivity and outlet pressure and three outputs are outlet temperature, reactor power and outlet flow rate. The boundary positions are also recorded. A flowchart to calculate the dynamic model is shown in Fig 3.11.
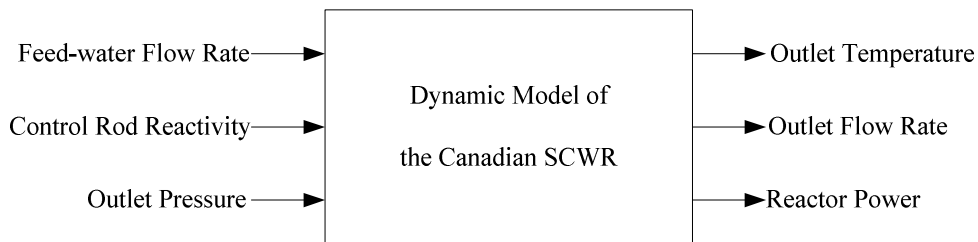
Fig 3.10 Dynamic model structure of the Canadian SCWR
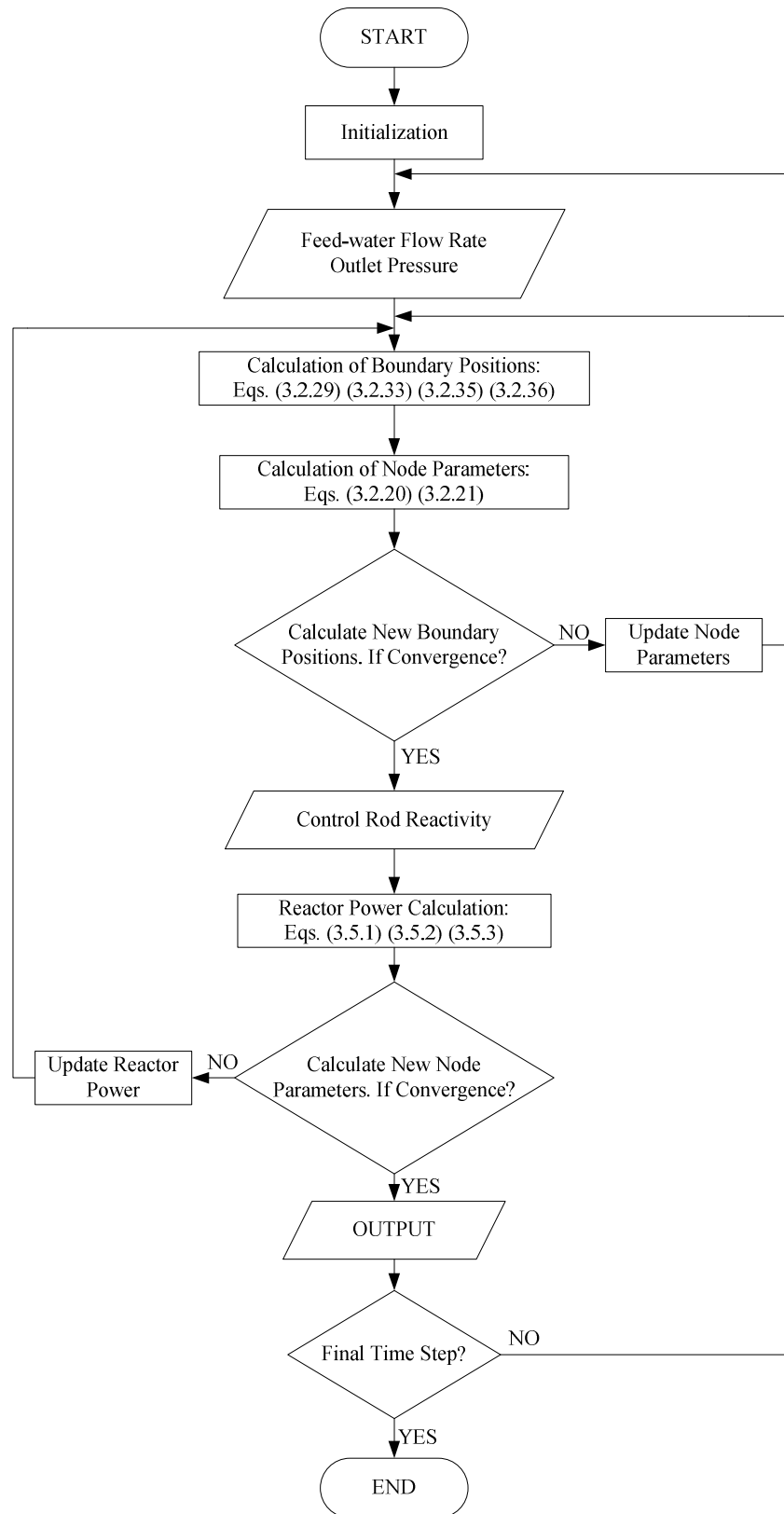
Fig 3.11 A flowchart of dynamic model construction of the Canadian SCWR

3.5.1 Steady-state Analysis

It has been tested that there are no major differences on the dynamic responses of the Canadian SCWR using 10 nodes and 20 nodes in the dynamic model. Therefore, 10 nodes are adopted: 2 for Liquid Region I, 2 for Liquid Region II and 6 for Vapour Region. The time step is chosen to be 0.1s. The results of the steady-state simulation are presented in Fig 3.12. As shown in Fig 3.12(a), the outlet temperature reaches 625.0°C, which agrees well with the design parameter. The maximum cladding temperature is 705.2°C below the limit temperature (850°C). As shown in Fig 3.12(b), the heat transfer coefficients in the Liquid Region II are higher than those in other regions. The boundary positions between regions are 0.876m and 2.067m, respectively.

(a) Temperature distributions   (b) Heat transfer coefficient distribution
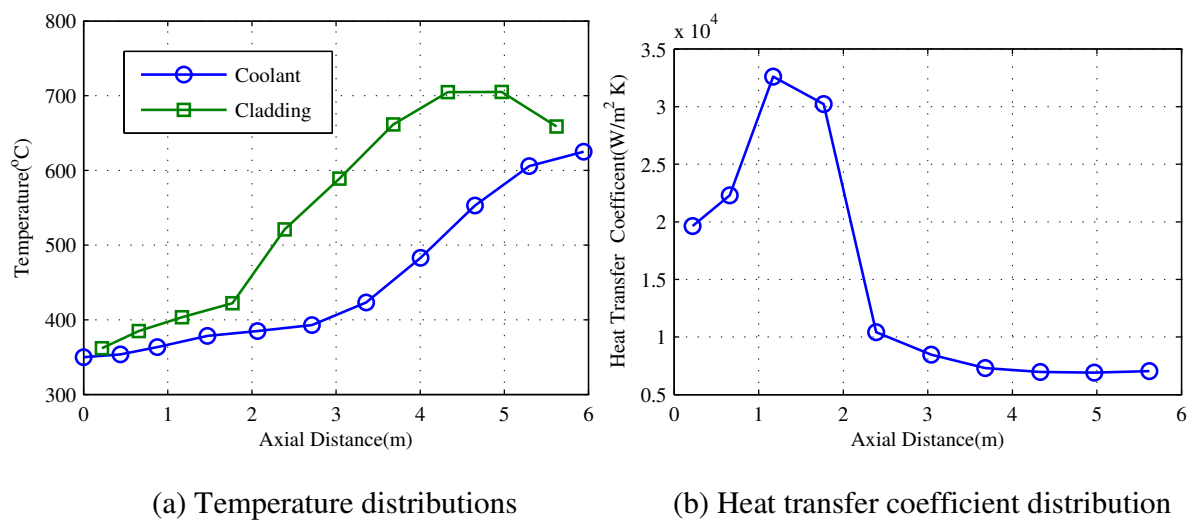
Fig 3.12 Results of the steady-state simulation

3.5.2 Transient Analysis

To investigate the dynamic behaviours of the Canadian SCWR to different disturbances, perturbations are introduced to the input variables. In each case, one input variable is perturbed from its designed value, while the others are kept unchanged at the designed values. All disturbances to inputs are introduced at 0 second.

3.5.2.1 A Step Decrease in the Feed-water Flow Rate

The responses to a step decrease from 4.4kg/s to 4.0kg/s in the feed-water flow rate are shown in Fig 3.13. The outlet flow rate decreases as the feed-water flow rate decreases. As a result, the outlet temperature increases. The reactor power decreases because of the negative reactivity caused by the decrease in the coolant density and increase in the fuel temperature. The outlet temperature then decreases as a result of the decrease in the reactor power. It finally stabilizes at 665.9°C. Because of the reactivity feedback, the reactor power decreases slightly and stabilizes at 96.2%FP. During this process, the boundary positions between the regions decrease with the increase in the coolant temperature. The position of the pseudo-critical point is decreased by 0.064m.

3.5.2.2 A Step Decrease in the Feed-water Temperature

The responses to a step decrease from 350°C to 345°C in the feed-water temperature are shown in Fig 3.14. The density of the coolant increases as the coolant temperature decreases and the outlet flow rate decreases accordingly. The outlet temperature increases because of the decrease in the outlet flow rate. The outlet flow rate increases promptly to balance the feed-water flow rate. At the same time, the outlet temperature decreases. The reactor power increases for the positive reactivity caused by the decrease in the fuel temperature and increase in the coolant density. As a result of the increase in the reactor power, the outlet temperature increases and finally stabilizes at 619.4°C. The reactor power slightly increases for the reactivity feedback and stabilizes at 100.9%FP. During this process, the boundary positions between regions decrease with the increase in the coolant temperature and decrease with the increase in the coolant temperature. The position of the pseudo-critical point is increased by 0.063m.

(a) The outlet temperature

(b) The normalized reactor power

(c) The outlet flow rate

(d) Boundary position between Liquid Regions I and II

(e) The position of the pseudo-critical point

Fig 3.13 Responses to a step decrease in the feed-water flow rate from 4.4kg/s to 4.0kg/s

(a) The outlet temperature
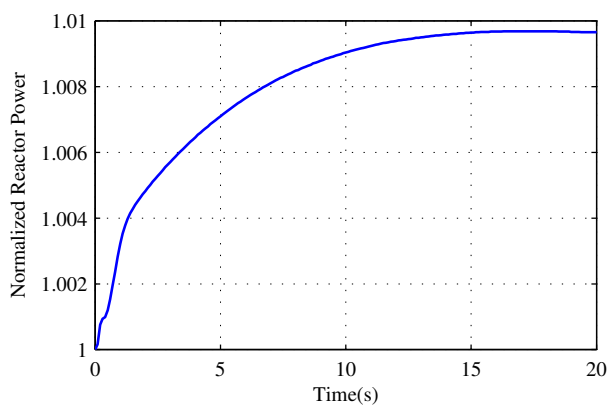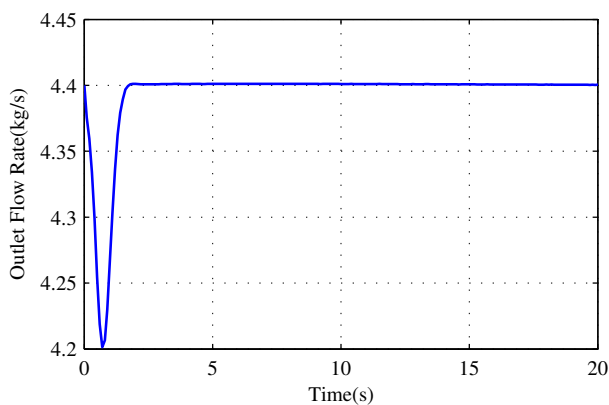
(b) The normalized reactor power

(c) The outlet flow rate

(d) Boundary position between Liquid Regions I and II
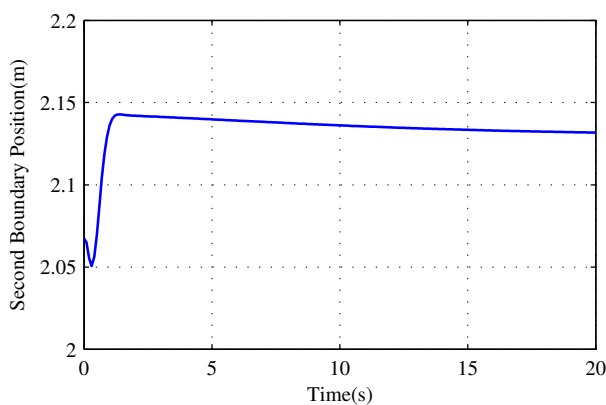
(e) The position of the pseudo-critical point

Fig 3.14 Responses to a step decrease in the feed-water temperature from 350°C to 345°C

3.5.2.3 A Step Decrease in the Outlet Pressure

The responses to a step decreases from 25MPa to 24.5MPa in the outlet pressure are shown in Fig 3.15. The step decrease in the outlet pressure results in a sudden increase in the outlet flow rate. The outlet temperature decreases as the outlet flow rate increases. Subsequently, the outlet flow rate decreases to balance the feed-water flow rate. Consequently, the outlet temperature increases accordingly. The reactor power changes slightly for a small change in the coolant density and the fuel temperature. The outlet temperature and the reactor power stabilize at $624.5^{\circ}C$ and 100.05%FP, respectively. The position of the pseuo-critical point is decreased by 0.020m.

3.5.2.4 A Step Increase in the Control Rod Reactivity

The responses to a step increase from 0 to 0.05$ in the control rod reactivity are shown Fig 3.16. The reactor power increases in response to the added positive reactivity. The outlet temperature increases as the reactor power increases and the coolant density decreases accordingly. The decrease of the coolant density results in the increase of the outlet flow rate. The reactor power then decreases because of the negative reactivity introduced by the increase in the fuel temperature and decrease in the coolant density. It is finally stabilized at 104.6%FP. The outlet temperature decreases as the reactor power decreases and stabilizes at $656.2^{\circ}C$. During this process, the boundaries between regions decrease with the increase in the coolant temperature and decrease with the increase in the coolant temperature. The position of the pseudo-critical point is decreased by 0.050m.
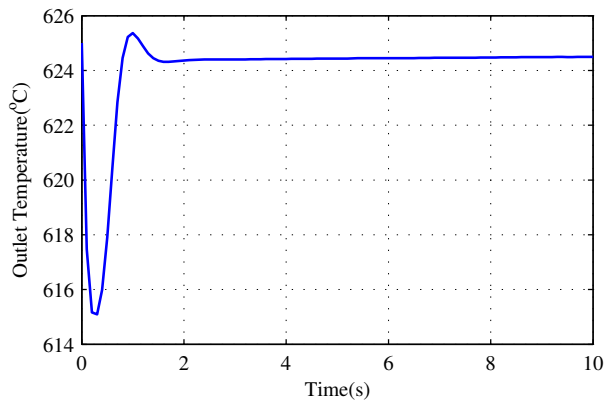
(a) The outlet temperature
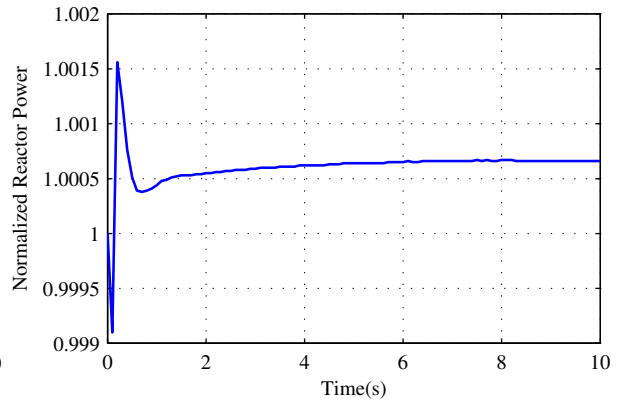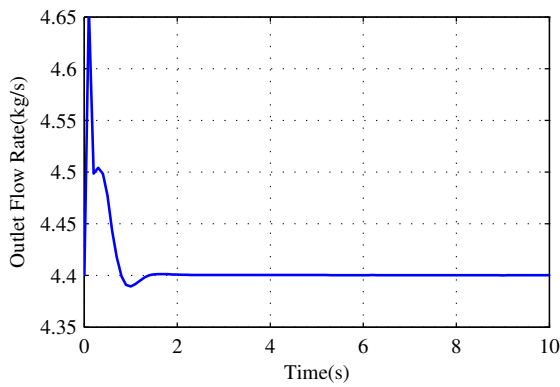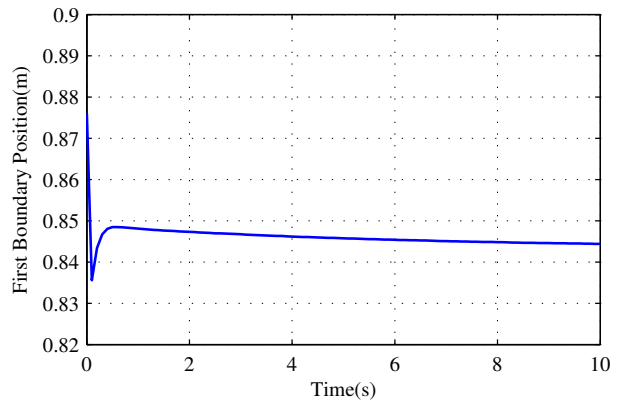
(b) The normalized reactor power

(c) The outlet flow rate

(d) Boundary position between Liquid Regions I and II
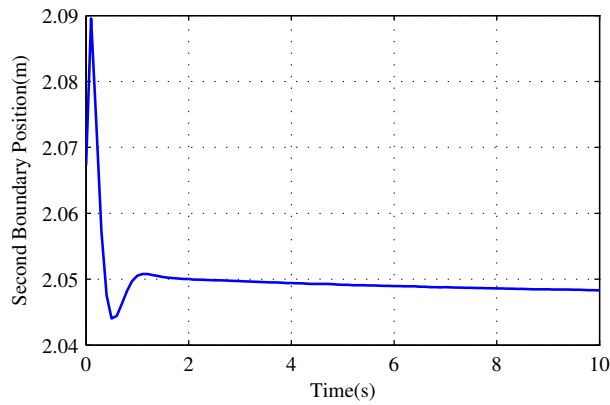
(e) The position of the pseudo-critical point

Fig 3.15 Responses to a step decrease in the outlet pressure from 25MPa to 24.5MPa
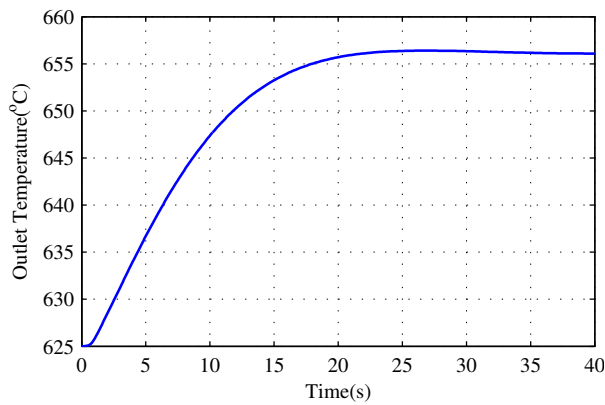
(a) The outlet temperature
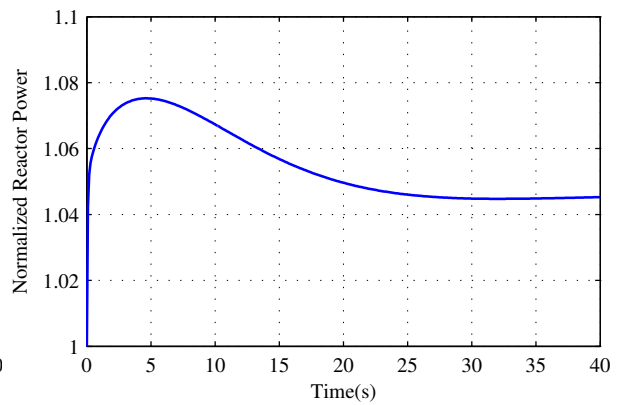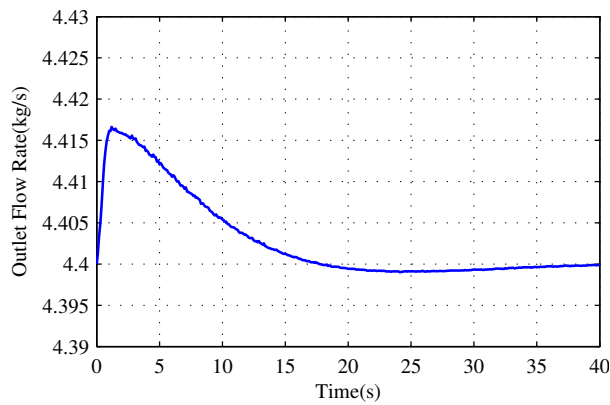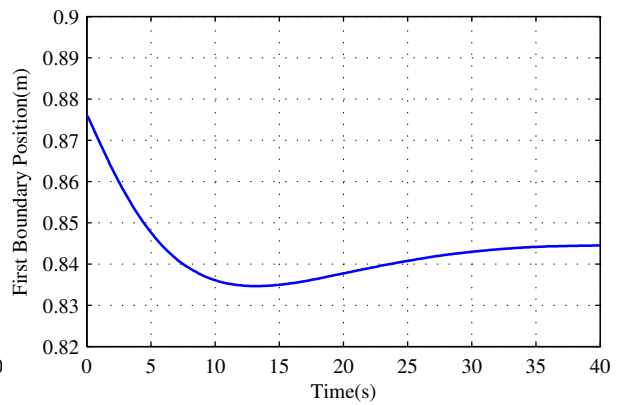
(b) The normalized reactor power

(c) The outlet flow rate

(d) Boundary position between Liquid Regions I and II
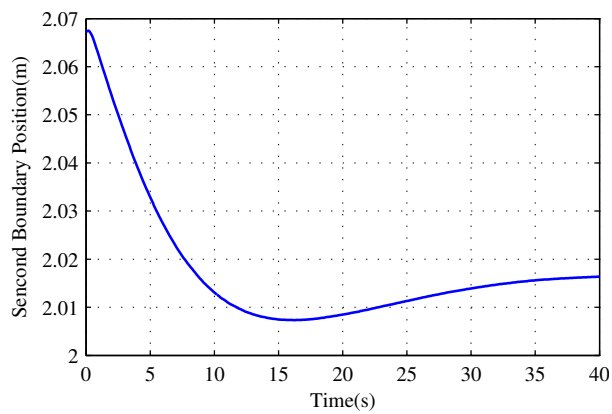
(e) The position of the pseudo-critical point

Fig 3.16 Responses to a step increase in the control rod reactivity from 0 to 0.05$

3.5.3 Comparisons between Dynamics of Canadian SCWR and ACR

A dynamic model of an ACR-700 is developed using CATHENA [20]. CATHENA is a system code developed by AECL, primarily for the analysis of postulated accident conditions in CANDU reactors. If the feed-water temperature of the ACR-700 in the model is $280^{o}C$ as designed, the void fraction at the outlet will be around 2.0% and the coolant is two-phase fluid. The coolant in the Canadian SCWR is single phase. For the convenience of comparison, the feed-water temperature of the ACR-700 is decreased by $10^{o}C$ to ensure that the coolant at the outlet is also in a single phase state. 2% step perturbations are introduced to the input variables. The simulation results are shown in Figs 3.17, 3.18 and 3.19.
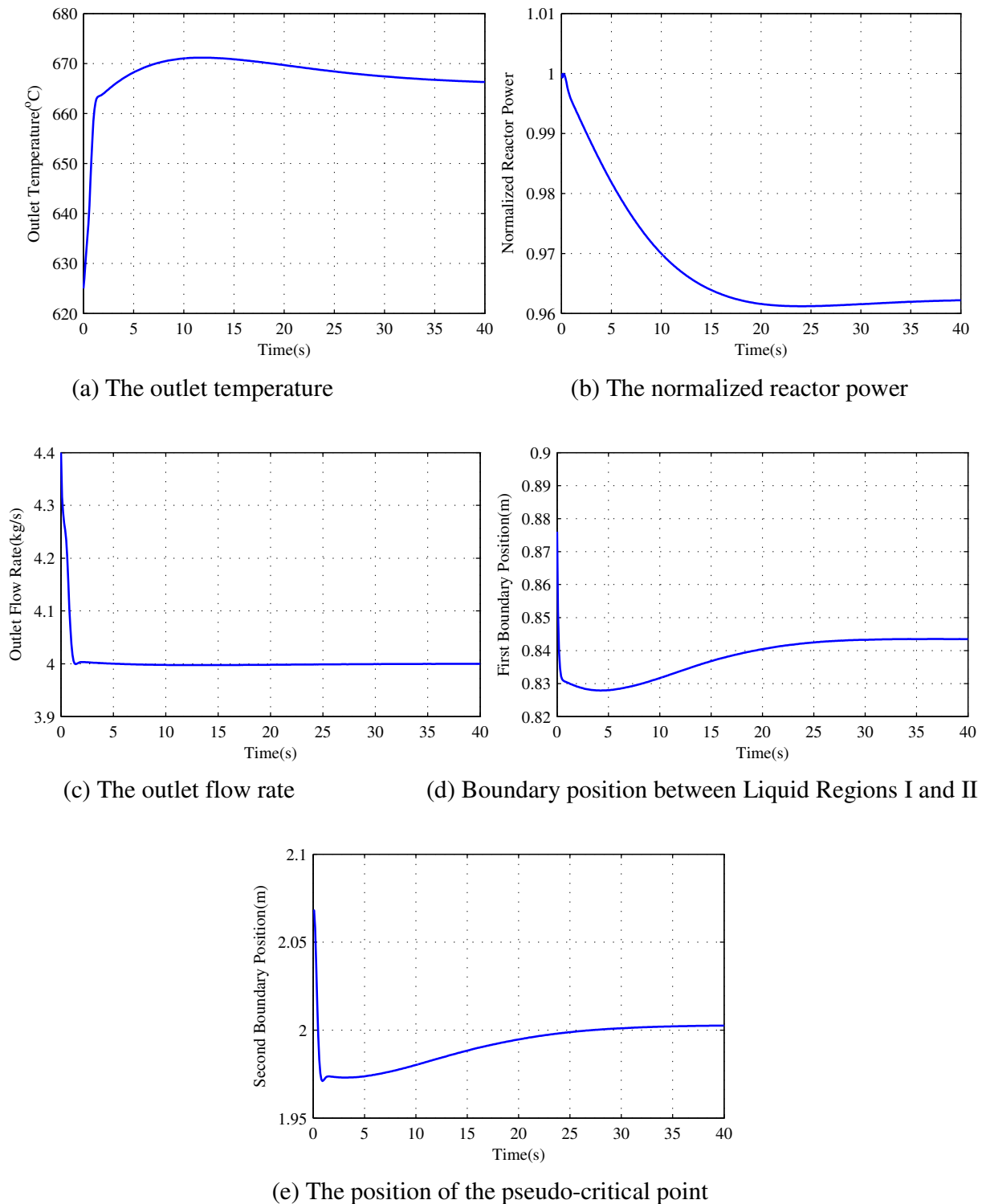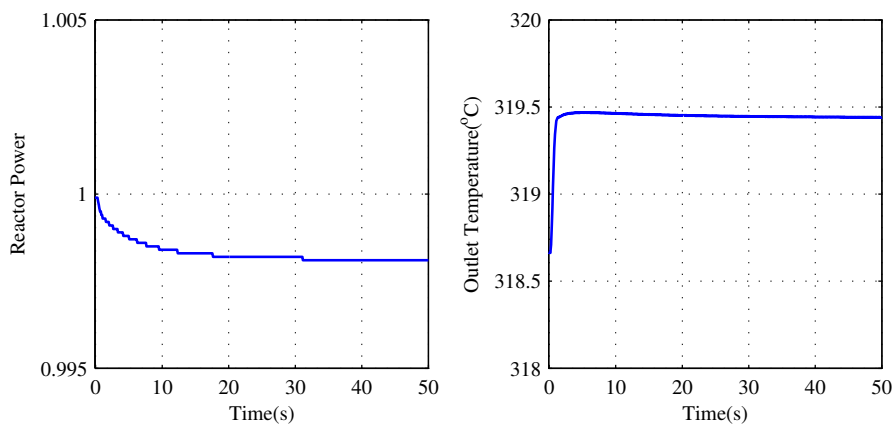

Fig 3.17 Responses to a 2% step decease in the feed-water flow rate
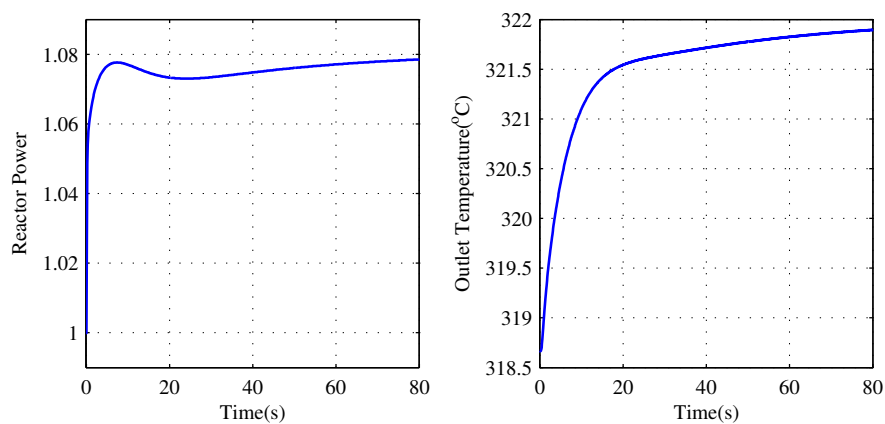
Fig 3.18 Responses to a step increase in the control rod reactivity
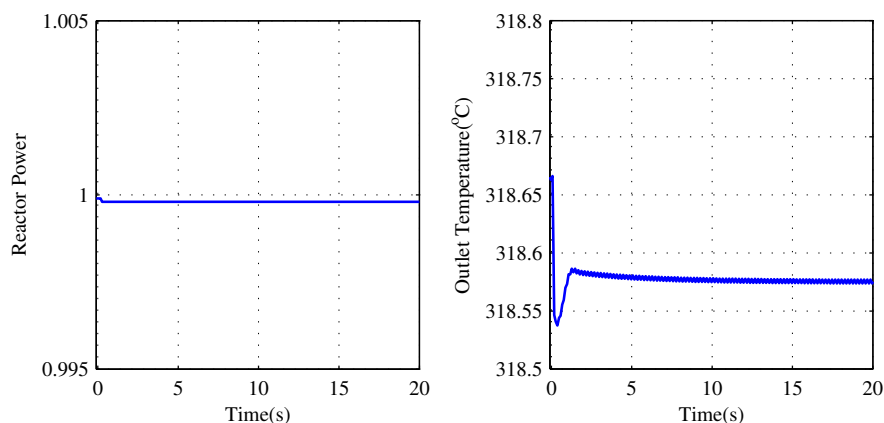
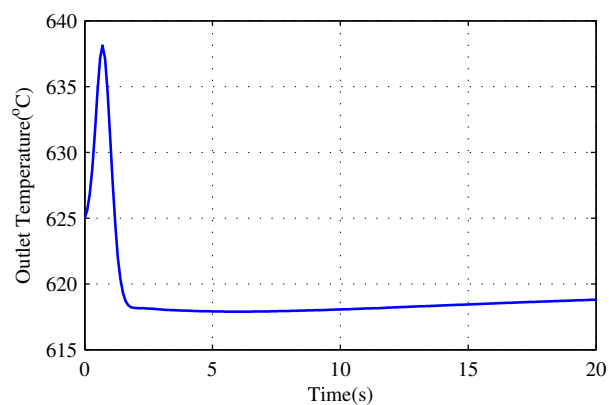Fig 3.19 Responses to a 2% step decrease in the outlet pressure

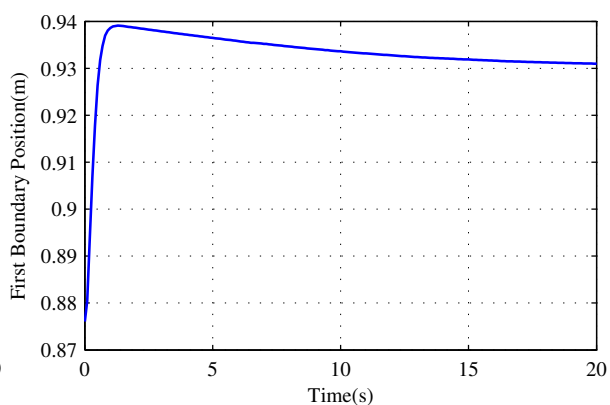The responses to a step decrease in the feed-water flow rate from 26kg/s to 25.48kg/s are shown in Fig 3.17. The outlet temperature increases as the feed-water flow rate decreases and stabilizes at 319.5°C. The reactor power decreases as the negative reactivity feedback induced by the decrease in the coolant density and the increase in the fuel temperature. The settling time of the reactor power and the outlet temperature is 32.3 seconds and 1.2 seconds, respectively. The reactor power is decreased by about 0.2% and the outlet temperature is increased by about 0.9°C.

The responses to a step increase in the control rod reactivity by 0.005\$ are shown in Fig 3.18. The reactor power increases for the addition of positive reactivity. The outlet temperature increases as the reactor power increases and stabilizes at 321.8°C. The settling time of the reactor power and the outlet temperature is 57.4 seconds and 60.3 seconds, respectively. The reactor power and the outlet temperature is increased by 7.9% and 3.2°C, respectively.

The responses to a step decrease in the outlet pressure from 12MPa to 11.76kMPa are shown in Fig 3.19. The reactor power is almost unaffected by the disturbance in the outlet pressure. At 0.3 seconds, the outlet temperature reaches its lowest value. However, the final outlet temperature is decreased by less than 0.1°C.

The main differences on the dynamics of the outlet temperature between the Canadian SCWR and the ACR-700 are summarized in Tables 3.3 and 3.4. The settling time to the feed-water flow rate and the outlet pressure disturbances of the ACR-700 is less than that of the Canadian SCWR. The settling time to the control rod reactivity disturbance of the ACR-700 is greater than that of the Canadian SCWR. The response magnitude in the outlet temperature of the ACR-700 is lower than that of the Canadian SCWR for its lower power-to-flow ratio. The response magnitude to the control rod reactivity disturbance in the reactor power of ACR-700 is higher than that of the Canadian SCWR for its lower reactivity feedback. These differences demonstrate that the dynamics of the Canadian SCWR are different from those of ACR. The outlet temperature is significantly affected by the feed-water flow rate and control rod reactivity. The response sensitivity and cross-coupling make the Canadian SCWR more challenging to control.

Table 3.3 Comparisons on the dynamics of the outlet temperature between the Canadian SCWR and ACR-700

Input Disturbances	Canadian SCWR		ACR-700	
	Settling Time	Response Magnitude	Settling Time	Response Magnitude
Feed-water Flow Rate	35.5s	8.5°C	1.2s	0.9°C
Control Rod Reactivity	19.5s	31.2°C	60.3s	3.2°C
Outlet Pressure	0.3s*	0.5°C	0.3s*	0.1°C

Note: * it is the time to reach the lowest temperature.

Table 3.4 Comparisons on the dynamics of the reactor power between the Canadian SCWR and ACR-700

Input Disturbances	Canadian SCWR		ACR-700	
	Settling Time	Response Magnitude	Settling Time	Response Magnitude
Feed-water Flow Rate	16.2s	0.8%	0.4s	0.2%
Control Rod Reactivity	28.0s	4.6%	57.4s	8.0%
Outlet Pressure	0.4s	0.1%	0.3s	0.0%

3.6 Linear Dynamic Model Development for the Canadian SCWR

A nonlinear dynamic model of the Canadian SCWR has been developed in Sections 3.2 and 3.5. However, this model is complicated and cannot be used directly for control system design and analysis. To facilitate the control system design, a set of linear dynamic models are preferred. For the complexity of the model, it is difficult to derive the linear dynamic models directly from the developed nonlinear model. A system identification technique is used to construct a set of linear dynamic models. The process of linear dynamic model development involves two steps: (1) input and output data set generation; and (2) construction of linear models in the form of transfer functions. The system identification toolbox of MATLAB/SIMULINK^{TM} is used in the model building process.

As shown in Fig 3.10, there are three inputs and three outputs in the Canadian SCWR dynamic model structure. But considering that the average coolant density change and the average fuel temperature change can induce the reactivity feedback in the reactor kinetics model, which is considered as internal feedback, the linear dynamic models for the Canadian SCWR dynamic model cannot be derived directly. As mentioned in Section 3.1, the Canadian SCWR dynamic model consists of a thermal-hydraulic model and a reactor kinetics model. The linear dynamic model development should be carried out independently for these two models. The relationship between these two models can be shown in Fig 3.20. The normalized reactor power, the output of the reactor kinetics model, is an input to the thermal-hydraulic model.
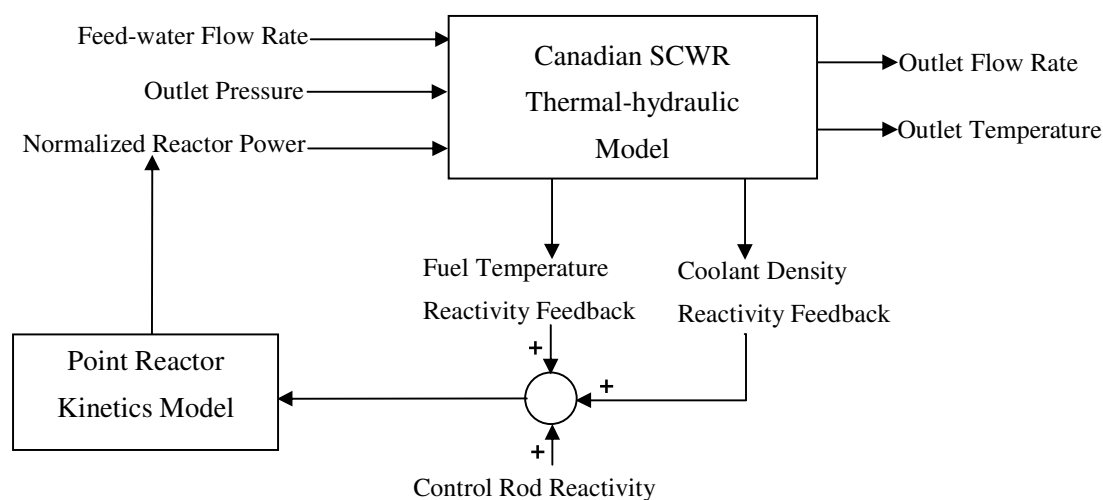
Fig 3.20 Linear dynamic model development structure

There are three inputs and four outputs in the thermal-hydraulic model of the Canadian SCWR as shown in Fig 3.4. Low amplitude perturbing signals are introduced at the thermal-hydraulic model of the Canadian SCWR inputs around the design point. The Canadian SCWR thermal-hydraulic model is used to generate the corresponding output signals. Each time only one input variable is perturbed. The perturbations consist of step changes from the initial value to the final value, as summarized in Table 3.5. The simulation time is 100 seconds in total.

Table 3.5 Input perturbations for system identification

Input Variables	0s	10s	20s	30s	40s
Feed-water Flow Rate (kg/s)	4.488	4.444	4.312	4.356	4.4
Normalized Reactor Power	102%	101%	98%	99%	100%
Outlet Pressure (MPa)	25.5	25.25	24.5	24.75	25

With each input perturbation, four output responses are recorded. In total, there are 12 sets of input and output data. Least-square based system identification techniques are used to fit these data sets to generate the corresponding linear dynamic models. Based on this analysis, the transfer functions can be obtained and presented in Table 3.6.

Table 3.6 Transfer functions of the linear dynamic models

Input / Output	Feed-water Flow Rate	Outlet Pressure	Normalized Reactor Power
Outlet Temperature	$\dfrac{-2624.00(s+4.97E-5)}{(s+33.74)(s+0.70)(s+2.10E-5)}$	$\dfrac{23.24(s+0.04+0.10i)(s+0.04-0.10i)}{(s+2.24)(s+4.95E-3)}$	$\dfrac{-58.17(s-1.79)}{(s+2.32)(s+0.07)}$
Outlet Flow Rate	$\dfrac{1.86}{s+1.86}$	$\dfrac{-0.50(s-0.10)(s+0.10)(s+3.81-10.21i)(s+3.81+10.21i)}{(s+21.28)(s+2.86-4.79i)(s+2.86+4.79i)(s+5.24E-3)}$	$\dfrac{2.09(s-0.02-0.07i)(s-0.02+0.07i)}{(s+8.18)(s+0.03)(s+0.01)}$
Average Coolant Density Change	$\dfrac{61.61(s+0.11)(s+1.52E-8)}{(s+2.56)(s+0.10)(s+8.86E-4)}$	$\dfrac{35.68(s+9.30E-6)}{(s+5.94)(s+6.35E-3)}$	$\dfrac{-108.20(s+8.02E-6)}{(s+7.39)(s+0.10)(s+9.75E-4)}$
Average Fuel Temperature Change	$\dfrac{-61.61(s+5.81E-8)}{(s+7.67)(s+0.07)(s+3.91E-5)}$	$\dfrac{0.54(s-1.20E-7)}{(s+0.14)(s+8.04E-3)}$	$\dfrac{84.10(s+2.18E-8)}{(s+0.06)(s+4.70E-4)}$

Even though the transfer functions are derived based on the data generated by the Canadian SCWR thermal-hydraulic model, the simulations are carried out by perturbing one input at a time and during transfer function development process, outputs are considered independently, which represents a SISO system. To ensure that the linear dynamic models can truly represent the dynamic behaviours of the Canadian SCWR around the design point, it is important to validate them using different sets of inputs to test the generality of the developed linear dynamic models.

The input perturbations for validation can be described as follows: a step increase in the feed-water flow rate from 4.4 kg/s to 4.532 kg/s at 0 second; a step increase in the outlet pressure from 25MPa to 25.75MPa at 10 seconds; a step increase in the normalized reactor power from 100%FP to 103%FP at 20 seconds; a step decrease in the feed-water flow rate from 4.532kg/s to 4.356kg/s at 30 seconds; a step decrease in the outlet pressure from 25.75MPa to 24.75MPa at 40 seconds; and a step decrease in the normalized reactor power from 103%FP to 99%FP at 50 seconds. All perturbations in input variables are set to zero at 60 seconds. The period of the simulation is 100 seconds.

The simulation results based on the Canadian SCWR thermal-hydraulic model and the linear dynamic model are shown in Fig 3.21. The differences between responses are shown in Table 3.7. Even though the disturbances are larger than those used for the linear dynamic model construction, the linear dynamic models agree well with the Canadian SCWR thermal-hydraulic model around the design point.

(a) The outlet temperature

(b) The outlet flow rate

(c) Average fuel temperature change

(d) Average coolant density change
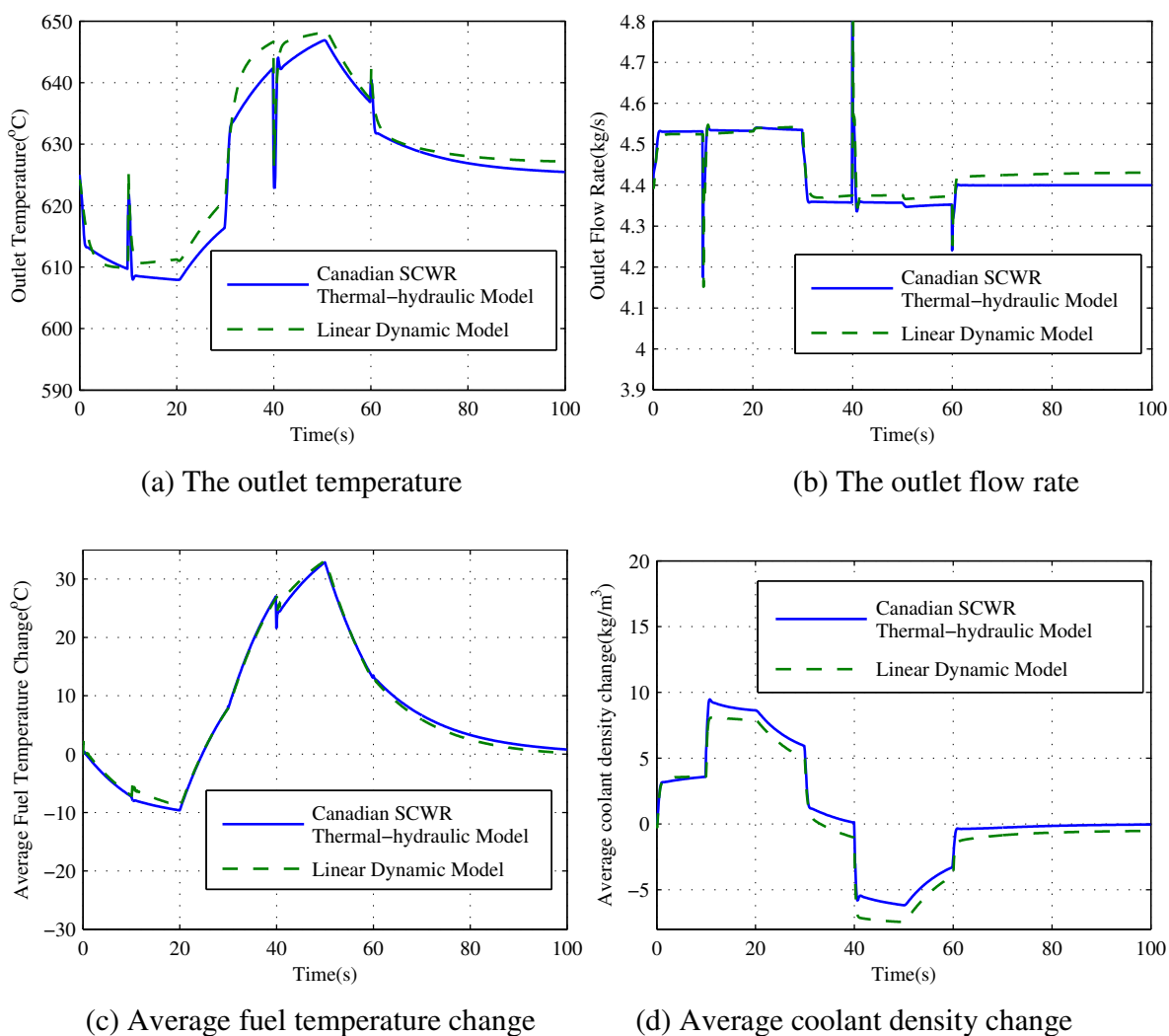
Fig 3.21 Linear dynamic model verification for the Canadian SCWR thermal-hydraulic model

Table 3.7 Differences between response of the linear dynamic models and the Canadian SCWR

thermal-hydraulic model

Outputs	Outlet Temperature (^{o}C)	Outlet Flow Rate (kg/s)	Average Fuel Temperature Change (^{o}C)	Average Coolant Density Change (kg/m^3)
Average Difference	0.83	1.48E-2	4.18E-2	7.21E-1
Standard Difference	1.75	3.11E-2	7.25E-1	8.31E-1

The transfer function of the point reactor kinetics model can be easily derived following the

method in [116], which gives

$$\frac{\Delta N(s)}{\Delta \mathrm{K}_N(s)} = \frac{1}{\Lambda s} \frac{1}{1 + \dfrac{1}{\Lambda} \sum_{j=1}^{6} \dfrac{\varphi_j}{s + \lambda_j}}.$$

where, $\Delta N(s)$ and $\Delta \mathrm{K}_N(s)$ are the Laplace transforms of $n(t)$ and κ_N in Eq (3.5.1), respectively.

Thus, the transfer function is

$$\frac{\Delta N(s)}{\Delta \mathrm{K}_N(s)} = \frac{3030.30(s+3.79)(s+1.39)(s+0.32)(s+0.12)(s+0.03)(s+6.00E-4)}{s(s+18.22)(s+3.45)(s+0.17)(s+0.08)(s+5.40E-3)}.$$

Even though the linear dynamic models for the thermal-hydraulic of the Canadian SCWR have

been verified separately, it is still necessary to verify whether the linear dynamic models

developed can indeed represent the dynamic behaviours of the Canadian SCWR. The input

perturbations used for validation are: a step increase in the feed-water flow rate from 4.4 kg/s to

4.532 kg/s at 0 second; a step increase in the outlet pressure from 25MPa to 25.75MPa at 10

seconds; a step increase in the control rod reactivity from 0 to 0.0001k at 20 seconds; a step

decrease in the feed-water flow rate from 4.532 kg/s to 4.356 kg/s at 30 seconds; a step decrease

in the outlet pressure from 25.75MPa to 24.75MPa at 40 seconds; a step decrease in the control

rod reactivity from 0.0001k to -0.0002k at 50 seconds. At 60 seconds, all the input variables return to their original values. The period of the simulation is 100 seconds.

The responses of the Canadian SCWR dynamic model and the linear dynamic model are shown in Fig 3.22. The differences in output responses are summarized in Table 3.8. As can be seen, the linear dynamic models agree well with the Canadian SCWR dynamic model around the design point.
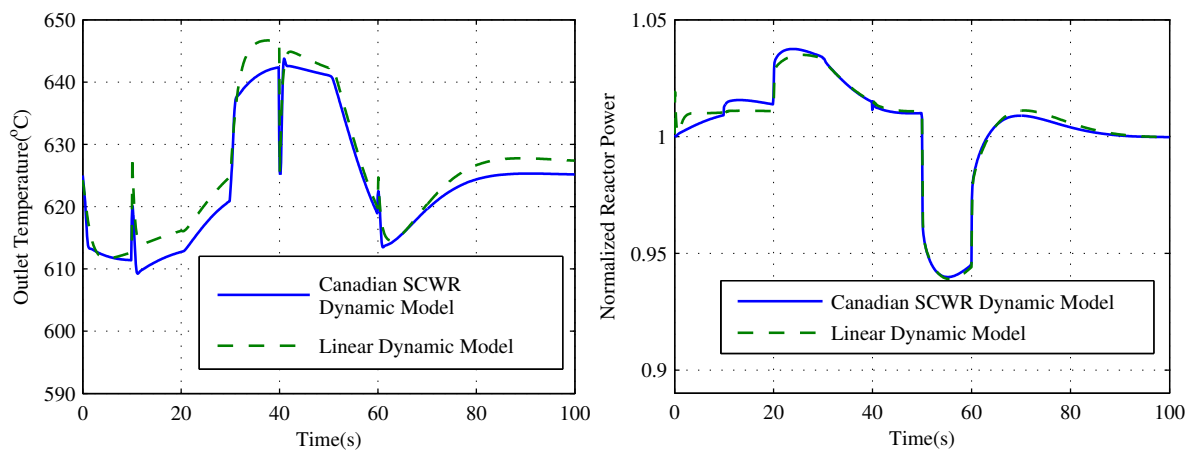
(a) The outlet temperature

(b) The normalized reactor power
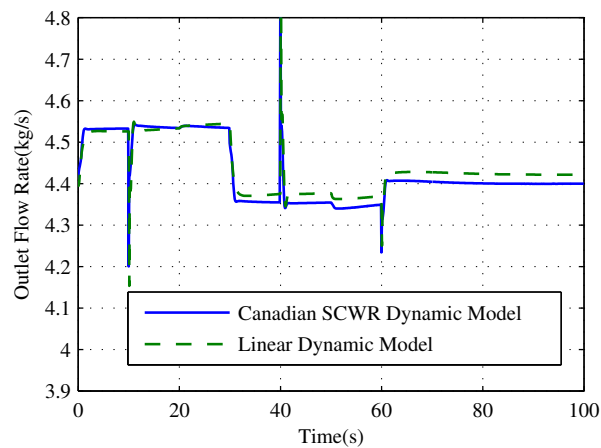
(c) The outlet flow rate

Fig 3.22 Linear dynamic model validation for the Canadian SCWR dynamic model

Table 3.8 Differences between responses of the linear dynamic models and the Canadian SCWR

dynamic model

Outputs	Outlet Temperature (^{o}C)	Outlet Flow Rate (kg/s)	Normalized Reactor Power
Average Difference	1.04	1.42E-2	6.43E-4
Standard Difference	1.68	3.02E-2	1.90E-3

The linear dynamic models shown in Table 3.6 are developed around the design point and they are valid only around the design point. The further question is whether the linear dynamic models constructed at one operating point are still valid for another one. For the operation of the Canadian SCWR, the feed-water flow rate is required to be proportional to the reactor power to keep the temperature of the reactor outlet at a constant. At different operating points, the position of the pseudo-critical point is unchanged. As long as the operating point is not far away from the design point, the nonlinear characteristics of the Canadian SCWR are relatively uniform. To illustrate this, operating conditions at four different reactor powers, ±10%FP and ±5%FP away from the design point are considered. At these operating points, the feed-water flow rate is adjusted according to the reactor power while the outlet pressure is kept at 25MPa.

The same dynamic inputs for the validation of the linear dynamic models at 100%FP are applied to the four operating points. The standard differences are shown in Table 3.9. It can be seen that using the dynamic models at the operating points other than the design point lead to larger standard differences. However, the standard errors at the operating points within ±10%FP variation around the design point are not too much higher than those at the design point. Thus, it is possible to apply the linear dynamic models, constructed at the design point, within 90%~110%FP operating range.

Table 3.9 Response errors of the linear dynamic models for the Canadian SCWR dynamic model

at different power levels

Outputs	90%FP	95%FP	100%FP	105%FP	110%FP
Outlet Temperature (^{o}C)	1.97	1.72	1.68	1.69	1.82
Outlet Flow Rate (kg/s)	3.01E-2	3.01E-2	3.02E-2	3.03E-2	3.06E-2
Normalized Reactor Power	2.67E-3	2.20E-3	1.90E-3	1.98E-3	2.51E-3

4   CONSTRUCTION OF A LINEAR DYNAMIC MODEL

4.1   Introduction

A linear dynamic model is preferred for dynamic analysis and control system design. The dynamic models for SCFR and SCLWR-H have been developed for plant transient analysis [83, 84]. However, no transfer functions or state space representations have been derived for dynamic system analysis and plant controller design. The control strategies for a BWR have been directly adopted for the control of SCFR and SCLWR-H, and sequential loop closing and trial and error methods have been used to tune the controller parameters. The strong cross-coupling among inputs and outputs has not been explicitly considered in the design of the existing works. For example, the reactor power is designed to satisfy requirements on the overshoot and response time. But if the reactor power follows a setpoint change, the variation of 'steam' temperature can be significant. Although the feed-water control system has been reconsidered for control performance improvement [85], the design is still based on a trial and error approach due to a lack of dynamic models. Many proven techniques for control system design and analysis cannot be utilized. Thus, it is highly desirable to develop a comprehensive set of dynamic models, so that a systematic approach can be applied to analyze the system dynamics and to deal with cross-coupling and nonlinearities in the system.

There are generally two approaches to construct a dynamic model: white-box first principle modeling and black-box approach based on system identification. A linear dynamic model can be directly obtained through system identification techniques, once the proper data sets of the process are available. For the case of the Canadian SCWR plant system, there are many internal feedbacks, which make the application of system identification techniques complicate and

challenging. Furthermore, the linear dynamic model obtained at one operating point is only valid in a small region around this point. The system identification needs to be carried out again to obtain a linear dynamic model at another operating point. Although the white-box first principle modeling is time-consuming and needs detailed knowledge of the process, it will supply the insight information of the process. A linear dynamic model can be constructed by linearizing the nonlinear dynamic model around any chosen operating point. The linear dynamic models at other operating points can be easily obtained by changing the values of corresponding parameters according to their operating conditions. Therefore, first principle modeling is more suitable and adopted to construct the dynamic model of the Canadian SCWR plant system.

The thermal-hydraulic model of the Canadian SCWR reactor core has been developed using the moving boundary method in Chapter 3. Since the thermal parameters of the Canadian SCWR are implicitly coupled with one another, it is difficult and complex to linearize such a model directly using traditional methods. In the current work, an empirical correlation is introduced to evaluate the coolant flow rate to decouple it from the reactor power and the pressure. Due to a large number of nodes chosen in the thermal-hydraulic model, the order of linear model turns out to be very high. Consequently, the thermal-hydraulic model is further simplified to two regions by means of the moving boundary. For other system components in the plant, lower order models, which capture the main dynamics, are used in the design and analysis process.

This rest of the chapter is organized as follows. A simplified dynamic model of the Canadian SCWR plant system and its linearization are presented in Section 4.2. The thermal-hydraulic model of the reactor core based on the moving boundary technique is briefly discussed. The linear dynamic model is obtained and described in Section 4.3. The open-loop system responses

are obtained by perturbing the system inputs in Section 4.4. Validation of the linearized models is carried out in both time domain and frequency domain.

4.2   Development of a Simplified Dynamic Model

An illustrative diagram of the Canadian SCWR plant system in this study is shown in Fig 4.1. The feed-water to the reactor core is pumped through the inlet plenum by the feed-water pump. The reactivity is controlled by the movement of the control rods. The supercritical coolant flows through the fuel channels. The coolant absorbs the heat generated in the fuel rods without going through a boiling process. The main 'steam' is then used to drive the turbine from the outlet feeder and outlet header. The turbine control valve is used to regulate the main 'steam' flow rate. The boundary conditions are set at the feed-water pump and the turbine.
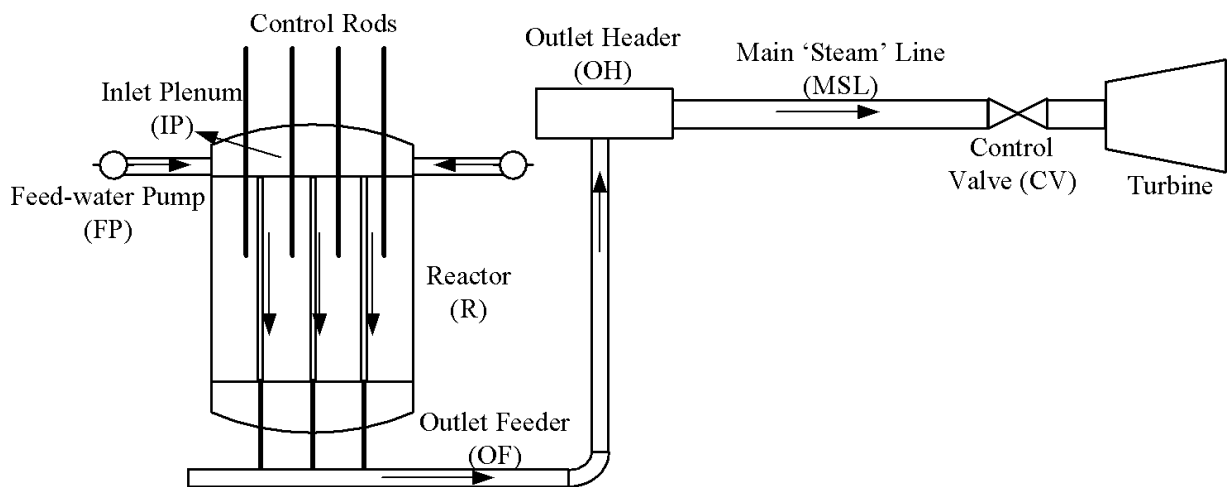
Fig 4.1 An illustrative diagram of a Canadian SCWR plant system

A simplified low order dynamic model with clear physical meanings is preferred for dynamic analysis and control system design. This low order dynamic model captures the dynamic input-output behaviours of the system. Meanwhile, it is easier to use engineering judgement during its

verification because the variables of this model have clear physical meanings [96, 117]. The lumped parameter method is considered in the modeling process, which is based on the fundamental conservation equations of mass, energy and momentum as follows:

Mass balance

$$\dot{m} = M_{in} - M_{out}$$

Energy balance

$$\frac{d(mh)}{dt} = M_{in}h_{in} - M_{out}h_{out} + Q_{in} - W$$

Pressure balance

$$P_{out} = P_{in} - \xi \frac{M_{in}^2}{\rho_{in}}$$

where, m is the total mass in the system, M is the mass flow rate, Q is the heat absorption rate of the system, W is the work, ξ is the pressure loss coefficient.

The major assumption for the modeling of the Canadian SCWR is that the Canadian SCWR plant system is nodalized to many nodes and each node has uniform properties such as pressure, temperature and flow rate, which is the requirement of the lumped parameter modeling.

The system model is linearized at the 100%FP operating point. The linearization is carried out by the perturbation theory [118]. In the following sub-sections, the dynamic model of each system component as shown in Fig 4.1 is developed.

4.2.1 Feed-water Pump

The main function of the variable speed feed-water pump is to push the feed-water through the reactor core. The feed-water flow rate can be regulated by the speed of the pump. The

relationship between the feed-water flow rate and the reactor core pressure is shown Fig 4.2, which is chosen to be the same as that in a previous study [84].
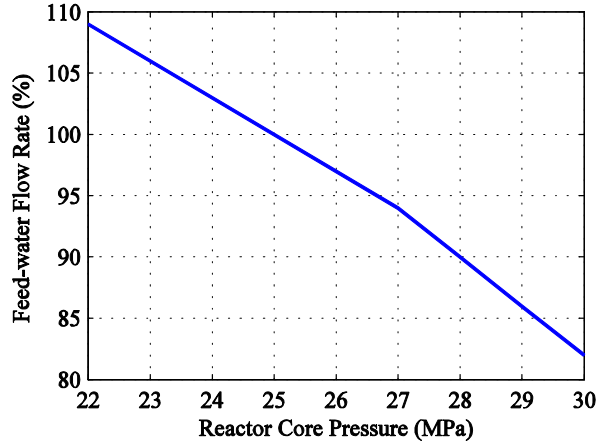
Fig 4.2 Feed-water flow rate at different reactor core pressure

The feed-water flow rate is perturbed and linearized at the 100%FP operating point and the feed-water flow rate is also at 100%. The following relationship between the mass flow rate and the pressure can be obtained:

$$\delta M_{FP,P} = -3\% M_{FP} \delta P_R \tag{4.2.1}$$

where, $\delta M_{FP,P}$ is the change in the mass flow rate of the feed-water pump caused by reactor pressure change, M_{FP} is the mass flow rate of the feed-water pump, and P_R is the reactor core pressure.

4.2.2 Inlet Plenum

The inlet plenum is assumed to be a well-mixed volume having neither pressure drop nor energy exchange with the environment. Applying mass and energy conservation equations, the dynamic relationships for the inlet plenum can be described by

$$V_{IP} \frac{d\rho_{IP}}{dt} = M_{FP,N} - M_{IP} \tag{4.2.2}$$

$$V_{IP} \frac{d(\rho_{IP}T_{IP})}{dt} = M_{FP,N}T_{FP} - M_{IP}T_{IP} \tag{4.2.3}$$

where, $M_{FP,N} = M_{FP} + M_{FP,P}$, V_{IP} is the volume of the inlet plenum, ρ_{IP} is the water density in the inlet plenum, M_{IP} is the mass flow rate of the inlet plenum, T_{IP} is the water temperature of the inlet plenum, and T_{FP} is the feed-water temperature. In the development of Eq. (4.2.3), the specific heat is assumed to be constant.

Substituting Eq. (4.2.2) into Eq. (4.2.3), one can obtain

$$\frac{dT_{IP}}{dt} = \frac{M_{FP,N}(T_{FP} - T_{IP})}{\rho_{IP}V_{IP}} \tag{4.2.4}$$

The density of the supercritical water depends on its temperature and pressure, and the derivative of the supercritical water density can be presented as

$$\frac{d\rho}{dt} = \left(\frac{\partial\rho}{\partial T}\right)_P \frac{dT}{dt} + \left(\frac{\partial\rho}{\partial P}\right)_T \frac{dP}{dt} \tag{4.2.5}$$

Since the pressure-flow process is much faster than the enthalpy-temperature process, the pressure dynamics in Eq. (4.2.5) is neglected [119]. Based on this assumption, the mass flow rate is obtained from the Eqs. (4.2.2) and (4.2.5)

$$M_{IP} = M_{FP,N} - V_{IP} \frac{d\rho_{IP}}{dT_{IP}} \frac{dT_{IP}}{dt} \tag{4.2.6}$$

Perturbing and linearizing Eqs. (4.2.4) and (4.2.6), the following dynamic relationships are obtained

$$\frac{d\delta T_{IP}}{dt} = \frac{M_{FP,N}(\delta T_{FP} - \delta T_{IP})}{\rho_{IP}V_{IP}} \qquad (4.2.7)$$

$$\delta M_{IP} = \delta M_{FP,N} - V_{IP}\frac{d\rho_{IP}}{dT_{IP}}\frac{d\delta T_{IP}}{dt} \qquad (4.2.8)$$

Thus, Eqs. (4.2.7) and (4.2.8) can be used to describe the linear dynamics of the inlet plenum.

4.2.3 Reactor Core

A simplified dynamic model of the reactor core is developed for dynamic system studies. The coolant model shown in Fig 4.3 has been divided into *Liquid Region* and *Vapour Region* by the pseudo-critical point. The fuel rod model has the same node distribution as that in the coolant model. A more detailed treatment of the model development can be found in [120].

4.2.3.1 Coolant Model
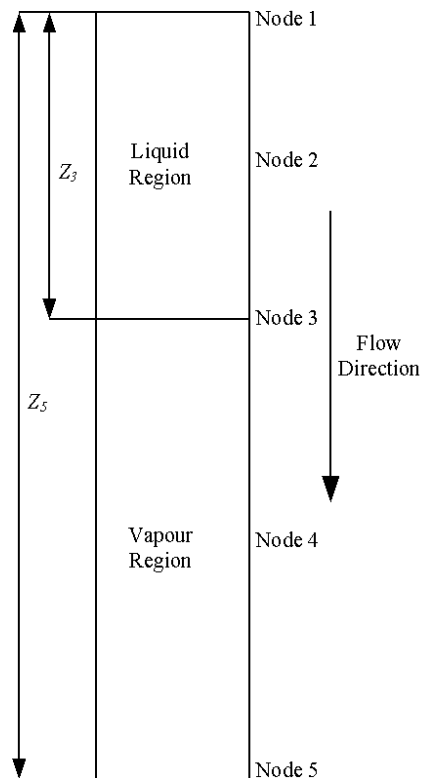
Fig 4.3 Two regions coolant model

The coolant flow is assumed to be 1D. The momentum equation is not considered in the model development process [120]. An extra model is added to calculate the pressure drop along the fuel channel. Eqs. (4.2.9) and (4.2.10) can be obtained by applying Leibnitz theorem to the mass and energy conservation equations (Eqs. (3.2.7) and (3.2.8)) for the *Liquid Region*:

$$\frac{d(\rho_2 Z_3)}{dt} - \rho_3 \frac{dZ_3}{dt} + (D_3 - D_1) = 0 \tag{4.2.9}$$

$$\frac{d(\rho_2 h_2 Z_3)}{dt} - \rho_3 h_3 \frac{dZ_3}{dt} + D_3 h_3 - D_1 h_1 = Q_2''' Z_3 \tag{4.2.10}$$

It is assumed that the coolant flow rate and the specific enthalpy at node 2 are

$$D_2 = \frac{D_1 + D_3}{2} \tag{4.2.11}$$

$$h_2 = \frac{h_1 + h_3}{2} \tag{4.2.12}$$

The boundary position between the *Liquid Region* and the *Vapour Region* is obtained from Eqs. (4.2.9), (4.2.10), (4.2.11) and (4.2.12) as

$$\frac{dZ_3}{dt} = \frac{(D_1 + D_3)(h_1 - h_3)/2 + Q_2''' Z_3 - \rho_2 Z_3 (\dot{h}_1 + \dot{h}_3)}{\rho_3 (h_1 - h_3)/2} \tag{4.2.13}$$

The specific enthalpy at node 3, that is, the pseudo-critical point, only depends on its pressure. Since the pressure effect on the dynamics is not considered herein, the terms related to perturbation and derivative of h_3 are omitted in the subsequent equations.

Taking into account of the transport delay in the *Liquid Region*, the feed-water specific enthalpy at node 1 and the flow rate at node 3 can be empirically approximated as [96]

$$\frac{dh_1}{dt} = \frac{h_{IP} - h_1}{\tau} \tag{4.2.14}$$

$$\frac{dD_3}{dt} = \frac{D_1 - D_3}{\tau} \tag{4.2.15}$$

where, $\tau = \dfrac{Z_3 \rho_2}{2D_1}$.

Eqs. (4.2.13), (4.2.14) and (4.2.15) are perturbed and linearized as

$$\frac{d\delta Z_3}{dt} = \frac{(\delta D_1 + \delta D_3)(h_1 - h_3)/2 + (D_1 + D_3)\delta h_1/2 + Q_2'''\delta Z_3 + Z_3 \delta Q_2''' - \rho_2 Z_3 \dot{\delta h_1}}{\rho_3(h_1 - h_3)/2} \tag{4.2.16}$$

$$\frac{d\delta h_1}{dt} = \frac{\delta h_{IP} - \delta h_1}{\tau} \tag{4.2.17}$$

$$\frac{d\delta D_3}{dt} = \frac{\delta D_1 - \delta D_3}{\tau} \tag{4.2.18}$$

The following equations are obtained by applying Leibnitz theorem to the mass and energy conservation (Eqs. (3.2.7) and (3.2.8)) for the *Vapour Region*:

$$\frac{d(\rho_4(Z_5 - Z_3))}{dt} + \rho_3 \frac{dZ_3}{dt} + D_5 - D_3 = 0 \tag{4.2.19}$$

$$\frac{d(\rho_4 h_4(Z_5 - Z_3))}{dt} + \rho_3 h_3 \frac{dZ_3}{dt} + (D_5 h_5 - D_3 h_3) = Q_4'''(Z_5 - Z_3) \tag{4.2.20}$$

It is assumed that the flow rate and the specific enthalpy at node 4 are described by

$$D_4 = D_5 = D_3 \tag{4.2.21}$$

$$h_4 = \frac{h_3 + h_5}{2} \tag{4.2.22}$$

The specific enthalpy at the reactor outlet is obtained from Eqs. (4.2.19), (4.2.20), (4.2.21) and (4.2.22) as

$$\frac{dh_5}{dt} = \frac{\rho_3(h_5 - h_3)\dot{Z}_3 / 2 + (h_3 - h_5)D_3 + Q_4'''(Z_5 - Z_3)}{\rho_4(Z_5 - Z_3) / 2} \tag{4.2.23}$$

Eq. (4.2.23) is further perturbed and linearized as

$$\frac{d\delta h_5}{dt} = \frac{\rho_3(h_5 - h_3)\delta\dot{Z}_3 / 2 + (h_3 - h_5)\delta D_3 - \delta h_5 D_3 - Q_4'''\delta Z_3 + (Z_5 - Z_3)\delta Q_4'''}{\rho_4(Z_5 - Z_3) / 2} \tag{4.2.24}$$

One extra model is used to calculate the pressure drop along the fuel channel. Since the gravity term is negligible as compared to the friction term, the pressure drop can be obtained as

$$P_{IP} - P_R = \sum_{i=2,4}(f\frac{Z_{i+1} - Z_{i-1}}{D_e} + k_g)\frac{D_i^2}{2\rho_i} \tag{4.2.25}$$

where, k_g is the friction coefficient at the spacer grid.

Eq. (4.2.25) is then perturbed and linearized as

$$\delta P_{IP} - \delta P_R = \sum_{i=2,4}(f\frac{Z_{i+1} - Z_{i-1}}{D_e} + k_g)\frac{D_i\delta D_i}{\rho_i} + \sum_{i=2,4}f\frac{\delta Z_{i+1} - \delta Z_{i-1}}{D_e}\frac{D_i^2}{2\rho_i} \tag{4.2.26}$$

Therefore, the linear dynamic model for the coolant can be obtained from Eqs. (4.2.16), (4.2.17), (4.2.18), (4.2.23) and (4.2.26).

4.2.3.2 Fuel Rod Model

A lumped dynamic model for fuel rod developed by BNL is adopted [114]. The average fuel pin temperature can be described by Eq. (3.2.5). The relationship among the average fuel pin temperature, bulk temperature and cladding temperature is described as [114] and shown in Eq. (3.2.6).

Substituting Eq. (3.2.6) into Eq. (3.2.5), perturbing and linearizing the average fuel pin temperature equation result in:

$$\delta \dot{\overline{T}}_{pin_i} = -\frac{2}{R_3} \frac{\delta q''_{w_i}}{(\rho c_P(\overline{T}_{pin_i}))_f} + \left(\frac{R_1}{R_2}\right)^2 \frac{\delta q'''_i}{(\rho c_P(\overline{T}_{pin_i}))_f} - \frac{\dot{Z}_{i+1} - \dot{Z}_{i-1}}{Z_{i+1} - Z_{i-1}} \delta \overline{T}_{pin_i} - \overline{T}_{pin_i} \frac{\delta \dot{Z}_{i+1} - \delta \dot{Z}_{i-1}}{Z_{i+1} - Z_{i-1}}$$
$$+ \frac{\left(c_P\left(\frac{\overline{T}_{pin_i} + \overline{T}_{pin_{i+1}}}{2}\right)\right)_f}{(c_P(\overline{T}_{pin_i}))_f} \frac{\overline{T}_{pin_i} + \overline{T}_{pin_{i+1}}}{2} \frac{\delta \dot{Z}_i}{Z_{i+1} - Z_{i-1}} - \frac{\left(c_P\left(\frac{\overline{T}_{pin_{i-1}} + \overline{T}_{pin_i}}{2}\right)\right)_f}{(c_P(\overline{T}_{pin_i}))_f} \frac{\overline{T}_{pin_{i-1}} + \overline{T}_{pin_i}}{2} \frac{\delta \dot{Z}_{i-1}}{Z_{i+1} - Z_{i-1}} \qquad (4.2.27)$$

where, $q''_w = H(T_c - T_b)$.

Perturbing and linearizing Eq. (4.2.27), and combining it with $q''_w = H(T_c - T_b)$ result in:

$$\frac{\delta q''_w}{H} - \frac{q''_w}{H} \frac{\delta H}{H} + \frac{(C_{gm} + F_{pr})(R_3 - R_2)}{k_c} \delta q''_w = \delta \overline{T}_{pin} - \delta T_b \qquad (4.2.28)$$

The following equation is obtained by rearranging Eq. (4.2.28)

$$\delta q''_w = \frac{\delta \overline{T}_{pin} - \delta T_b + \frac{q''_w}{H} \frac{\delta H}{H}}{\frac{1}{H} + \frac{(C_{gm} + F_{pr})(R_3 - R_2)}{k_c}} \qquad (4.2.29)$$

δH is obtained by perturbing and linearizing the Yamagata correlation equation [112]:

$$\delta H = 0.85 \frac{\delta D}{D} H \qquad (4.2.30)$$

4.2.3.3 Reactor Kinetics Model

The power distribution in the reactor core along the fuel channel is assumed to be a cosine function. A point kinetics model with six groups of delayed neutrons is used to model the neutron flux in the reactor core and the equations are shown in Eqs (3.5.1) and (3.5.2). Since the neutron flux is proportional to the reactor power, $n(t)$ is converted to the normalized reactor power in this study.

Eqs. (3.5.1) and (3.5.2) are perturbed and linearized as

$$\delta \dot{n}(t) = \frac{\Delta \kappa_N - \varphi}{\Lambda} \delta n(t) - \frac{\delta \Delta \kappa_N}{\Lambda} n(t) + \sum_{j=1}^{6} \lambda_j \delta C_j(t) \qquad (4.2.31)$$

$$\delta \dot{C}_j(t) = \frac{\varphi_j}{\Lambda} \delta n(t) - \lambda_j \delta C_j(t), \, j = 1...6 \qquad (4.2.32)$$

The reactivity feedback considered in this model is due only to changes in the coolant density and the fuel temperature. Thus, the total reactivity can be calculated as shown in Eq. (3.5.3).

Eq. (3.5.3) is perturbed and linearized as

$$\delta \Delta \kappa_N = \alpha_d \delta \Delta \overline{d} + \alpha_T \delta \Delta \overline{T} + \delta \Delta \kappa_{CR} \qquad (4.2.33)$$

The reactivity coefficients are assumed to be constant.

Since the average coolant density change and average fuel temperature change cannot be accurately obtained from the simplified thermal-hydraulic model shown in Section 4.2.3.1 and 4.2.3.2 due to their distributed and nonlinear nature, the transfer functions between them and the feed-water flow rate as well as the reactor power are derived based on the detailed thermal-hydraulic model through system identification techniques as explained in Section 3.6. The results are presented in Section 4.3.

4.2.4 Outlet Feeder

The coolant is heated up in the reactor core and flows into the outlet header through the outlet feeder. It is assumed that there is no energy exchange with the environment in the outlet feeder.

Considering the dynamic response, the temperature of the outlet feeder is described as

$$\dot{T}_{OF} = \frac{T_5 - T_{OF}}{\tau} \qquad (4.2.34)$$

where, $\tau = \dfrac{V_{OF}\rho_{OF}}{M_5}$.

The pressure of the outlet header is described as

$$P_{OF} = P_R - \xi \frac{M_5^2}{\rho_5} \qquad (4.2.35)$$

Eqs. (4.2.34) and (4.2.35) are perturbed and linearized as

$$\delta \dot{T}_{OF} = \frac{\delta T_5 - \delta T_{OF}}{\tau} \qquad (4.2.36)$$

$$\delta P_{OF} = \delta P_R - 2\xi \frac{M_5 \delta M_5}{\rho_5} \qquad (4.2.37)$$

The subscript 5 in Eqs. (4.2.36) and (4.2.37) corresponds to the reactor outlet (node 5) as shown in Fig 4.3.

4.2.5 Outlet Header

The outlet header is assumed to be a well-mixed volume having no pressure drop and no energy exchange with the environment. There are 336 outlet feeders connecting to the outlet header. Applying the mass and energy conservation equations, one can obtain

$$V_{OH} \frac{d\rho_{OH}}{dt} = 336 M_{OF} - M_{OH} \qquad (4.2.38)$$

$$V_{OH} \frac{d(\rho_{OH}T_{OH})}{dt} = 336 M_{OF} T_{OF} - M_{OH} T_{OH} \qquad (4.2.39)$$

Substitute Eq. (4.2.38) into Eq. (4.2.39) and the following equations can be obtained

$$\frac{dT_{OH}}{dt} = \frac{336 M_{OF}(T_{OF} - T_{OH})}{\rho_{OH} V_{OH}} \qquad (4.2.40)$$

$$M_{OH} = 336M_{OF} - V_{OH} \frac{d\rho_{OH}}{dT_{OH}} \frac{dT_{OH}}{dt} \qquad (4.2.41)$$

Eqs. (4.2.40) and (4.2.41) are perturbed and linearized as

$$\delta \dot{T}_{OH} = \frac{336M_{OF}(\delta T_{OF} - \delta T_{OH})}{\rho_{OH}V_{OH}} \qquad (4.2.42)$$

$$\delta M_{OH} = 336\delta M_{OF} - V_{OH} \frac{d\rho_{OH}}{dT_{OH}} \delta \dot{T}_{OH} \qquad (4.2.43)$$

A linear dynamic model for the outlet header is obtained from Eqs. (4.2.42) and (4.2.43).

4.2.6 Main 'Steam' Line

It is assumed that there is no energy exchange with the environment in the main 'steam' line. The pressure drop along the main 'steam' line is calculated as

$$P_{MSL} = P_{OH} - \xi \frac{M_{OH}^2}{\rho_{OH}} \qquad (4.2.44)$$

The temperature in the main 'steam' line is described as

$$\frac{dT_{MSL}}{dt} = \frac{M_{OH}(T_{OH} - T_{MSL})}{\rho_{MSL}V_{MSL}} \qquad (4.2.45)$$

Applying the mass conversation to the main 'steam' line, one can obtain

$$V_{MSL} \frac{d\rho_{MSL}}{dt} = M_{OH} - M_{MSL} \qquad (4.2.46)$$

The main 'steam' density can be considered as a function of its pressure and temperature. Thus, the main 'steam' pressure is presented as

$$\dot{P}_{MSL} = \frac{M_{OH} - M_{MSL}}{V_{MSL} \dfrac{d\rho_{MSL}}{dP_{MSL}}} - \frac{\dfrac{d\rho_{MSL}}{dT_{MSL}}}{\dfrac{d\rho_{MSL}}{dP_{MSL}}} \dot{T}_{MSL} \tag{4.2.47}$$

Eqs. (4.2.44), (4.2.45) and (4.2.47) are perturbed and linearized as

$$\delta P_{MSL} = \delta P_{OH} - 2\xi \frac{M_{OH} \delta M_{OH}}{\rho_{OH}} \tag{4.2.48}$$

$$\frac{d\delta T_{MSL}}{dt} = \frac{M_{OH}(\delta T_{OH} - \delta T_{MSL})}{\rho_{MSL} V_{MSL}} \tag{4.2.49}$$

$$\delta\dot{P}_{MSL} = \frac{\delta M_{OH} - \delta M_{MSL}}{V_{MSL} \dfrac{d\rho_{MSL}}{dP_{MSL}}} - \frac{\dfrac{d\rho_{MSL}}{dT_{MSL}}}{\dfrac{d\rho_{MSL}}{dP_{MSL}}} \delta\dot{T}_{MSL} \tag{4.2.50}$$

The flow rate in the main 'steam' line δM_{MSL} can be determined from the control valve model.

4.2.7 Control Valve

The control valve model in [84] is selected for the current studies. Its characteristic is shown in Fig 4.4. The control valve opening can be adjusted to regulate the flow rate. The flow rate is more sensitive to the opening at the lower flow area than at the higher flow area.
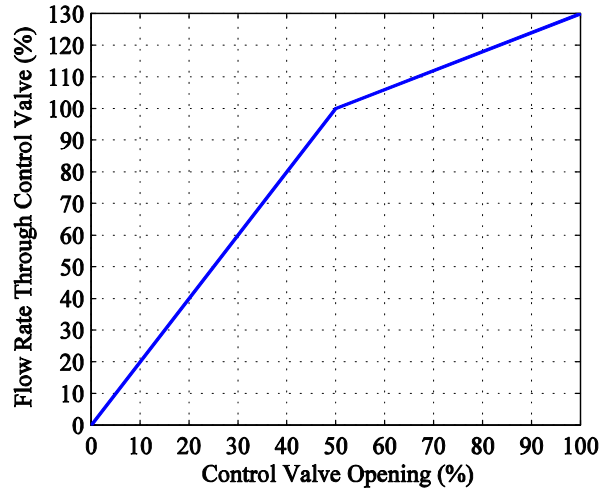
Fig 4.4 Flow rate profile of the control valve

The flow rate through the control valve, i.e., the flow rate out of the main 'steam' line, is described as [121]

$$M_{MSL} = \begin{cases} 2E_{CV}\dfrac{P_{MSL}}{\sqrt{T_{MSL}}}A_{CV}, A_{CV} \leq 50\% \\[4mm] E_{CV}\dfrac{P_{MSL}}{\sqrt{T_{MSL}}}(0.6A_{CV}+0.7), A_{CV} > 50\% \end{cases} \tag{4.2.51}$$

where E_{CV} is the control valve coefficient, A_{CV} is the percentage of the control valve opening.

One can perturb Eq. (4.2.51) to obtain a linearized model as

$$\delta M_{MSL} = \begin{cases} 2E_{CV}\dfrac{\delta P_{MSL}}{\sqrt{T_{MSL}}}A_{CV} - E_{CV}\dfrac{P_{MSL}}{\sqrt{T_{MSL}^3}}A_{CV}\delta T_{MSL} + 2E_{CV}\dfrac{P_{MSL}}{\sqrt{T_{MSL}}}\delta A_{CV}, A_{CV} \leq 50\% \\[4mm] E_{CV}[\dfrac{\delta P_{MSL}}{\sqrt{T_{MSL}}}(0.6A_{CV}+0.7) - \dfrac{P_{MSL}}{2\sqrt{T_{MSL}^3}}(0.6A_{CV}+0.7)\delta T_{MSL} \\[4mm] +0.6\dfrac{P_{MSL}}{\sqrt{T_{MSL}}}\delta A_{CV}], A_{CV} > 50\% \end{cases} \tag{4.2.52}$$

The linearization is divided into two parts for the two sections of the control valve characteristics as shown in Fig 4.4.

4.3 Linear Dynamic Model of the Canadian SCWR

A set of linear dynamic models for each subsystem component of the Canadian SCWR plant system has been developed in Section 4.2 by perturbation and linearization techniques. To facilitate control system design, the linearized models are represented in the form of transfer functions using Laplace transforms in the frequency domain. A block diagram representation of the open-loop system is shown in Fig 4.5. The block diagram in Fig 4.5(a) represents the overall system, while the reactor core is represented in Fig 4.5(b), which corresponds to G_3 in Fig 4.5(a). Fig 4.5(c) represents the input-output relationship of the Canadian SCWR and the detailed transfer matrix is shown in Appendix A. In these models, the feed-water temperature is assumed to be constant.
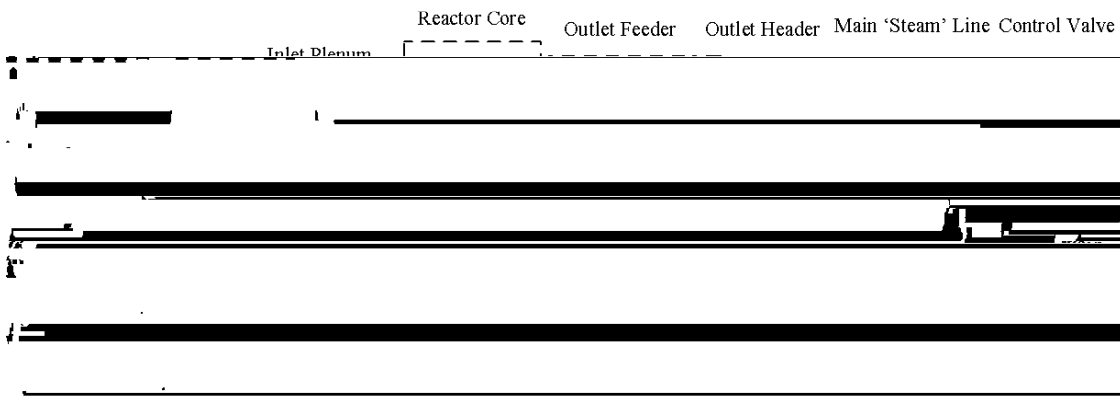
(a) Block diagram of the Canadian SCWR overall system
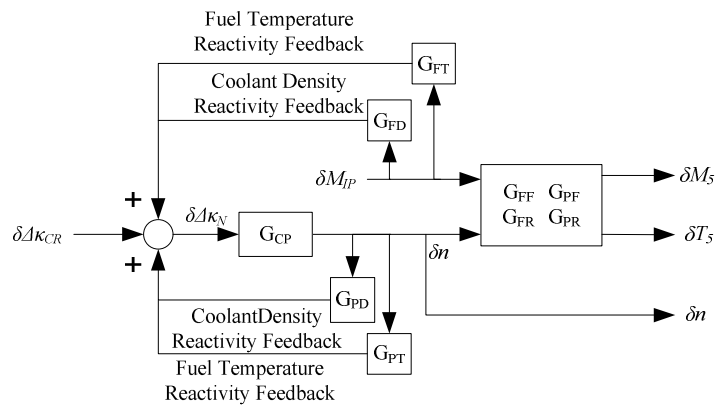
(b) Block diagram of the Canadian SCWR reactor core
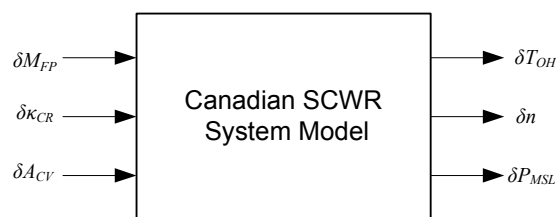
(c) Input-output relationship of Canadian SCWR

Fig 4.5 Block diagram representation of the linearized model for a Canadian SCWR

The main inputs to the system model are the feed-water mass flow rate M_{FP}, the control rod reactivity $\Delta\kappa_{CR}$ and the control valve opening A_{CV}. The main outputs are the reactor power n, the outlet header temperature T_{OH}, and the turbine inlet pressure P_{MSL}.

The physical descriptions of the inputs and the outputs for the different system components are provided in Table 4.1. The mathematical representations of the transfer functions shown in Fig 4.5(a) are detailed as follows

$$G_{1P} = \left[\frac{\delta M_{FP,P}(s)}{\delta P_R(s)}\right] = \left[-39.6\right]$$

$$G_2 = \left[\frac{\delta M_{FP,N}(s)}{\delta M_{IP}(s)}\right] = \left[1\right]$$

$$G_4 = \begin{bmatrix} \dfrac{\delta T_{OF}(s)}{\delta T_5(s)} & \dfrac{\delta T_{OF}(s)}{\delta M_5(s)} \\ \dfrac{\delta M_{OF}(s)}{\delta T_5(s)} & \dfrac{\delta M_{OF}(s)}{\delta M_5(s)} \end{bmatrix} = \begin{bmatrix} \dfrac{0.69}{s+0.69} & 0 \\ \dfrac{7.45*10^{-3}}{s+0.69} & 1 \end{bmatrix}$$

$$G_{4P} = \left[\frac{\delta P_R(s)}{\delta P_{OF}(s)} \quad \frac{\delta P_R(s)}{\delta M_5(s)}\right] = \left[1 \quad 0.13\right]$$

$$G_5 = \begin{bmatrix} \dfrac{\delta T_{OH}(s)}{\delta T_{OF}(s)} & \dfrac{\delta T_{OH}(s)}{\delta M_{OF}(s)} \\ \dfrac{\delta M_{OH}(s)}{\delta T_{OF}(s)} & \dfrac{\delta M_{OH}(s)}{\delta M_{OF}(s)} \end{bmatrix} = \begin{bmatrix} \dfrac{4.68}{s+4.68} & 0 \\ \dfrac{1.14s}{s+4.68} & 336 \end{bmatrix}$$

$$G_{5P} = \left[\frac{\delta P_{OH}(s)}{\delta P_{OF}(s)}\right] = \left[1\right]$$

$$G_6 = \begin{bmatrix} \dfrac{\delta T_{MSL}(s)}{\delta T_{OH}(s)} & \dfrac{\delta T_{MSL}(s)}{\delta M_{OH}(s)} & \dfrac{\delta T_{MSL}(s)}{\delta M_{MSL}(s)} \\[3mm] \dfrac{\delta P_{MSL}(s)}{\delta T_{OH}(s)} & \dfrac{\delta P_{MSL}(s)}{\delta M_{OH}(s)} & \dfrac{\delta P_{MSL}(s)}{\delta M_{MSL}(s)} \end{bmatrix} = \begin{bmatrix} \dfrac{0.70}{s+0.70} & 0 & 0 \\[3mm] \dfrac{3.00*10^{-2}}{s+0.70} & \dfrac{1.31*10^{-2}}{s} & -\dfrac{1.31*10^{-2}}{s} \end{bmatrix}$$

$$G_{6P} = \begin{bmatrix} \dfrac{\delta P_{MSL}(s)}{\delta P_{OH}(s)} & \dfrac{\delta P_{MSL}(s)}{\delta M_{OH}(s)} \end{bmatrix} = \begin{bmatrix} 1 & 6.45*10^{-5} \end{bmatrix}$$

$$G_7 = \begin{bmatrix} \dfrac{\delta M_{MSL}(s)}{\delta A_{CV}(s)} & \dfrac{\delta M_{MSL}(s)}{\delta T_{MSL}(s)} & \dfrac{\delta M_{MSL}(s)}{\delta P_{MSL}(s)} \end{bmatrix} = \begin{cases} \begin{bmatrix} 2640 & -0.37 & 26.74 \end{bmatrix}, A_{CV} \leq 50\% \\ \begin{bmatrix} 792 & -0.37 & 26.74 \end{bmatrix}, A_{CV} > 50\% \end{cases}$$

For G_3,

$$G_{CP} = \begin{bmatrix} \dfrac{\delta n(s)}{\delta \kappa_N(s)} \end{bmatrix} = \begin{bmatrix} \dfrac{3030.30(s+3.78577)(s+1.38922)(s+0.317638)(s+0.12185)(s+0.0315532)(s+0.612382e\text{-}3)}{s(s+0.0054)(s+0.0776)(s+0.1732)(s+1.4069)(s+3.4507)(s+18.2217)} \end{bmatrix}$$

$$G_{FD} = \begin{bmatrix} \dfrac{\delta \kappa_{FD}(s)}{\delta M_{IP}(s)} \end{bmatrix} = \begin{bmatrix} \dfrac{4.9561*10^{-5}}{s+1.888} \end{bmatrix}$$

$$G_{FT} = \begin{bmatrix} \dfrac{\delta \kappa_{FT}(s)}{\delta M_{IP}(s)} \end{bmatrix} = \begin{bmatrix} \dfrac{1.8548*10^{-5}}{s+0.07176} \end{bmatrix}$$

$$G_{PD} = \begin{bmatrix} \dfrac{\delta \kappa_{PD}(s)}{\delta n(s)} \end{bmatrix} = \begin{bmatrix} \dfrac{-2.6429*10^{-5}}{s+0.1014} \end{bmatrix}$$

$$G_{PT} = \begin{bmatrix} \dfrac{\delta \kappa_{PT}(s)}{\delta n(s)} \end{bmatrix} = \begin{bmatrix} \dfrac{-3.8119*10^{-4}}{s+0.06566} \end{bmatrix}$$

$$G_{FF} = \begin{bmatrix} \dfrac{\delta M_5(s)}{\delta M_{IP}(s)} \end{bmatrix} = \begin{bmatrix} \dfrac{2.38}{s+2.38} \end{bmatrix}$$

$$G_{PF} = \begin{bmatrix} \dfrac{\delta M_5(s)}{\delta n(s)} \end{bmatrix} = \begin{bmatrix} 0 \end{bmatrix}$$

$$G_{FR} = \left[\frac{\delta T_5(s)}{\delta M_{IP}(s)} \right] = \left[\frac{143.8439(s-6.077)(s+4.978)(s+0.2915)(s+0.1103)}{(s+7.167)(s+5.257)(s+2.380)(s+0.2974)(s+0.06833)} \right]$$

$$G_{PR} = \left[\frac{\delta T_5(s)}{\delta n(s)} \right] = \left[\frac{-369.6109(s-5.47)(s+0.2564)}{(s+7.167)(s+5.257)(s+0.2974)(s+0.06833)} \right]$$

Table 4.1 Physical meanings of the input and the output variables

Variables	Physical Meanings
A_{CV}	Control valve opening
κ_{CR}	Reactivity caused by moving the control rod
κ_{FD}	Coolant density reactivity caused by change in the feed-water flow rate
κ_{FT}	Fuel temperature reactivity caused by change in the feed-water flow rate
κ_N	Net reactivity
κ_{PD}	Coolant density reactivity caused by change in the reactor power
κ_{PT}	Fuel temperature reactivity caused by change in the reactor power
M_5	Reactor outlet mass flow rate
M_{IP}	Mass flow rate of the inlet plenum
M_{IH}	Mass flow rate of the inlet header
M_{FP}	Mass flow rate of the feed-water pump
$M_{FP,N}$	Net feed-water mass flow rate
$M_{FP,P}$	Feed-water mass flow rate change caused by the reactor pressure
M_{MSL}	Main 'steam' mass flow rate
M_{OF}	Mass flow rate of the outlet feeder
M_{OH}	Mass flow rate of the outlet header
n	Normalized reactor power
P_{MSL}	Main 'steam' pressure
P_R	Reactor pressure
P_{OF}	Pressure of the outlet feeder
P_{OH}	Pressure of the outlet header
T_5	Reactor outlet temperature
T_{MSL}	Main 'steam' temperature
T_{OF}	Temperature of the outlet feeder
T_{OH}	Temperature of the outlet header

4.4 Dynamic Characteristics and Verification of the Open-loop System

To examine the dynamic behaviours of the Canadian SCWR system with respect to variations at

the inputs, up to 2% magnitude changes are introduced at each individual input one at a time.

The responses to these perturbations are then observed. The responses of the three system output variables are shown in Figs 4.6, 4.7 and 4.8, respectively. In these figures, SM represents the response based on the linearized Simplified Model developed in Section 4.2. DM stands for Detailed Model, in which the reactor model developed in [120] is adopted. In this detailed model analysis, 8 nodes for the inlet plenum, 8 nodes for the outlet feeder, 1 node for the outlet header and 10 nodes for the main 'steam' line are used. RM corresponds to RETRAN Model [19], in which the heat transfer correlation of this code has been modified for supercritical conditions and 20 nodes are used for the reactor model. For other system components, the node number is chosen to be the same as those in DM. It is important to point out that the RM is used herein for validation purpose only. However, DM and SM have been used to describe the system dynamics in MATLAB/SIMLINK^{TM} environment for further control system design and evaluation studies.

4.4.1 Open-loop Dynamic Characteristics

The dynamic behaviours of the open-loop system are to be examined in the following subsections based on the SM.

4.4.1.1 Step Decrease in the Feed-water Flow Rate

A 2% step decrease is applied to the feed-water flow rate, while the control rod position and the turbine control valve opening are unchanged. This decrease in the feed-water flow rate results in a decrease in the coolant flow rate. Therefore, the temperature at the outlet header increases and the main 'steam' pressure decreases. The normalized reactor power decreases because of the negative reactivity feedback caused by the increase in the fuel pin temperature and the decrease in the coolant density. The normalized reactor power is stabilized at 99.2%. The temperature at the outlet header increases by 8.4^{o}C, and the main 'steam' pressure decreases by 0.4MPa.

4.4.1.2 Withdrawal of the Control Rods

A positive reactivity (0.1mk) is added to the reactor core by withdrawing the control rods. The feed-water flow rate and the turbine control valve opening remain unchanged. The normalized reactor power promptly increases. The temperature at the outlet header increases because of the increase in the reactor power. The temperature settles finally at 636.6°C. The negative reactivity feedback is caused by the increase in the fuel temperature and decrease in the coolant density. As a result of the negative reactivity feedback, the normalized reactor power exhibits a peak first and then stabilizes at 101.5%. At the steady-state, the main 'steam' pressure has increased by as much as 0.1MPa.

4.4.1.3 Step Decrease in the Control Valve Opening

Under this test, the control valve opening is reduced stepwise from 50% to 49%. The control rod position and the feed-water flow rate remain unchanged. In response to this adjustment, the main 'steam' pressure increases rapidly and stabilizes at 25.0MPa. The increase in the reactor core pressure leads to the decrease in the feed-water flow rate, which results in a decrease in the outlet header temperature. The normalized reactor power is decreased due to the negative reactivity feedback as a result of the increase in the fuel pin temperature and the decrease in the coolant density. The outlet header temperature and the normalized reactor power stabilize at 628.4°C and 99.6%, respectively.

From Fig 4.6, it can be seen that the outlet header temperature is affected by any of the three inputs. However, the simulations have indicated that it is most effective to control the outlet header temperature using the feed-water flow rate because of its sensitivity and faster response. Reactivity variations induced by moving the control rods can have a quick and significant effect on the reactor power as shown in Fig 4.7. Similarly, the main 'steam' pressure can be effectively controlled through proper adjustment of the control valve opening or the feed-water flow rate as

shown in Fig 4.8. However, the control valve opening is much more sensitive to affect the main

'steam' pressure than the feed-water flow rate.
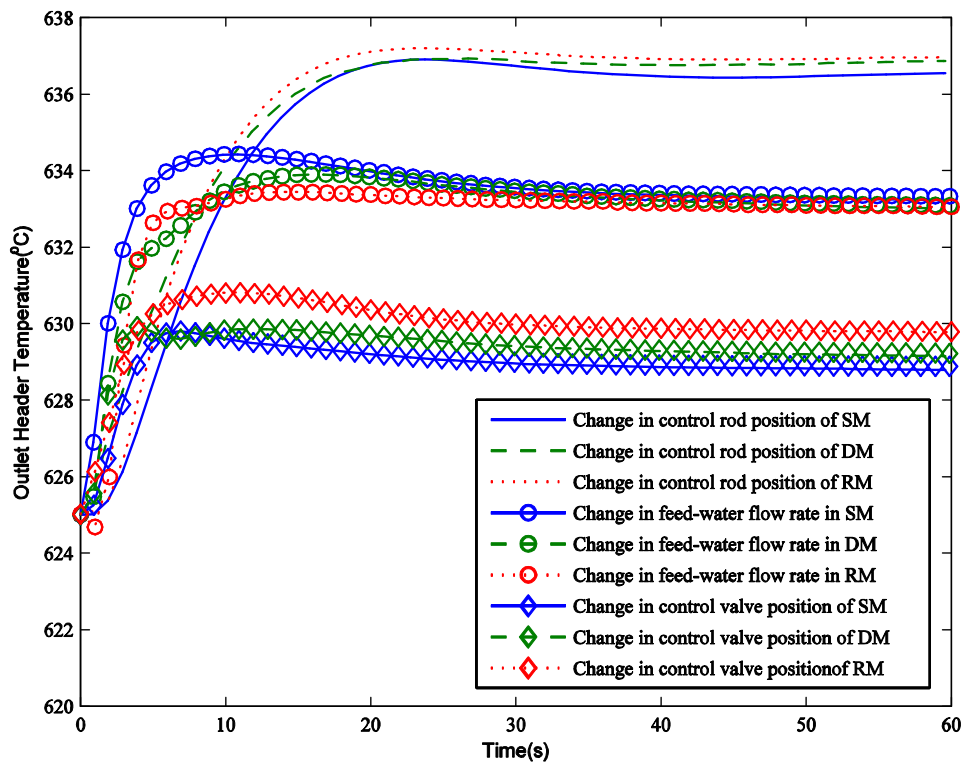
Fig 4.6 Responses of the outlet header temperature to changes at different inputs
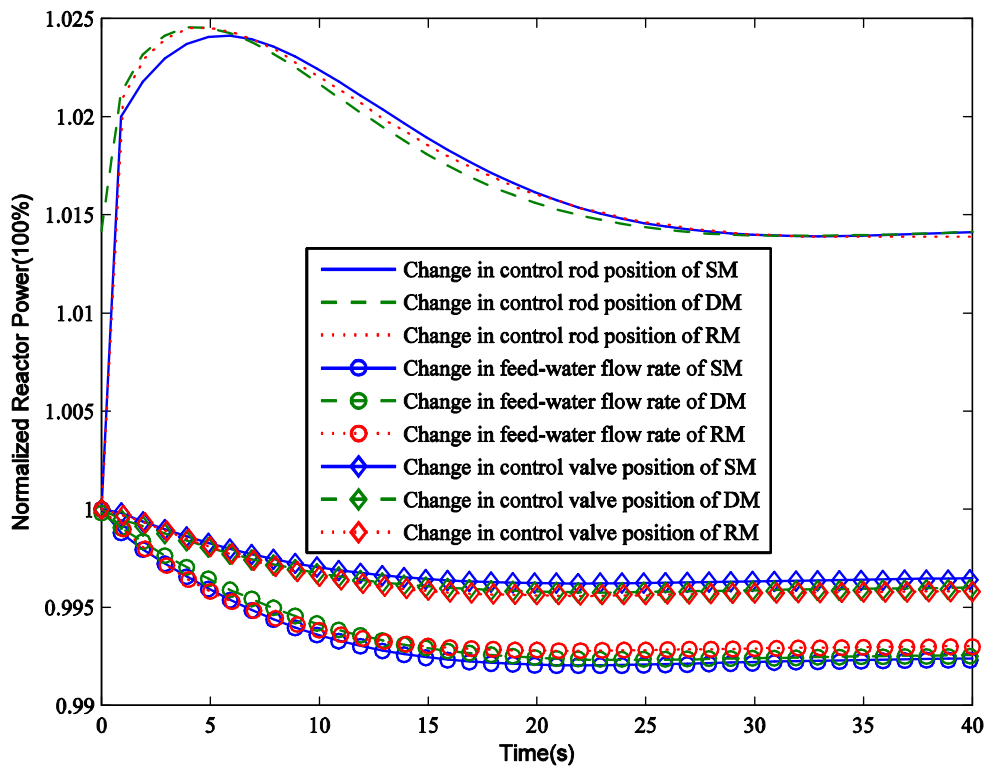
Fig 4.7 Responses of the normalized reactor power to changes at different inputs
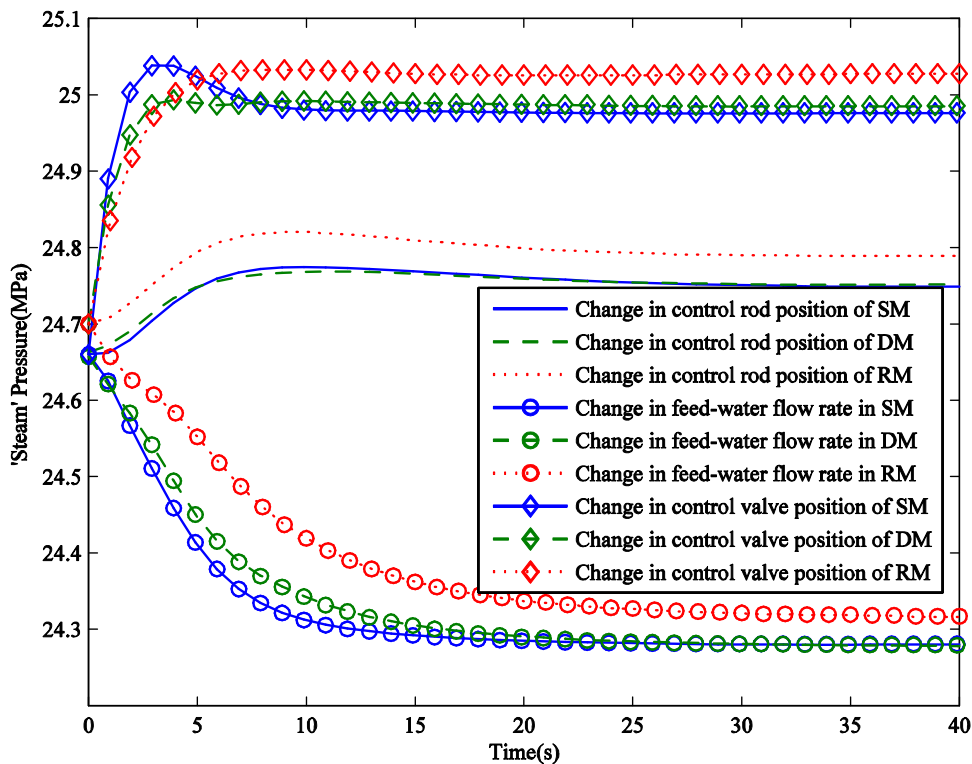
Fig 4.8 Responses of the main 'steam' pressure to changes at different inputs

4.4.2 Dynamic Model Verification

The developed linearized dynamic model is verified in both time domain and frequency domain techniques. The time domain analysis provides information, such as speed of responses and steady-state gains, while the frequency domain can provide more detailed information on the relative stability of the system and the degree of cross-coupling at different frequency bands. Both types of information are valuable in the selection of control system variables and design of control algorithms.

4.4.2.1 Model Validation in Time Domain

From Figs 4.6, 4.7 and 4.8, it can be observed that the step-responses of the system based on the DM and RM agree well. There is a difference of less than 0.05MPa in the main 'steam' pressure

between these two models at the steady-state. The differences in the outlet header temperature are due to feed-water flow rate difference caused by changes in the reactor pressure.

Compared with the DM, the coolant flow rate in the reactor core based on the SM is evaluated. The reactor outlet flow rate only depends on the reactor inlet flow rate. Therefore, the difference in responses between the DM and SM is mainly at the beginning part of the main 'steam' pressure and the outlet header temperature response.

The reason why the response based on the SM is closer to that based on the DM than on the RM is because the SM and DM have similar pressure distribution.

To illustrate the differences on the responses between the SM and RM of Figs 4.6, 4.7 and 4.8, the average and standard differences are listed in Table 4.2 and 4.3.The differences caused by the control rod reactivity as an input are smaller than those caused by the feed-water flow rate or the control valve opening as an input.

Table 4.2 Average differences of the responses between the SM and the RM

Output Input	Outlet Temperature (^{o}C)	Main 'Steam' Pressure (MPa)	Normalized Reactor Power
Feed-water Flow Rate	6.35E-1	5.55E-2	5.80E-4
Control Rod Reactivity	5.10E-1	4.13E-2	1.28E-5
Control Valve Opening	9.85E-1	4.11E-2	4.90E-4

Table 4.3 Standard differences of the responses between the SM and the RM

Output Input	Outlet Temperature (^{o}C)	Main 'Steam' Pressure (MPa)	Normalized Reactor Power
Feed-water Flow Rate	9.34E-1	6.36E-2	6.33E-4
Control Rod Reactivity	5.77E-1	4.14E-2	3.31E-4
Control Valve Opening	1.00E0	5.09E-2	5.37E-4

4.4.2.2 Model Validation in Frequency Domain

Bode plots of the SM and numerical data obtained based on the DM simulation are carried out to obtain the frequency responses from different system inputs to the outputs. The results are presented in Figs 4.9, 4.10 and 4.11. In these figures, the solid curves are Bode plot based on the SM and the dots are calculated at particular frequency points using the DM.

When the feed-water flow rate is used as the input (Fig 4.9), the main discrepancies are only at the high frequency end in the main 'steam' pressure. This is because, at low frequencies, the pressure effect on the flow rate is small. At high frequencies, the effect becomes more profound.
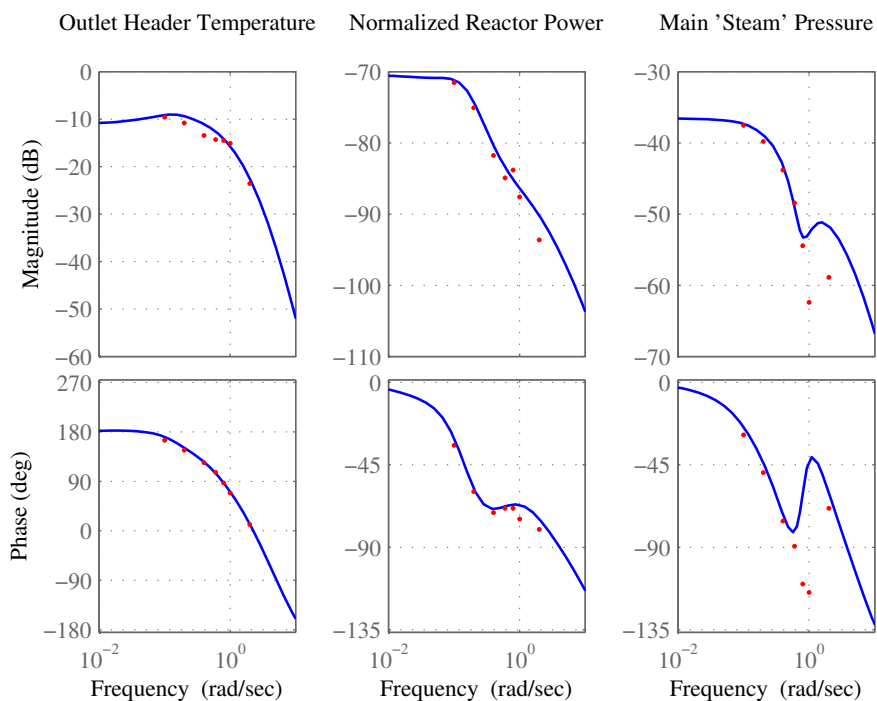
Fig 4.9 Model verification in frequency domain using the feed-water flow rate as the input

When the control rod reactivity is used as the input as shown in Fig 4.10, some inconsistencies have been observed at the high frequency end and in the main 'steam' pressure. This is because,

in the SM, the reactor outlet flow rate is assumed to be only dependent on the reactor inlet flow rate.
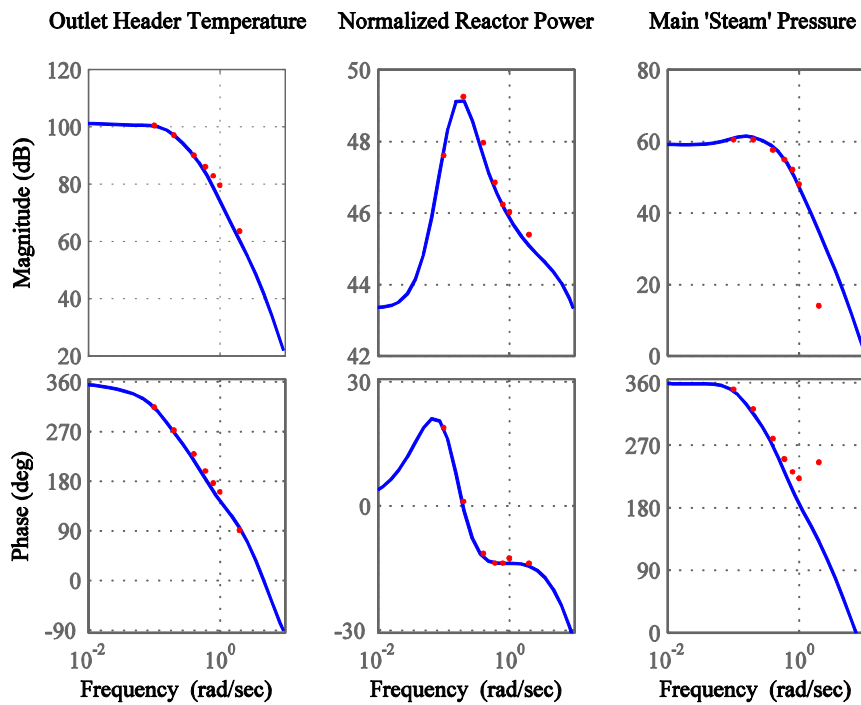
Fig 4.10 Model verification in frequency domain using the control rod as the input

When the control valve opening is treated as the input as shown in Fig 4.11, it can be seen that there are some differences for all three outputs. The main reason is that the pressure effect on the coolant flow rate is not modelled in the SM. Nevertheless, the differences are relatively small.

Even though the dynamic behaviours of SM are slightly different from those of the DM and RM, Such differences can be treated as modeling uncertainties and dealt with effectively at the control system design stage [122]. The significant reduction in the model complexity fully justifies the bounded differences in this simplified models.
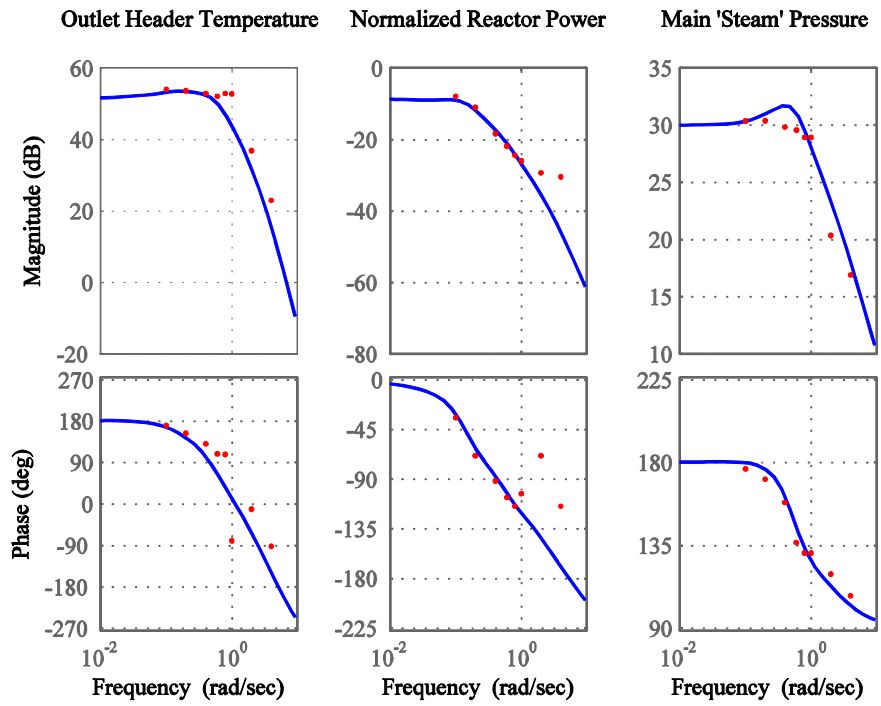
Fig 4.11 Model verification in frequency domain using the control valve opening as the input

5 DYNAMIC ANALYSIS OF THE CANADIAN SCWR

5.1 Introduction

In the Canadian SCWR, the coolant flow rate has to be maintained in a correct proportion to the reactor power output so that the main 'steam' temperature can be maintained constant. Therefore, at a lower power level, the coolant flow rate is lower, which leads to a larger percentage change in the flow rate for a disturbance of the same magnitude. Also, at the low power level the heat transfer coefficient is also low, and the time constant is larger. Thus, the gain and the time constant of the system vary as the power level changes. This represents a typical behaviour of a nonlinear dynamic system.

From an input and output perspective, a Canadian SCWR is a MIMO system similar to a BWR. However, the Canadian SCWR has a much stronger cross-coupling among different system variables. For example, in a BWR, when the load increases rapidly, more steam will be drawn from the reactor core. Since there is a large water inventory in the reactor, the steam loss can be recovered through boiling. The feed-water flow and the reactor power can be gradually adjusted to re-establish the desired water level. In a Canadian SCWR, the above scenario has to be dealt with differently. If there is a rapid increase in load, more 'steam' has to be supplied to the turbine immediately. Since there is no boiling taken place in the SCWR to act as a cushion to supply this additional 'steam', the feed-water flow rate needs to be increased immediately and the reactor power should also be increased quickly to compensate for the increase in the feed-water flow rate. If this is not done properly, there will be excessive variations in the main 'steam' temperature, which is highly undesirable and should be strictly avoided.

Even though an SCFPP is also highly nonlinear with strong cross-couplings among its variables [123], the dynamics of a Canadian SCWR are more complicated than those of an SCFPP. This is because the heat flux in the boiler of an SCFPP is lower and the length of the heated tubes is much longer. Therefore, the response time is larger and the dynamic is slower. Furthermore, there is no reactivity feedback issue in an SCFPP. In fact, the intermediate temperature at the outlet of an evaporation section in an SCFPP can be measured and this information can be used, not only for predicting the water inventory in the boiler, but also for controlling the temperature of the main 'steam'. Unfortunately, the coolant temperature distribution in the fuel channel of the Canadian SCWR reactor is not available during operation. The only operational information that can be obtained is the feed-water temperature and the reactor outlet temperature. Therefore, there is no way to locate the pseudo-critical point as an index for water inventory which would be useful information for controlling the Canadian SCWR.

In summary, the high power-to-flow ratio, high degree of nonlinearities due to different dynamics at different power levels and the movement of the pseudo-critical point, and strong cross-coupling among different system variables pose difficulties and challenges for control system design of a Canadian SCWR.

Even though the dynamic analysis and control system design for SCFR and SCLWR-H [83, 84] have been carried out, the dynamics of a Canadian SCWR are very different from those of an SCFR and SCLWR-H. To be more precise, the feed-water flow rate of the Canadian SCWR is less than that of SCFR and SCLWR-H for the same amount of thermal power generation. This means that a Canadian SCWR is more sensitive to disturbances in the feed-water. Furthermore, the Canadian SCWR is a thermal reactor while the SCFR is a fast reactor. In the modeling process of SCFR, Dittus-Boelter correlation is adopted, which is not recommended for heat

transfer coefficient calculation under supercritical conditions. In addition, the Canadian SCWR is moderated by heavy water, which is separated from the supercritical light water coolant. Therefore, the coolant density reactivity feedback will have less effect on the neutron kinetics than that in an SCLWR-H. Hence, the existing results for SCFR and SCLWR-H cannot be applied to the Canadian SCWR directly.

The Canadian SCWR is a multivariable system. There are mainly three approaches to control a multivariable plant: decentralized control, two-step decoupling control and multivariable optimal control.

An intuitive approach to design a controller for a multivariable plant is decentralized control. Decentralized control is valid only if the multivariable plant is weakly coupled or close to diagonal of its transfer function matrix, because in such a case the multivariable plant to be controlled is a collection of independent SISO sub-plants in essence. The performance of the decentralized control may deteriorate in case of the existence of large off-diagonal elements, because no attempts are made to compensate the interactions. The interactions may lead to stability problems. Therefore, it is necessary to select good input-output parings in the decentralized control, such that the effects of the interactions is minimized. The design of a decentralized control system typically involves two steps: input-output pairing and parameter tuning of each controller. There are three main approaches to the tuning of each controller: fully coordinated design, independent design and sequential design. In the fully coordinated design approach, all diagonal controller elements are designed simultaneously based on the complete model of the plant. In the independent design approach, each controller element is designed based on the corresponding diagonal element of the plant. In the sequential design approach, the controllers are designed sequentially one at a time, with the previously designed controllers

implemented. In theory, fully coordinated design is the optimal approach in the decentralized control, but it is not commonly used in practice. Independent control is used when the system is close to diagonal while sequential design is used when the system outputs can be decoupled in time.

Another approach to multivariable control is achieved by a two-step procedure: a decoupling compensator is designed to deal with the interactions and then a diagonal controller is designed using classical SISO techniques. The most common approach for decoupling compensator is to use a pre-compensator, which counteracts the interactions in the plant and leads to a new pre-compensated plant. The new plant is more diagonal and easier to control than the original plant.

There are three possible cases to the pre-compensator design:

    a)   Dynamic decoupling: the pre-compensated plant is diagonal at all frequencies selected. The elements of the pre-compensator are dynamics and are a function of frequencies.

    b)   Steady-state decoupling: the pre-compensated plant is kept diagonal at steady-state only. It may be obtained by selecting a constant pre-compensator: inverse of the plant at the steady-state.

    c)   Approximate decoupling at a certain frequency: the pre-compensated plant is diagonal at some selected frequencies. Similar to the steady-state decoupling, it can be obtained by choosing a constant pre-compensator: inverse of the plant at the selected frequencies.

Common pre-compensator design techniques in frequency domain are Nyquist array methods [124] and eigenvalue based characteristic locus method [125, 126]. The decoupling can also be achieved by state feedback and output feedback [127]. The pre-compensator approach may be

extended by introducing a post-compensator. The Singular Value Decomposition (SVD) controller is a special case of a pre-compensator and post-compensator design [128, 129].

The optimal design approach to multivariable control is to synthesize directly a multivariable controller based on minimizing/maximizing some objective functions or norms. The multivariable plant is considered as a whole and only one centralized multivariable controller is obtained. The measure of the quality of the multivariable controller is formulated in terms of the objective function or the norm. Optimization in controller design became prominent in the 1960s. The optimal control problem can be addressed as follows: find a control that minimizes/maximizes an objective function over all admissible controls. From an engineering point of view, optimality provides a very useful design principle and the cost to be minimized or the profit to be maximized is contained in the problem formulation. Examples of multivariable optimal design techniques include Linear Quadratic Regulator (LQR) control, H_2 and H-infinity control.

Before choosing a suitable control strategy and approach for the Canadian SCWR, dynamic analysis is necessary to investigate its dynamic characteristics. Based on the results shown in Chapter 4, the Canadian SCWR is a MIMO system with three inputs and three outputs as shown in Fig 4.5(c). This means that variations in any single input will result in changes in all three outputs. The dynamic cross-coupling among inputs and outputs can be observed from the step responses in the time domain and Bode plots in the frequency domain in Section 4.4.2. The degree of interaction at the steady-state and the dynamic conditions of the Canadian SCWR is investigated so that the most effective input-output pairing and most appropriate control strategies can be determined for control system design and analysis.

The rest of the chapter is organized as follows. In Section 5.2, the steady-state coupling is analyzed using RGA. The degree of the dynamic coupling is evaluated using direct Nyquist array in Section 5.3. Based on the analysis on the cross-coupling, the appropriate input-output pairing is determined. The analysis on the cross-coupling at different operating conditions is also performed in Section 5.4. The nonlinearities of the Canadian SCWR are analyzed.

5.2 Steady-state Cross-coupling Analysis

An effective way to describe the cross-coupling among different inputs and outputs of a MIMO system at steady-state conditions is the RGA [130]. The RGA is a normalized form of the gain matrix that measures the impact of a control input on an output, relative to its impact on the other outputs. The RGA has the following basic properties:

a) It is independent of input and output scaling;

b) Each row and each column should sum to unity;

c) The input and output should be paired when their corresponding element in the RGA is most closest to one; and

d) The plant with large RGA elements (typically 5-10) is fundamentally difficult to control due to strong interactions and sensitivity to uncertainties [131].

Based on an analysis on the RGA, the most effective control input can be selected for a particular system output. The steady-state gain matrix of the Canadian SCWR is obtained based on the dynamic model developed in Section 4.3 as

$$\begin{bmatrix} \delta T_{OH} \\ \delta n \\ \delta P_{MSL} \end{bmatrix} = \begin{vmatrix} -2.73*10^{-1} & 6.05*10^{4} & -1.81*10^{2} \\ 6.00*10^{-4} & 1.53*10^{2} & 3.82*10^{-1} \\ 3.00*10^{-2} & 9.50*10^{2} & -3.14*10^{1} \end{vmatrix} \begin{bmatrix} \delta M_{FP} \\ \delta \kappa_{CR} \\ \delta A_{CV} \end{bmatrix} \qquad (5.2.1)$$

The RGA of the Canadian SCWR at 100%FP is calculated from the steady-state gain matrix as

$$RGA_{100\%} = \begin{vmatrix} 0.35 & 0.47 & 0.18 \\ 0.27 & 0.53 & 0.20 \\ 0.38 & 0.00 & 0.62 \end{vmatrix} \qquad (5.2.2)$$

As indicated by this RGA, the Canadian SCWR is not a diagonally dominant system even at the steady-state condition. The temperature at the outlet header is affected significantly by all three input variables, of which the largest is the control rod reactivity. Because of the high power-to-flow ratio in the Canadian SCWR, any perturbation on the control rod reactivity or the feed-water flow rate will cause significant variations in the outlet header temperature. The control valve opening affects the outlet header temperature, because it can regulate the system pressure while the feed-water flow rate is changed by the effect of the reactor pressure on the feed-water pump. The reactor power is most sensitive to changes in the control rod reactivity. The Canadian SCWR is a heavy water moderated reactor with relatively low reactivity feedback. Thus, the changes in the control valve opening and the feed-water flow rate result in little reactivity feedback. Hence, these two inputs have little influence on the reactor power. The main 'steam' pressure is most sensitive to the control valve opening. The control rod reactivity can have large effect on the main 'steam' temperature, but not on the pressure. The main 'steam' flow rate must be balanced with the feed-water flow rate. Therefore, the feed-water flow rate has some influence on the main 'steam' pressure as well.

5.3 Analysis of Dynamic Cross-coupling

Even though RGA has widely been used to quantify interactions among system inputs and outputs at steady-state conditions, this approach may not be sufficient to account for all the interactions among system inputs and outputs at different frequencies in a dynamic way.

Several methods have been proposed to analyze the dynamic interaction in a MIMO system [132]. The direct Nyquist array can provide a basis for estimating the cross-coupling among system inputs and outputs as a function of frequency, and hence is adopted here since the open-loop transfer functions are now available.

The Nyquist array consists of a set of standard polar plots of the magnitude and the phase angle for each element in the transfer function matrix. It is a graphical representation of the open-loop relationship among inputs and outputs. The direct Nyquist array based on the dynamic model of the Canadian SCWR developed in Section 4.3 is shown in Fig 5.1. The units of inputs and outputs have been scaled by the maximum allowable change range in the inputs based on the assumption of the valid range for linearization, which is 5%FP. The degree of the interaction between input and output is measured by the magnitude of the Nyquist plots in the polar coordinates.

From the first row of Fig 5.1, it can be observed that the outlet header temperature is affected significantly by all three inputs. The dynamic effects of the feed-water flow rate on the outlet header temperature are larger than those of the control valve opening. The largest amount of influence is from the control rod reactivity. This is also the reason why it requires to maintain the power-to-flow ratio during operation to minimize the main 'steam' temperature variation in an SCFPP [133].

The reactor power is most sensitive to the change in the control rod reactivity as shown in the second row of Fig 5.1. The influences of the control valve opening and the feed-water flow rate on the reactor power are negligible.

From the last row of Fig 5.1, the main 'steam' pressure can be influenced by all three inputs. The dynamic effects of the feed-water flow rate and the control valve opening on the main 'steam' pressure are opposite. The effect of the control rod reactivity on the main 'steam' pressure is comparable with that of the feed-water flow rate and the control valve opening. But the control valve opening has dominant effect on the main 'steam' pressure among the three inputs at high frequencies, such as, at 0.5rad/s as shown in Fig 5.1.

Through the steady-state and dynamic interaction analysis, it can be concluded that the reactor power should be controlled by the control rod reactivity. The feed-water flow rate has a larger effect on the outlet header temperature. The control valve opening has comparable effect with the feed-water flow rate on the main 'steam' pressure at the steady-state, but has larger influence at high frequencies. The control valve opening and the main 'steam' pressure should be paired. Therefore, the appropriate input-output pairing can be selected as follows: (a) the outlet header temperature should mainly be regulated through the feed-water flow rate, (b) the reactor power should mainly be controlled by the control rod reactivity, and (c) the main 'steam' pressure should be manipulated by the control valve opening.
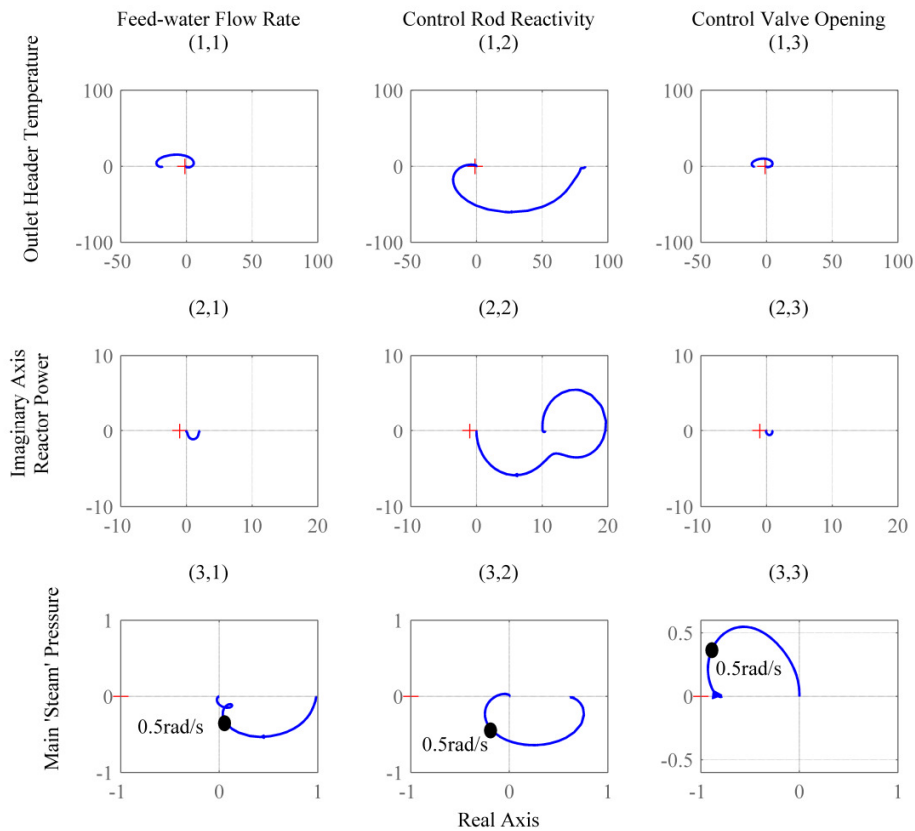
Fig 5.1 Direct Nyquist array of the Canadian SCWR system

5.4 Analysis of Cross-coupling at Different Operating Conditions

The analysis in the previous sections is based on the open-loop model obtained at 100%FP. Similar analyses have been performed at 80%FP and 60%FP levels as well. At different power levels, the corresponding feed-water flow rate and the control valve opening are adjusted to keep the outlet header temperature and the main 'steam' pressure constant, which is known as constant pressure operation in an SCFPP [133].

The RGA for the plant operating at 80%FP is

$$RGA_{80\%} = \begin{vmatrix} 0.38 & 0.44 & 0.18 \\ 0.25 & 0.56 & 0.19 \\ 0.36 & 0.00 & 0.64 \end{vmatrix} \qquad (5.4.1)$$

The RGA for the plant at 60%FP is

$$RGA_{60\%} = \begin{vmatrix} 0.38 & 0.41 & 0.21 \\ 0.24 & 0.59 & 0.17 \\ 0.39 & 0.00 & 0.61 \end{vmatrix} \qquad (5.4.2)$$

Comparing the corresponding elements in the RGAs at different power levels, the magnitude of each element does not change significantly, which means that the degree of the steady-state cross-coupling is relatively insensitive with respect to operating condition changes. The main trend is that the control rod reactivity becomes less dominant on the outlet header temperature as the power level decreases. This trend can also be observed from the Nyquist plots shown in Figs 5.2, 5.3, and 5.4. From these figures, it can be seen that the feed-water flow rate and the control valve opening have stronger influences on the outlet header temperature, while the control rod reactivity has a weaker effect on the outlet header temperature at a lower power level.
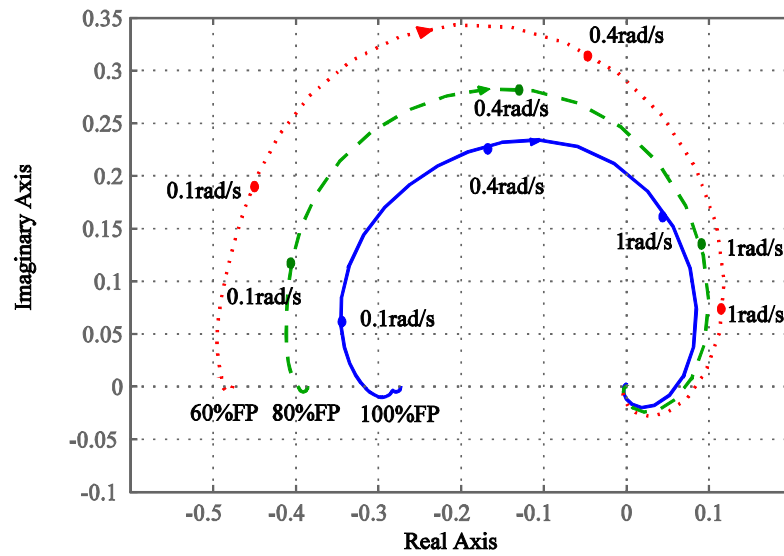
Fig 5.2 Effect of the feed-water flow rate on the outlet header temperature at different power
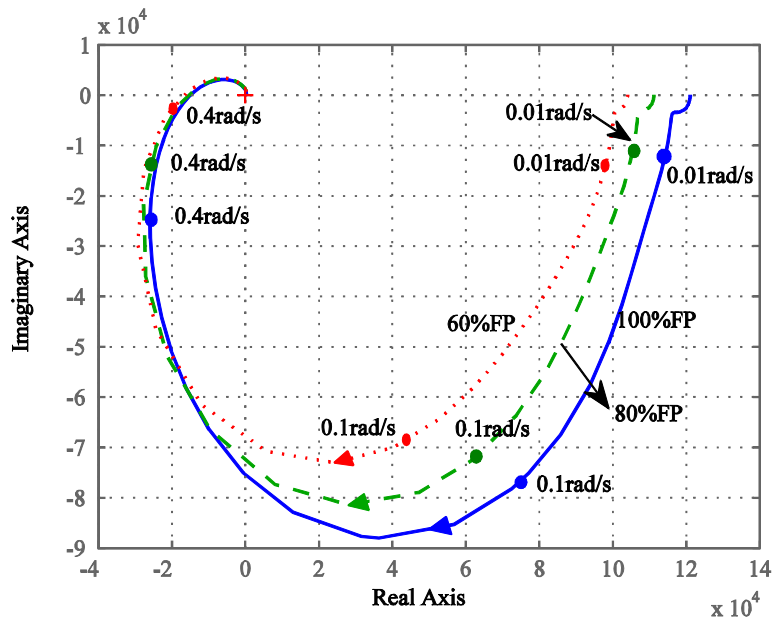
levels

Fig 5.3 Effect of the control rod reactivity on the outlet header temperature at different power
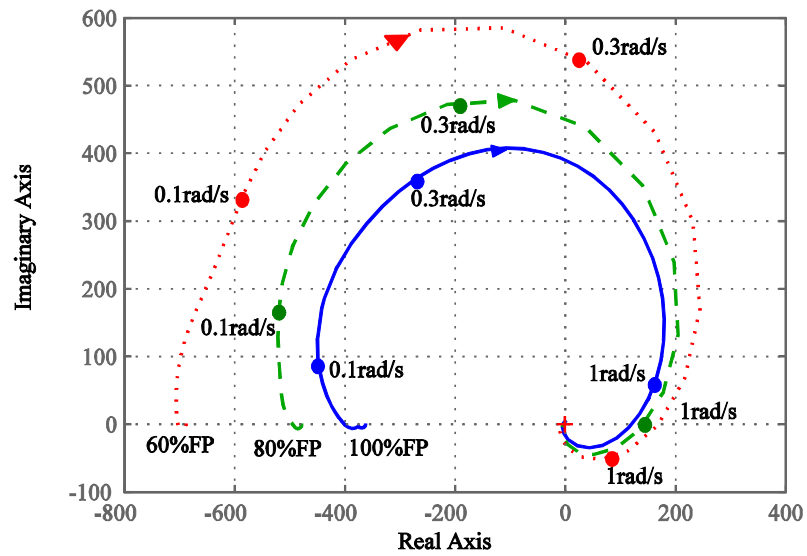
levels

Fig 5.4 Effect of the control valve opening on the outlet header temperature at different power
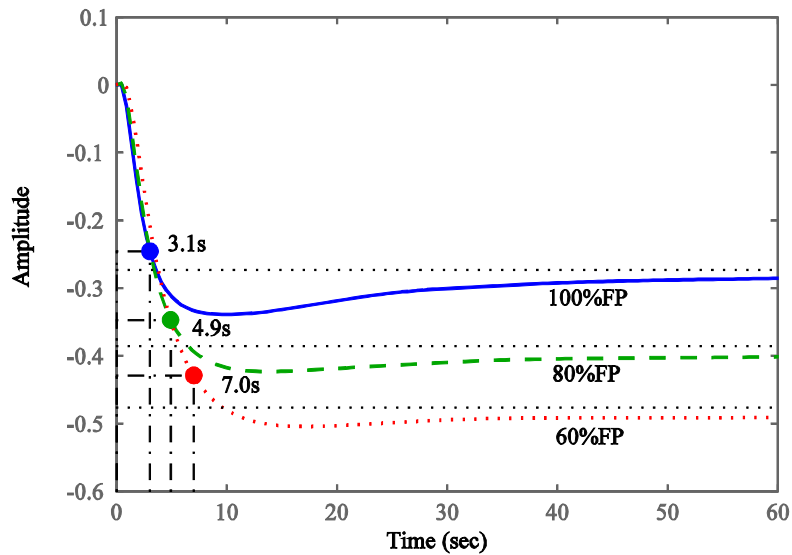
levels

Fig 5.5 Step responses of the temperature at the outlet header subject to changes in the feed-

water flow rate at different power levels
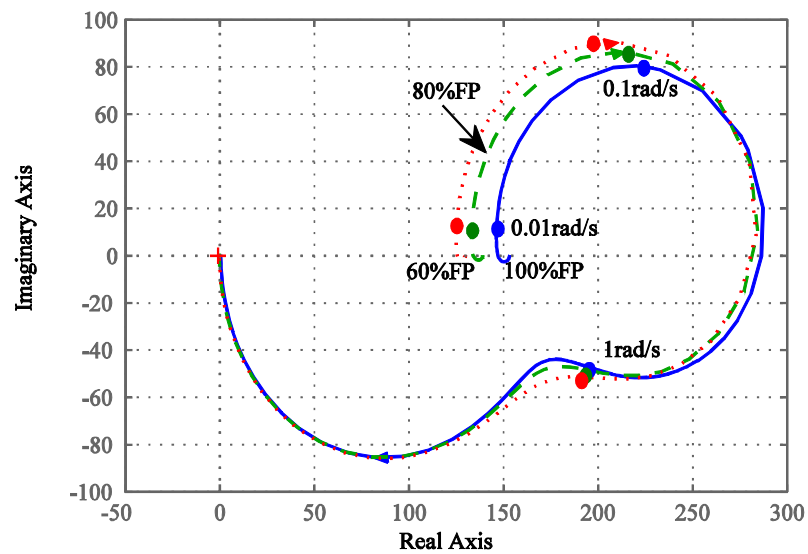
Fig 5.6 Effect of the control rod reactivity on the reactor power at different power levels
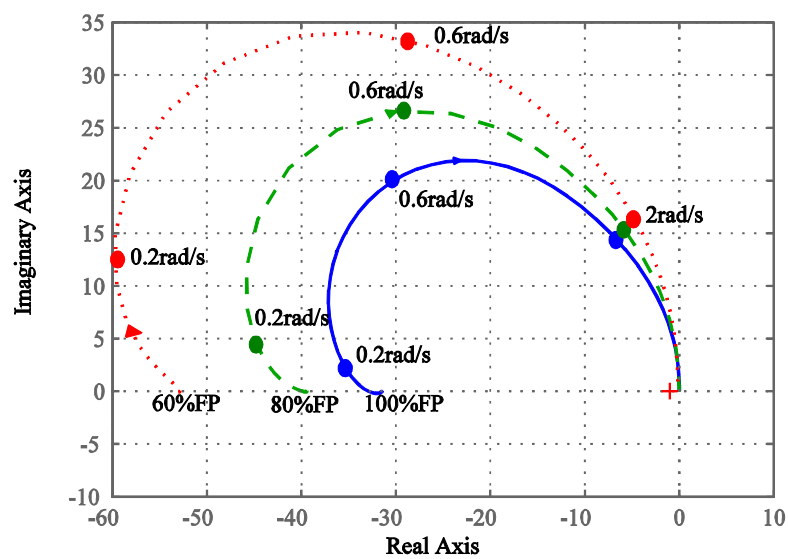
Fig 5.7 Effect of the control valve opening on the main 'steam' pressure at different power levels

As shown in Fig 5.2, the effect of the feed-water flow rate on the outlet header temperature increases as the power level decreases. In the time domain, the time constant increases as the

power level decreases, due to the decrease in the coolant flow rate and the heat transfer coefficient. These effects can be clearly seen from the step responses in Fig 5.5. The rise time of the step responses is also listed in Fig 5.5.

The effect of the control rod reactivity on the outlet header temperature decreases as the power level decreases as shown in Fig 5.3. The reason is that the effect of the control rod reactivity on the reactor power decreases as the power level decreases shown in Fig 5.6. The phenomenon shown in Fig 5.6 is due to the relative larger reactivity feedback at the lower power level.

The effect of the control valve opening becomes more significant with the decrease in the power level as shown in Fig 5.4. This can be explained by the effect of control valve opening on the main 'steam' pressure as shown in Fig 5.7. At a lower power level, the same magnitude change in the control valve opening can result in a larger pressure change, which further leads to larger change in the feed-water flow rate and the outlet header temperature.

In summary, the Canadian SCWR is a nonlinear MIMO system with strong cross-coupling between system inputs and outputs. Through the detailed analysis in this section, the dynamic characteristics of the Canadian SCWR have been revealed in both time and frequency domains. The dynamic analysis will play an important role in the subsequent control system design and analysis.

6   DECOUPLING CONTROL OF THE CANADIAN SCWR

6.1   Introduction

As indicated in Chapter 4, the Canadian SCWR can be modelled as a MIMO system. It has a large power-to-flow ratio, strong cross-coupling and a high degree of nonlinearities with respect to reactor power output. Because there is no steam generator to act as a cushion between the reactor and the turbine, the dynamics between the reactor and the turbine is strongly coupled. Any disturbances from the turbine side can have a direct effect on the reactor side. Due to the high power-to-flow ratio, the 'steam' temperature can be significantly influenced by minor changes in both the reactor power and the system pressure. For example, a 2% decrease in the reactor power can result in a 14°C decrease in the main 'steam' temperature. Furthermore, the system pressure can also affect the power-to-flow ratio, because any variation in the system pressure can have immediate effects on the feed-water flow rate through the feed-water pump.

Because of the strong coupling among system inputs and outputs, one can no longer treat a MIMO Canadian SCWR as three SISO systems. The cross-couplings have to be dealt with before a suitable control system can be designed. One way to reduce the effect of cross-coupling is to use a decoupling pre-compensator. Once the cross-couplings are softened, the pre-compensated system can be represented as a diagonal dominant MIMO system. Subsequently, the control system can be designed as if the system contains several relatively independent SISO systems. Once the control system is designed for the diagonal dominant system, the controller can be combined with the pre-compensator to form a multivariable control system. This controller will have the build-in decoupling effects.

From the operational experience of SCFPP, a large variation in the 'steam' temperature and pressure can cause a high degree of thermal stress on the system components, and therefore, to reduce their design life [134]. This is also true for SCWR. At the base load operation, such variations are relatively low due to mild regulations on system variables. However, for start-up or shutdown processes, during a setback or stepback manoeuvre, or load-following operations, the rate and the magnitude of the variations in the system variables can be significantly larger. In addition, if the correct proportion cannot be kept between the coolant flow rate and the reactor power, it will also lead to a large variation in the 'steam' temperature. The pre-compensator can reduce the effects of the reactor power and system pressure variations on the 'steam' temperature. Therefore, the power-to-flow ratio can follow the transient change of the reactor power and pressure changes adequately.

To design appropriate dynamic pre-compensator, the DNA method is used in the current work. This method relies on the frequency domain characteristics of the system [23]. From a dynamic point of view, the purpose of the pre-compensator is to maximize the diagonal dominance so that the cross-couplings among different system inputs and outputs can be minimized.

Furthermore, the Canadian SCWR is a highly nonlinear system. Its dynamic characteristics depends on the operating conditions of the reactor, in particular, the reactor power output. Thus, it is very difficult to synthesize a single controller to cover all operating conditions effectively. Under the constant pressure operation, the system pressure of the Canadian SCWR will remain unchanged. If the sliding pressure control mode is adopted, the pressure will be directly related to the reactor power. In both situations, the feed-water flow rate is required to be proportional to the reactor power to maintain the 'steam' temperature at a desired value. Thus, the operating condition is dictated by the reactor power and its dynamics also show strong dependence on the

reactor power. Therefore, in the current work, several operating conditions are selected, and the corresponding controllers are designed. Depending on the operating condition, the suitable controller is used. Since the reactor power is used to divide the nonlinear operating range into several linear approximations, a logic choice for the scheduling parameter would be the reactor power. The resulting control strategy is known as a gain scheduling control strategy.

Previous works on control system design and analysis for SCWR can be traced to SCFR [83] and SCLWR-H [84]. In the above work, the structures selected are simply multiple SISO feedback control loops. The effects of cross-coupling have just been ignored, which potentially limit the achievable performance. A sequential loop closing and trial-and-error approach have been used in the controller design. Although design improvements have been made subsequently [85], the adopted method is still not systematic due to lack of proper representation of dynamic relationships between inputs and outputs. Furthermore, all the design and analysis are based on the dynamic characteristics of the system around 100%FP operation, the operating condition induced nonlinearities have not been considered, either.

In the current work, cross-couplings among different system inputs and outputs have explicitly been considered in the control system design process. Gain scheduling strategy is adopted to deal with the nonlinearities. The results of the analysis have demonstrated that the inclusion of the above two steps can significantly improve the performance of the Canadian SCWR for both dynamic and steady-state operations. The closed-loop system is able to effectively reject disturbances to minimize the main 'steam' temperature variation.

The rest of the chapter is organised as follows. In Section 6.2, the DNA method is briefly introduced. In Section 6.3, design of a pre-compensator is carried out based on DNA method. In Section 6.4, a loop compensator is designed in the frequency domain. The performance of the

control system is evaluated through simulation in Section 6.5 under various operating scenarios. The nonlinearities of the system are dealt with by using a gain scheduling strategy in Section 6.6.

6.2 Direct Nyquist Array Method

A feedback control loop of the Canadian SCWR is shown in Fig 6.1, where $P(s)$ is the multivariable plant developed in Chapter 4 and shown in Appendix A, $K(s)$ is the decoupling pre-compensator whose transfer function matrix is shown in Eq. (6.2.1). Since $K(s)$ essentially makes the pre-compensated system diagonal dominant, the controller, $C(s)$ only contains diagonal elements as given in Eq. (6.2.2). From the controller design point of view, each controller on the diagonal can be designed independently. The signals $R(s)$, $E(s)$, $U(s)$ and $Y(s)$ are the desired setpoints, errors, system inputs and outputs in vector forms, respectively.

$$K(s) = \begin{bmatrix} k_{11}(s) & k_{12}(s) & k_{13}(s) \\ k_{21}(s) & k_{22}(s) & k_{23}(s) \\ k_{31}(s) & k_{32}(s) & k_{33}(s) \end{bmatrix} \tag{6.2.1}$$

$$C(s) = \begin{bmatrix} c_1(s) & 0 & 0 \\ 0 & c_2(s) & 0 \\ 0 & 0 & c_3(s) \end{bmatrix} \tag{6.2.2}$$
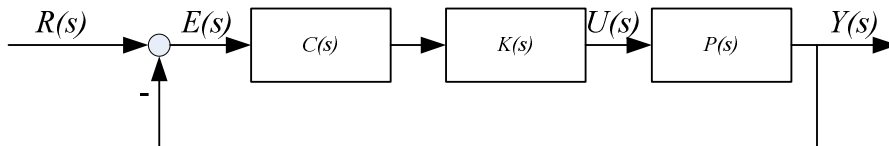
Fig 6.1 Feedback control loop of the Canadian SCWR

Let $G(s)$ be the pre-compensated plant and $Q(s)$ be the loop transfer function matrix defined as

$$G(s) = P(s)K(s) = \begin{bmatrix} g_{11}(s) & g_{12}(s) & g_{13}(s) \\ g_{21}(s) & g_{22}(s) & g_{23}(s) \\ g_{31}(s) & g_{32}(s) & g_{33}(s) \end{bmatrix} \tag{6.2.3}$$

$$Q(s) = P(s)K(s)C(s) = \begin{bmatrix} q_{11}(s) & q_{12}(s) & q_{13}(s) \\ q_{21}(s) & q_{22}(s) & q_{23}(s) \\ q_{31}(s) & q_{32}(s) & q_{33}(s) \end{bmatrix} \tag{6.2.4}$$

To maintain the closed-loop system stability, the controller $C(s)$ must be chosen so that the loop transfer function can satisfy the DNA stability theorem, which is stated as follows [124]:

Let the Gershgorin bands based on $q_{ii}(s)$ exclude the point (-1+j0). Let the ith Geshgorin band encircles the point (-1+j0) N_i time anti-clockwise. Then, the closed-loop system is stable if and only if

$$\sum_{i=1}^{n} N_i = p_0$$

where p_0 is the number of unstable poles of $Q(s)$. The Gershgorin bands can be obtained as follows: on the loci of $q_{ii}(j\omega)$ superimpose, at each point, a circle of radius $\sum_{\substack{j=1 \\ j \neq i}}^{n} |q_{ij}(j\omega)|$ or

$\sum_{\substack{j=1 \\ j \neq i}}^{n} |q_{ji}(j\omega)|$, n is the highest order of the denominator polynomial of the loop transfer function matrix. Based on the analysis of the SM, the Canadian SCWR plant is a stable process. Hence, it leads $p_0 = 0$.

The control system design using the DNA method consists of two steps:

(1) First, the pre-compensator $K(s)$ is designed to decouple the system $P(s)$ as much as possible, i.e. to maximize the diagonal dominance of $G(s)$. Using the DNA method, the

objective is to maximize the column dominance. There are two possible solutions to this problem:

One is steady-state decoupling. The decoupling matrix can be obtained by selecting $K(s) = P^{-1}(0)$. Using the steady-state decoupling, it can only achieve column dominance at the steady-state or for very low frequency.

The other option is dynamic decoupling, while the elements of the pre-compensator are a function of frequency. In the current case, the dynamic decoupling has to be used, because the amount of cross-coupling of *P(s)* at different frequencies is different.

(2) Once diagonal dominance is achieved, the loop compensator *C(s)* is synthesized to shape the Gershgorin bands in such a way that they do not encircle the point (-1+j0) to achieve the closed-loop system stability [23, 124].

6.3 Design of the Pre-compensator

Since the DNA method focuses on column dominance, a measure of column dominance for the *j*th column is calculated as

$$d_j(\omega) = \frac{\sum_{\substack{i=1 \\ i \neq j}}^{3} \left| p_{ij}(j\omega) \right|}{\left| p_{jj}(j\omega) \right|} \tag{6.3.1}$$

The column dominance can be considered as the effects of one specific input to the off-diagonal outputs over the diagonal one. If any value of $d_j(\omega)$ is greater than unity, this column will no longer be considered as column dominant. The frequency range considered in the current study is from 0.001 to 10.0rad/s. The column dominance of the SM at different frequencies is shown in

Fig 6.2. As can be seen, the first column is column dominant already, which means that the feed-water flow rate has dominant influence on the outlet header temperature as compared to the reactor power and the main 'steam' pressure. The second column is not column dominant. This means that the control rod reactivity can have significant influence on both the outlet header temperature and the reactor power. Neither does the third column, which means that the control valve opening can affect both the outlet header temperature and main 'steam' pressure significantly. Further decoupling is needed for these two input-output pairs.
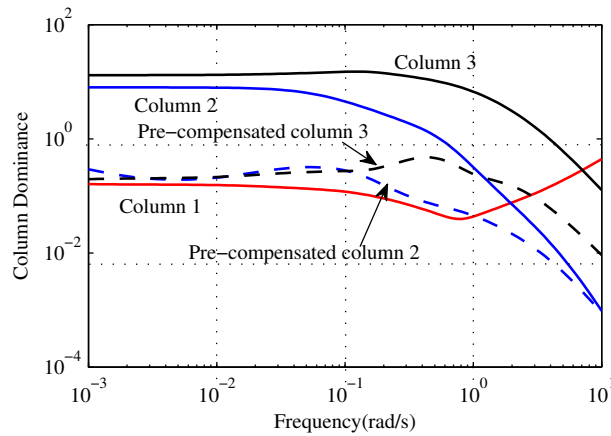
Fig 6.2 Column dominance of the original and pre-compensated plant

The pre-compensator $K(s)$ is designed to decouple $P(s)$ so that the compensated system becomes column dominant. Pseudo-diagonalization method is adopted to synthesize $K(s)$. Assume that the dynamic pre-compensator can be represented as:

$$K(s) = [k_1(s), k_2(s), k_3(s)] \tag{6.3.2}$$

where $k_j(s) = [k_{1j}(s), k_{2j}(s), k_{3j}(s)]^T$ ($j = 1, 2, 3$), is a column vector having the form

$$k_j(s) = k_{0j} + \ldots + k_{\beta j}s^{\beta}$$

each k_{lj} ($l = 1, 2, \ldots, \beta$) is a column vector and β is the highest order of $k_j(s)$.

Thus,

$$g_{ij}(j\omega) = \gamma_i^T(j\omega)\eta_j \qquad (6.3.3)$$

where s is replaced by $j\omega$, and $\gamma_i^T(j\omega)$ is a row vector

$$\gamma_i^T(j\omega) = [p_i^T(j\omega), j\omega p_i^T(j\omega), ..., (j\omega)^\beta p_i^T(j\omega)]$$

in which $p_i^T(s) = [p_{i1}(s), p_{i2}(s), p_{i3}(s)]$, denotes the ith row of $P(s)$ and η_j is a column vector composed of the coefficients of $k_j(s)$

$$\eta_j = [k_{0j}^T, ..., k_{\beta j}^T]^T$$

To maximize the column dominance, one can minimize the following function

$$J_j = \frac{\displaystyle\sum_m w_m \left\{ \sum_{i \neq j} \left| \gamma_i^T(j\omega_m)\eta_j \right|^2 \right\}}{\displaystyle\sum_m w_m \left| \gamma_i^T(j\omega_m)\eta_j \right|^2} \qquad (6.3.4)$$

where w_m is the weight associated with frequency ω_m.

The multi-frequency ALIGN algorithm can be used to solve Eq. (6.3.4) [23]. During the pseudo-diagonalization process, the choice of frequency range and its associated weighting coefficient is of significant importance. The frequency range can be determined by considering the frequency contents of the input signals and disturbances. For the weighting coefficients, a trial-and-error method can be used. For example, if one set of coefficients does not satisfy the requirement for some frequencies, then the weighting coefficients can be adjusted for those frequencies in the subsequent calculation. The coefficients in each elements of the pre-compensator η_j can be determined using a procedure outlined in [135].

Once column dominance of *G(s)* is established, it will not be destroyed by any scaling on the column of *K(s)*. Therefore, a realizable compensator can be obtained by dividing $k_j(s)$ by any stable polynomial of degree β or greater to simplify the implementation.

6.3.1 First Column of the Pre-compensator

As shown in Fig 6.2, since the first column has already exhibited column dominance, the pre-compensator can be chosen as

$$k_1(s) = \begin{bmatrix} 1.0 & 0.0 & 0.0 \end{bmatrix}^T$$

6.3.2 Second Column of the Pre-compensator

The order of the polynomial in the three elements of the second column of the pre-compensator is set as 0, 1 and 0, respectively. The frequency weights are chosen to be uniform. The second column can be obtained as

$$\begin{bmatrix} 0.53 & 1.95s + 0.24 & 0.47 \end{bmatrix}^T$$

To ensure the pre-compensator is realizable, every element is divided by (1.95s+0.24). Hence, the second column now becomes:

$$k_2(s) = \begin{bmatrix} \dfrac{0.53}{1.95s + 0.24} & 1.0 & \dfrac{0.47}{1.95s + 0.24} \end{bmatrix}^T$$

Mathematically, the purpose of the second column of the pre-compensator is to enhance the dominance of the second element in the second column of *P(s)*, while to reduce that of the other two elements. The column dominance of the pre-compensated system can be seen in Fig 6.2.

Physically, it means that, with the pre-compensation, the control rod reactivity has the largest effects on the reactor power than any other inputs. Similarly, the effects of the control rod

reactivity on the outlet heater temperature and main 'steam' pressure are effectively reduced as well. This is demonstrated by the gain reductions in Fig 6.3.

6.3.3 Third Column of the Pre-compensator

The order of the polynomial in the three elements of the third column of the pre-compensator is set as 1, 0 and 2, respectively. The weightings in the frequency range are chosen to be uniform. The third column of the pre-compensator can be obtained as

$$\begin{bmatrix} -1.23s - 0.21 & 6.0*10^{-3} & 1.24s^2 + 1.16s + 0.23 \end{bmatrix}^T$$

Similarly, dividing every element by (1.24s^2+1.16s+0.23), a realizable third column of the pre-compensator can be obtained as

$$k_3(s) = \begin{bmatrix} \dfrac{-1.23s - 0.21}{1.24s^2 + 1.16s + 0.23} & \dfrac{6.0*10^{-3}}{1.24s^2 + 1.16s + 0.23} & 1.0 \end{bmatrix}^T$$

The column dominance of the third column has been achieved as shown in Fig 6.3.

Based on Eq. (6.3.2), the pre-compensator *K(s)* can be obtained as

$$K(s) = \begin{bmatrix} 1.0 & \dfrac{0.53}{1.95s + 0.24} & \dfrac{-1.23s - 0.21}{1.24s^2 + 1.16s + 0.23} \\ 0.0 & 1.0 & \dfrac{6.0*10^{-3}}{1.24s^2 + 1.16s + 0.23} \\ 0.0 & \dfrac{0.47}{1.95s + 0.24} & 1.0 \end{bmatrix} \tag{6.3.5}$$

The column dominance of the pre-compensated system is validated in time domain by applying a unit step change, one at a time, at each respective input; the responses are shown in Fig 6.3. For the outlet header temperature, the effects of the control rod reactivity and control valve opening are significantly reduced. For the reactor power, the dominance of the control rod reactivity is

slightly improved. The magnitude of the control valve opening on the main 'steam' pressure is larger than those of the feed-water flow rate and the control rod reactivity. Although the magnitude is not significantly larger, the speed of the response has been improved significantly.

In frequency domain, the Nyquist array of the pre-compensated system with Gershgorin bands for the diagonal elements is shown in Fig 6.4. The column dominance can also be shown by Gershgorin bands which reflect the magnitude of the off-diagonal transfer functions relative to the diagonal ones.
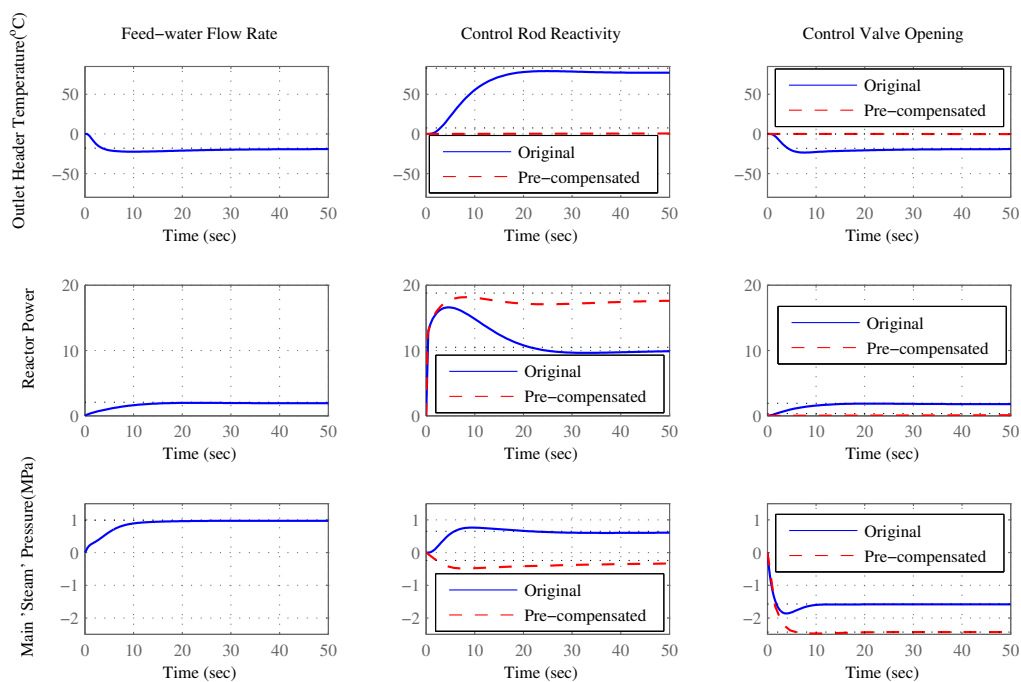
Fig 6.3 Step responses of the original and pre-compensated plant

Even though the DNA method is aimed at achieving column dominance, in fact, once column dominance is established, the row dominance is achieved as well. Physically, column dominance can be explained as the role of one specific input on the corresponding output related to the

diagonal of *P(s)*, while row dominance can be seen as the influence on one specific output from the corresponding input related to the diagonal of *P(s)*.
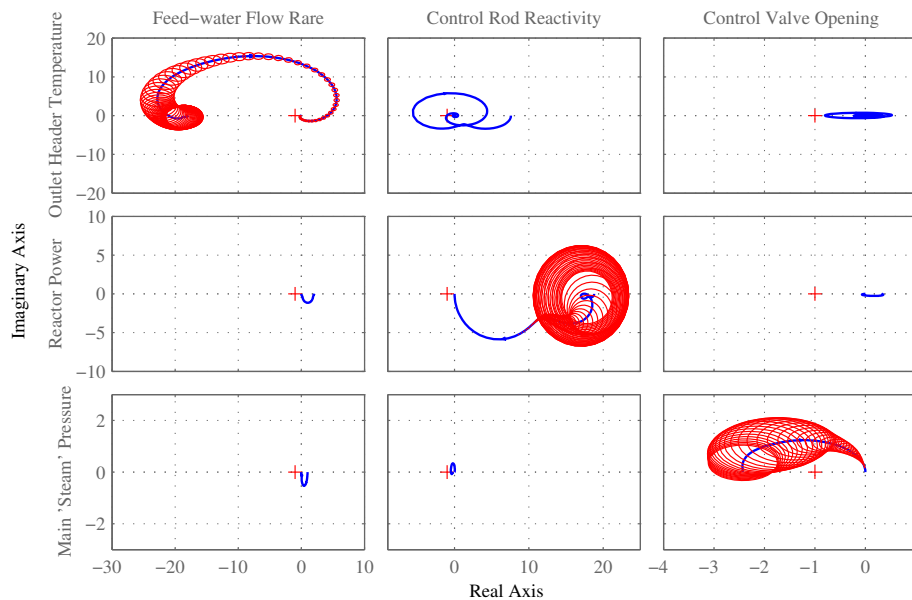
Fig 6.4 Direct Nyquist array with Gershgorin bands of the pre-compensated plant

6.4 Loop Compensator Design

With the pre-compensator, the new open-loop transfer function matrix is *G(s)*, which is diagonally dominant. For a diagonally dominant system, one can effectively treat the entire system as several SISO systems. Hence, control system design techniques for SISO system can be used. The stability of the system will be guaranteed as long as Gershgorin bands do not overlap the point (-1+j0) in Nyquist diagram. In this research, the design is carried out using Bode plots to shape the open-loop frequency responses of the pre-compensated plant as shown in Fig 6.5. The Bode plots of the uncompensated plant *G(s)* is also included for illustration purposes.

The control system should be designed to ensure that the permissible limits not be exceeded. The following specifications for the loop compensator design are [84]:

- The damping ratio should be larger than 0.75;

- The percentage of overshoot is less than 15%;

- DNA stability theorem must be satisfied.

6.4.1 Outlet Header Temperature Control

The outlet header temperature is regulated by the feed-water flow rate. To achieve zero steady-state error for a step setpoint change, a proportional plus integral (PI) compensator is selected. The PI compensator is designed as shown in Eq. (6.4.1) to satisfy the performance specifications

$$c_1(s) = -\frac{0.85s + 0.5}{s} \tag{6.4.1}$$

The Bode plot of the compensated outlet header temperature system is shown in Fig 6.5. The phase margin is 72degs and gain margin is 17dBs.

6.4.2 Reactor Power Control

The main control input for the reactor power is the control rods. When deviation of the reactor power from its setpoint is less than a certain value δ, the rate of the control rod drive is proportional to the error in power. If the error in power is larger than δ, the maximal rate is used. The control algorithm can be characterized by Eq. (6.4.2)

$$v = \begin{cases} v_{\max} \dfrac{q_{set} - q}{\delta}, (q_{set} - q < \delta) \\ v_{\max}, (q_{set} - q \geq \delta) \end{cases} \tag{6.4.2}$$

The rate of reactivity changes induced by the control rod is limited to 0.2mk/s. There is only one parameter δ to be determined. By considering the dynamics of the plant related to reactor

dynamics, the parameter δ is determined to be 0.04. A PI compensator is selected to achieve zero steady-state error. To achieve the requirements on the damping ratio and overshoot, the compensator is designed as

$$c_2(s) = 4.0 * 10^{-3} \frac{0.1s + 1.0}{s}$$

(6.4.3)

The Bode plot of the compensated reactor power system is shown in Fig 6.5. The phase margin is 82degs.

6.4.3 Main 'Steam' Pressure Control

The main 'steam' pressure is regulated by adjusting the control valve opening. The maximum rate of the valve stroke is limited to 100%/3.5s, which is chosen to be the same as that of a current BWR. A phase lag compensator is chosen to improve steady-state tracking accuracy and reduce cross-over frequency. To obtain the design specifications, the compensator is designed as

$$c_3(s) = -4.0 \frac{s + 1.0}{20.0s + 1.0}$$

(6.4.4)

The Bode plot of the compensated main 'steam' pressure system is shown in Fig 6.5 and the phase margin is 88degs.
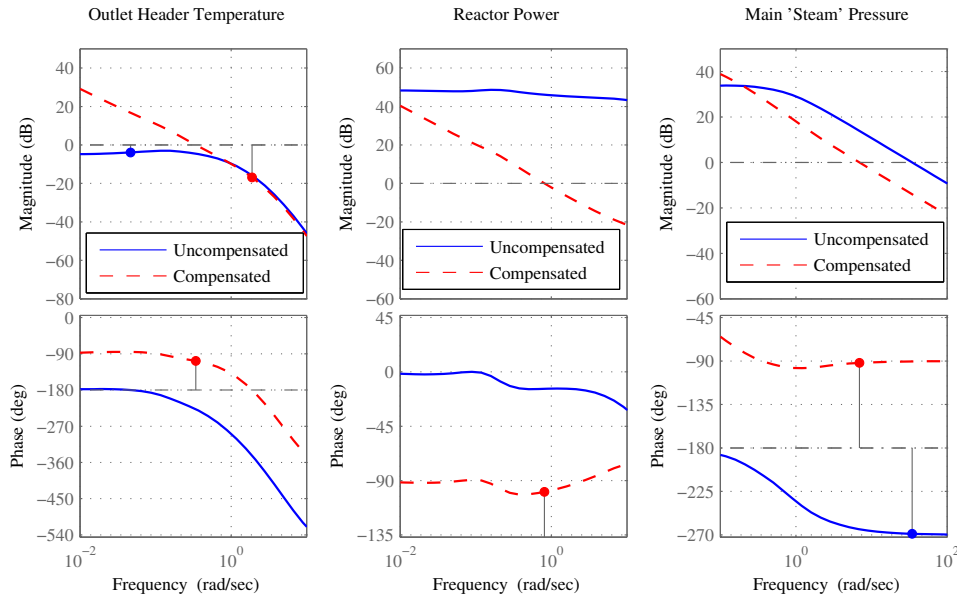
Fig 6.5 Bode plots the uncompensated and compensated system

The loop compensator is obtained as

$$C(s) = \begin{bmatrix} -\dfrac{0.85s+0.5}{s} & 0.0 & 0.0 \\ 0.0 & 4.0*10^{-3}\dfrac{0.1s+1.0}{s} & 0.0 \\ 0.0 & 0.0 & -4.0\dfrac{s+1.0}{20.0s+1.0} \end{bmatrix} \tag{6.4.5}$$

The direct Nyqist array of the compensated plant with Gershgorin bands is shown in Fig 6.6. It can be clearly seen that the DNA stability theorem is satisfied. If no loop controller can be found to satisfy the theorem, the diagonal dominance of the SM should be further improved.
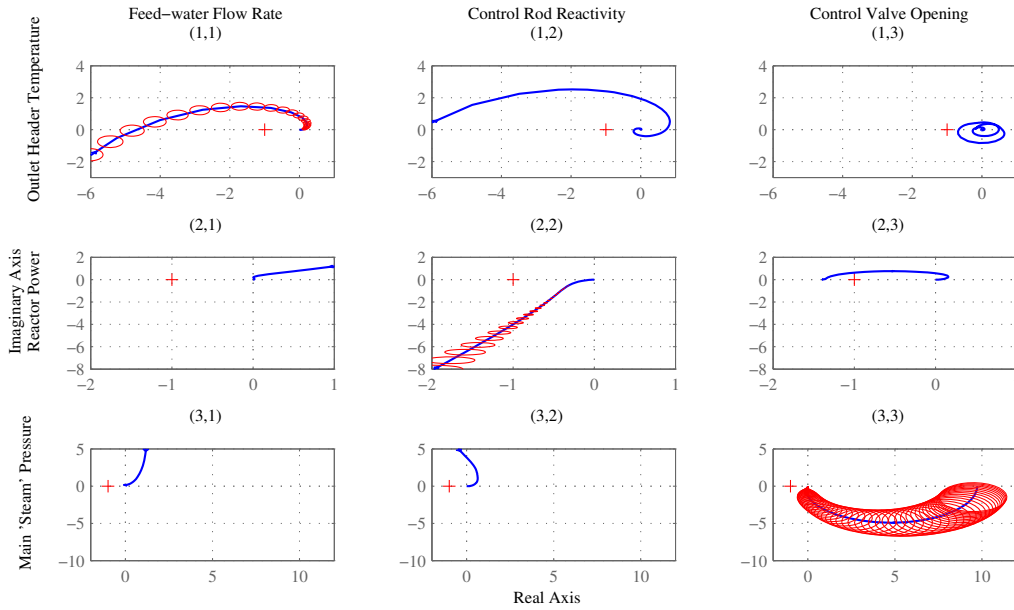
Fig 6.6 Direct Nyquist array with Gershgorin bands of the compensated plant

6.5 Performance Evaluation of the Designed Control System

Even though the control system design process has been divided into two steps (a) decoupling control via a pre-compensator and (b) three SISO controllers for the decoupled MIMO system, at the implementation stage, one can combine the pre-compensator and the diagonal controller into one single controller. The transfer function of the controller becomes

$$K(s)C(s) = \begin{bmatrix} -\dfrac{0.85s+0.5}{s} & \dfrac{2.12*10^{-3}(0.1s+1.0)}{s(1.95s+0.24)} & \dfrac{(4.92s+0.84)(s+1.0)}{(20.0s+1.0)(1.24s+1.16s+0.23)} \\[3mm] 0.0 & \dfrac{4.0*10^{-4}(0.1s+1.0)}{s} & -\dfrac{2.40*10^{-2}(s+1.0)}{(20s+1)(1.24s+1.16s+0.23)} \\[3mm] 0.0 & \dfrac{1.88*10^{-3}(0.1s+1.0)}{s(1.95s+0.24)} & -\dfrac{4.0(s+1.0)}{20.0s+1.0} \end{bmatrix} \quad (6.5.1)$$

The combined MIMO controller is represented by the shaded area in Fig 6.7. The part encircled by the dashed lines is the diagonal dominant version of the plant.
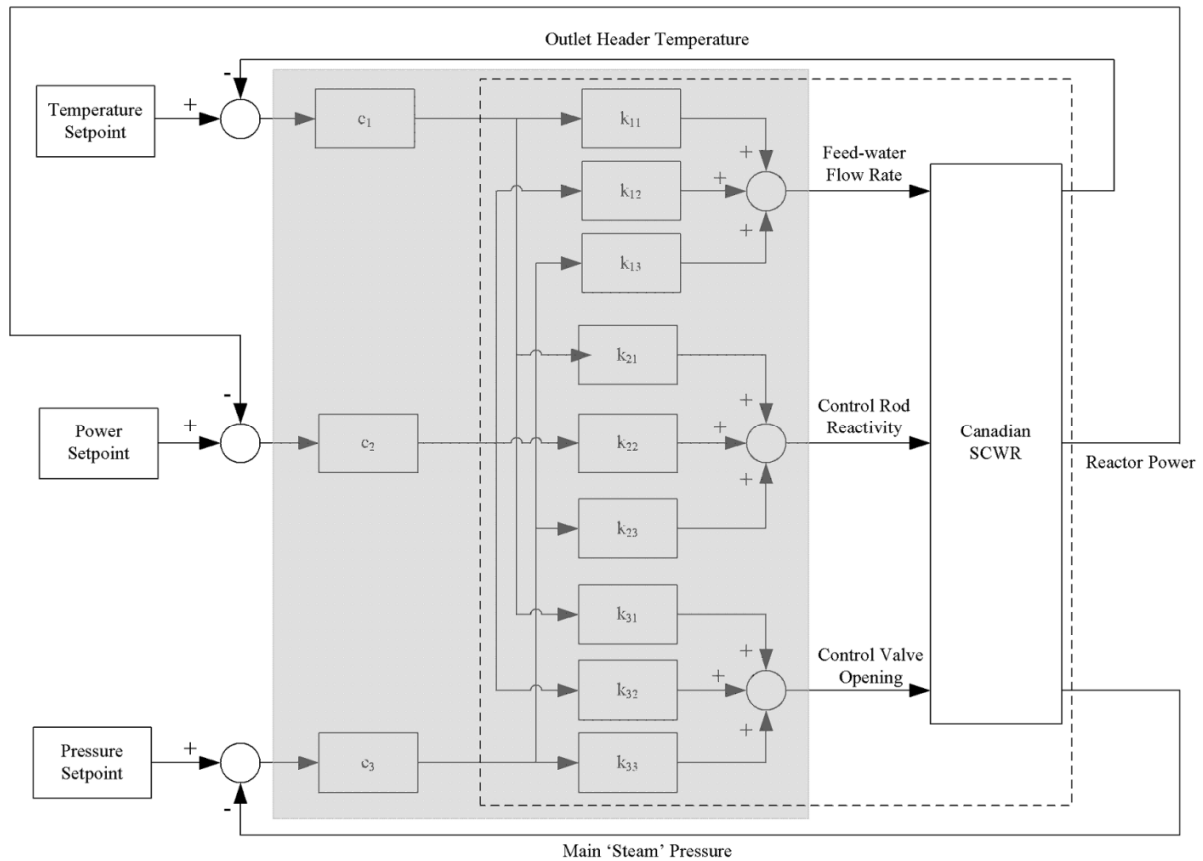
Fig 6.7 A block diagram representation of the decoupling control system

To evaluate the performance of the closed-loop system with the designed control system, simulations are carried out. The simulation involves introducing perturbations at 5 seconds: (a) a $5^{\circ}C$ step increase in the outlet header temperature setpoint, (b) a 5% step decrease in the reactor power setpoint, (c) a 0.2MPa step increase in the main 'steam' pressure setpoint, and (d) a $5^{\circ}C$ step decrease in the feed-water temperature.

The selected simulation scenarios are based on typical operations encountered of a power plant to comprehensively examine the performances of the designed control system. All simulations

are carried out with full nonlinear plant model: the DM, in which the reactor model is developed in Chapter 3.

6.5.1 Step Increase in the Outlet Header Temperature Setpoint

The responses of the DM to a 5°C step increase in the outlet header temperature setpoint are shown in Fig 6.8. The outlet header temperature increases and settles to its new setpoint as shown in Fig 6.8(a). The reactor power and main 'steam' pressure do not change much. Under the temperature control system, the feed-water flow rate decreases by detecting the setpoint change as shown in Fig 6.8(d). The feed-water flow rate is normalized. The regulation in the outlet header temperature has little influence on other systems because $k_{21}(s)$ and $k_{31}(s)$ are both zeros in Eq. (6.3.5), which are k_{21} and k_{31} in Fig 6.7.
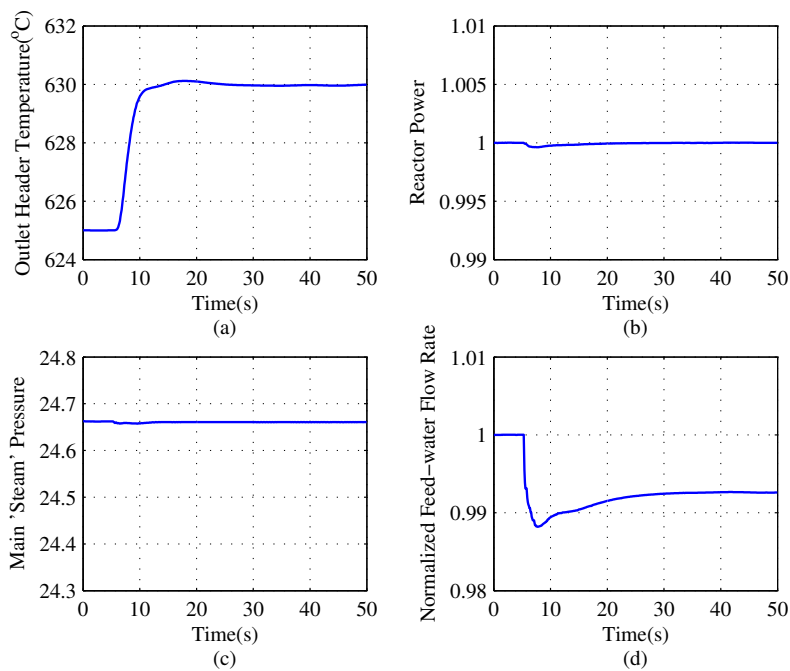
Fig 6.8 Responses to a step increase in the outlet header temperature setpoint

6.5.2 Step Decrease in the Reactor Power Setpoint

The setpoint of the reactor power is decreased stepwise by 5% at 5 seconds and the responses of the DM are shown in Fig 6.9. The reactor power promptly responds to its setpoint change and settles at 95% as shown in Fig 6.9(b). In the Fig 6.9(a), the outlet header temperature decreases with the decrease of the reactor power and returns to its setpoint under the temperature control system. The variation on the outlet header temperature from its setpoint is less than 1°C. Under the designed control system, the feed-water flow rate can response to the change of the reactor power quickly to suppress the temperature variation, which can be seen in Fig 6.9(d). During the process, there is only a minor fluctuation in the main 'steam' pressure as shown in Fig 6.9(c).
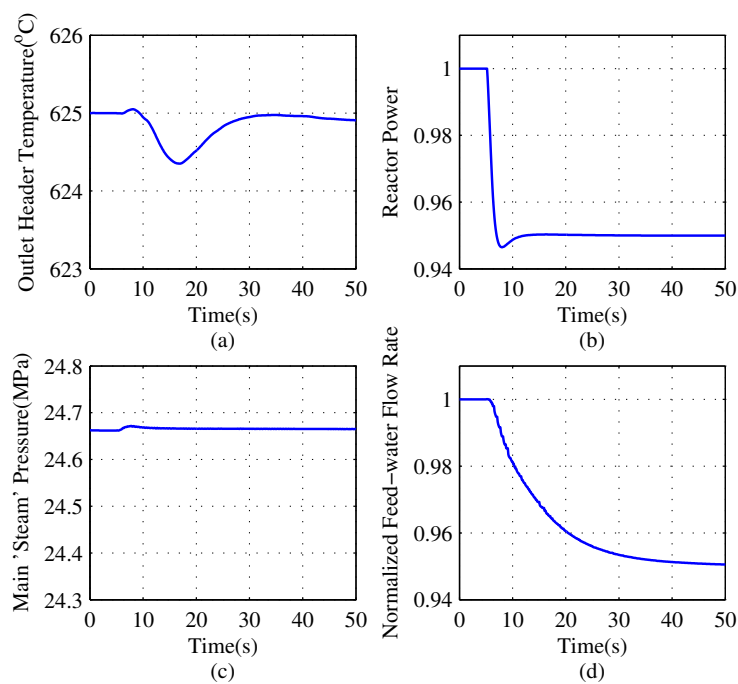
Fig 6.9 Responses to a step decrease in the reactor power setpoint

6.5.3 Step Increase in the Main 'Steam' Pressure Setpoint

The responses of the DM to a 0.2MPa step increase in the main 'steam' pressure setpoint at 5 seconds are shown in Fig 6.10. As shown in Fig 6.10(b), the fluctuation in the reactor power is

small. It can be seen from Fig 6.10(c) that the pressure quickly settles at the new setpoint by regulating the control valve opening. For the fast effect of the pressure change on the feed-water flow rate as shown in Fig 6.10(d), the feed-water flow rate has undergone a transient and then stabilizes at a steady-state value. Therefore, a peak value of the outlet header temperature occurs as shown in Fig 6.10(a).
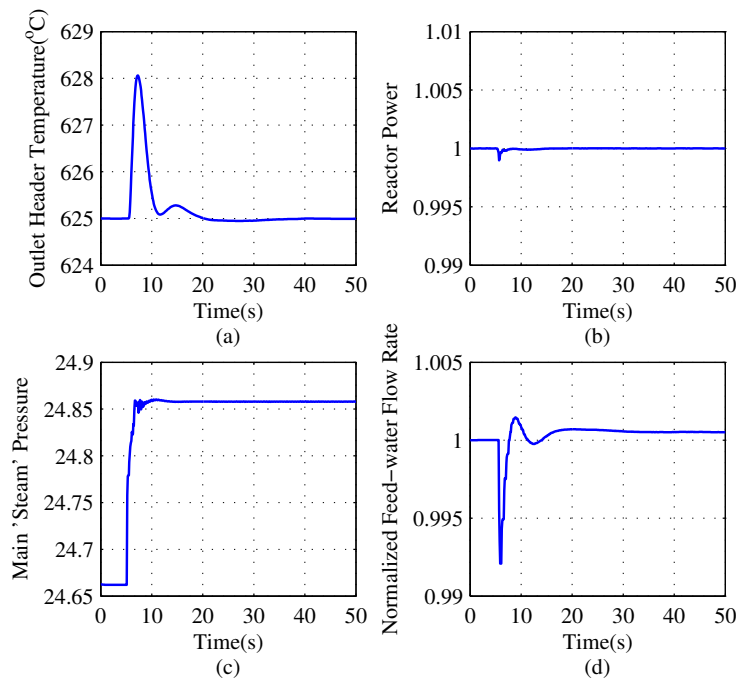
Fig 6.10 Responses to a step increase in the main 'steam' pressure setpoint

6.5.4 Step Decrease in the Feed-water Temperature

The responses of the DM to a 5°C step decrease in the feed-water temperature are shown in Fig 6.11. At the beginning, the outlet header temperature increases as a result of the decrease in the feed-water flow rate, which is a consequence of the decrease in the feed-water temperature. Then, the outlet header temperature decreases as a result of the decrease in the feed-water temperature. Finally, it increases to its setpoint by the temperature control system. During the process, the reactor power and the main 'steam' pressure do not change significantly. The normalized feed-

water flow rate is stabilized at 98.4%. It can be explained by Eq. (6.5.2) based on the energy conservation equation, where Pow is the reactor power; M is the feed-water mass flow rate; h_{out} is the specific enthalpy of the main 'steam' and h_{in} is the specific enthalpy of the feed-water. Specific enthalpy is a function of the fluid temperature and pressure. At the steady-state, the reactor power Pow, the main 'steam' pressure and the temperature are unchanged. Therefore, h_{out} is kept at its original value. h_{in} decreases for the decrease in the feed-water temperature and (h_{out}-h_{in}) is in fact increased. Thus, M is reduced to balance the energy conservation equation.

$$Pow = M(h_{out} - h_{in}) \tag{6.5.2}$$
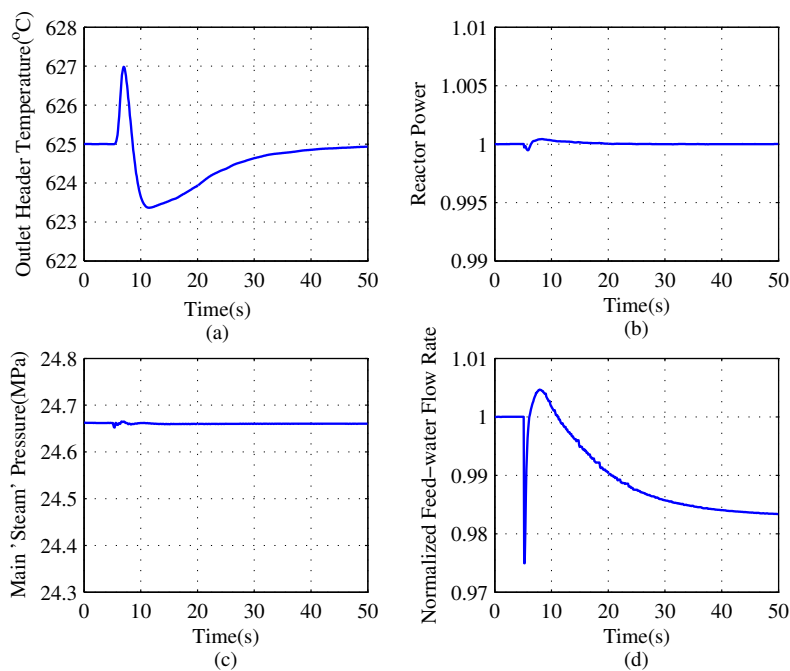
Fig 6.11 Responses to a step decrease in the feed-water temperature

The performance metrics of the designed control system to the setpoint changes are summarized in Table 6.1. It can be seen that the outputs follow their setpoints regulation with high accuracy

and the permissible limits are not exceeded. The ability to reject disturbances is also proven by introducing the feed-water temperature disturbance.

Table 6.1 Summary of the closed-loop system performance

Outputs	Rise Time	Settling Time	Overshoot/Undershoot	Steady-state Error
Outlet Header Temperature	7.5s	29.5s	2%	$0^{o}C$
Reactor Power	2.2s	13.2s	4%	0%
'Steam' Pressure	1.4s	4.5s	4%	0.003MPa

6.6 Gain Scheduling Control Strategies

As shown in Chapter 5, the dynamic characteristics of the Canadian SCWR are dependent on its operating points. The control system designed for 100%FP may not satisfy the performance requirements for other operating conditions. To illustrate such phenomena, three operating points are chosen: 60%FP, 80%/FP and 100%FP. The respective pre-compensators and loop controllers are designed. The linear dynamic models and their compensators at 80%FP and 60%FP are listed in Appendix B and C, respectively. The compensators are applied to regulate the plant at the selected operating points.

A 5% step increase in the reactor power setpoint is introduced at the 5th second at 80%FP. The compensators obtained at 80%FP and 100%FP are adopted. The responses of the DM are shown in Fig 6.12. Even though the reactor power responses are almost coincident in both cases as shown in Fig 6.12(b), it can be seen from the Fig 6.12(a) that the variation on the outlet header temperature with compensators at 80%FP is much less than that with compensators at 100%FP. Hence, the diagonal dominance of the plant at 80%FP cannot be achieved by the controller designed for 100%FP.
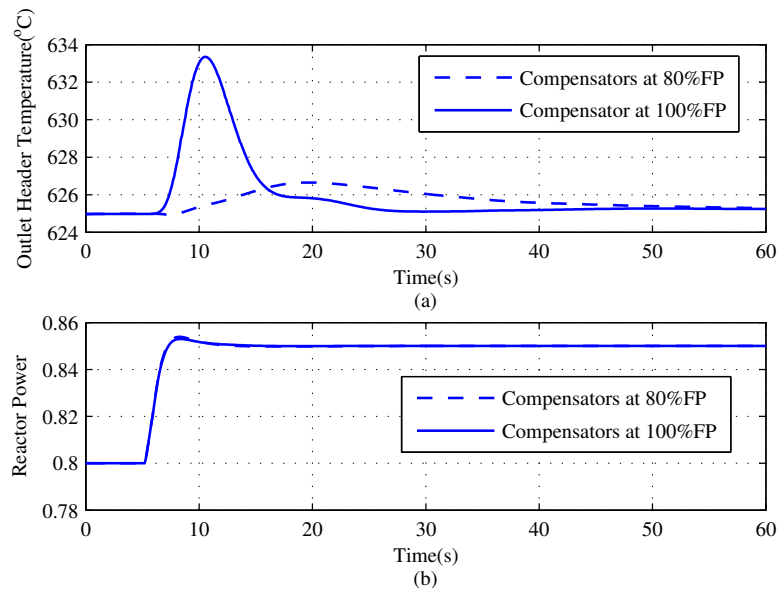
Fig 6.12 Responses to a 5% step increase in the reactor power setpoint at 80%FP

The largest closed-loop dominant eigenvalues at different operating points with three sets of compensators are shown in Table 6.2. At a lower power level, the eigenvalue is closer to the imaginary axis, therefore, it is more difficult to control. In other words, if the control system is designed based on the system information at 100%FP, but used to regulate the plant at 60%FP, the dominant closed-loop eigenvalues will be at $-0.19 \pm j0.22$, which are more vulnerable to model uncertainties.

Table 6.2 Largest closed-loop dominant eigenvalues at different operating points

Operating Point	Largest Dominant Eigenvalue		
	Compensators at 100%FP	Compensators at 80%FP	Compensators at 60%FP
100%FP	-0.80	-0.80	-0.82
80%FP	-0.50	-0.59	-0.63
60%FP	$0.19 \pm j0.22$	-0.33	-0.42

Under such a condition, if a $5^{o}C$ step increase in the outlet header temperature setpoint is introduced at the 5th second. The overshoot at the outlet header temperature can be as high as 44%

as shown in Fig 6.13. This is much larger than the design specification of 15% given in Section 6.4.
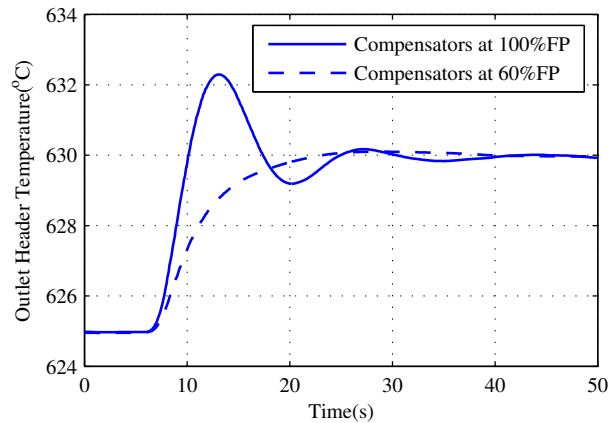
Fig 6.13 Outlet header temperature response to a 5°C step increase in its setpoint at 60%FP

Therefore, although a single set of compensators obtained at one operating point shows enough robustness to stabilize the plant, the control requirements may not be satisfied at another operating point.

One way to deal with this situation is to divide the entire system operating range into several smaller ranges. For each range, a set of controllers are synthesized. As the operating condition changes, the most appropriate set of controllers are used. Such a control strategy is known as 'gain scheduling' control [136]. To ensure smooth transitions from one range to another, the respective control signals in adjacent ranges can be combined through a weighted average operation.

A nuclear reactor power plant may have two operation modes: reactor-following-turbine or turbine-following-reactor. In the reactor-following-turbine mode, the reactor power is controlled to provide the right amount of power demanded by the turbine load to maintain the required reactor pressure. In the turbine-following-reactor mode, the turbine load is controlled to match

the reactor power output. Most of the existing nuclear power plants adopt the turbine-following-reactor operation mode to fully utilize the reactor capacity and to supply base load. In this current study, the turbine-following-reactor operation mode is selected.

In the turbine-following-reactor mode, the amount of power output is determined by the reactor power setpoint. The feed-water flow rate is proportional to the reactor power to maintain the 'steam' temperature constant. In a constant pressure operation, the main 'steam' pressure is kept constant. If a sliding pressure operation is used, the main 'steam' pressure will be dependent on the reactor power. The dynamic behaviour of the plant also changes with respect to changes in the reactor power.

In the constant pressure operation, the main 'steam' pressure is constant and the reactor is operated under the supercritical conditions. The operating range in this study is selected from 50% to 100%FP. For the sliding pressure operation, the main 'steam' pressure varies dependently on the reactor power output. At low power operations, the reactor may operate in a subcritical pressure region. This paper concentrates only on supercritical conditions. All designs are based on the constant pressure operation, but it has been tested for a sliding pressure operation at supercritical conditions.

Three fixed operating points have been selected to perform gain scheduling operation: 60%FP, 80%FP and 100%FP. Ranges around these operating points are also defined. These are shown in Fig. 6.14. The reactor power is chosen as the scheduling parameter. The actual control signals are the linear combination of respective compensators as shown in Fig 6.14. For example, the control signals at 90%FP are 50% from the compensators at 80%FP and 50% from the compensators at 100%FP.

Even though each of three set of compensators stabilizes the plant, the gain scheduling controller may not necessarily stabilize the same plant. If the switching between fixed controllers is slow with respect to the bandwidth of the plant, instability cannot occur [137]. The gain scheduling approach selected results in a smooth transition between the fixed controllers and the outputs of the adjacent controllers add through proper weights as the reactor power varies. One particular choice of these weights are shown in Fig 6.14. What's more, during the normal operation, the rate of the reactor power change is constrained. Therefore, the stability of the gain scheduling control can be maintained.
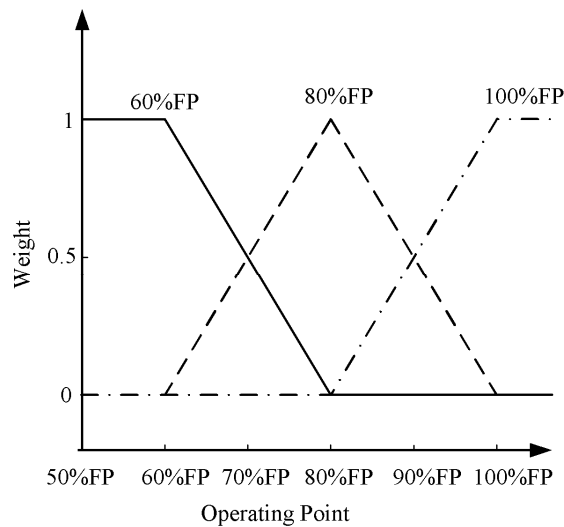
Fig 6.14 Gain scheduling control strategy based on weighted average

The permissible range of the main 'steam' temperature variation is limited during the operation of an SCFPP. A large variation of the 'steam' temperature from its desired value can cause undue thermal stress to the plant components and reduce the lifetime. In the current SCFPP, the temperature variation from its setpoint is $\pm 5^{\circ}C$ [138]. The same limit of an SCFPP is applied to test the performance of the designed control system based on two typical load patterns: 7%FP/min in the range of 90%-100%FP and 3%FP/min in the range of 50%-100%FP .

A load pattern 7%FP/min in the range of 90%-100%FP is applied at both constant and sliding pressure operation. For the sliding pressure operation, a typical load and pressure function of an SCFPP is adopted. The setpoint of the load is regulated as follows: decrease linearly from 100%FP to 90%FP from 100 seconds for a period 85.7 seconds, maintain at 90%FP for 200 seconds, then increase linearly from 90%FP to 100%FP in 85.7 seconds and stay at 100%FP to 600 seconds. The responses of the DM are shown in Fig 6.15.
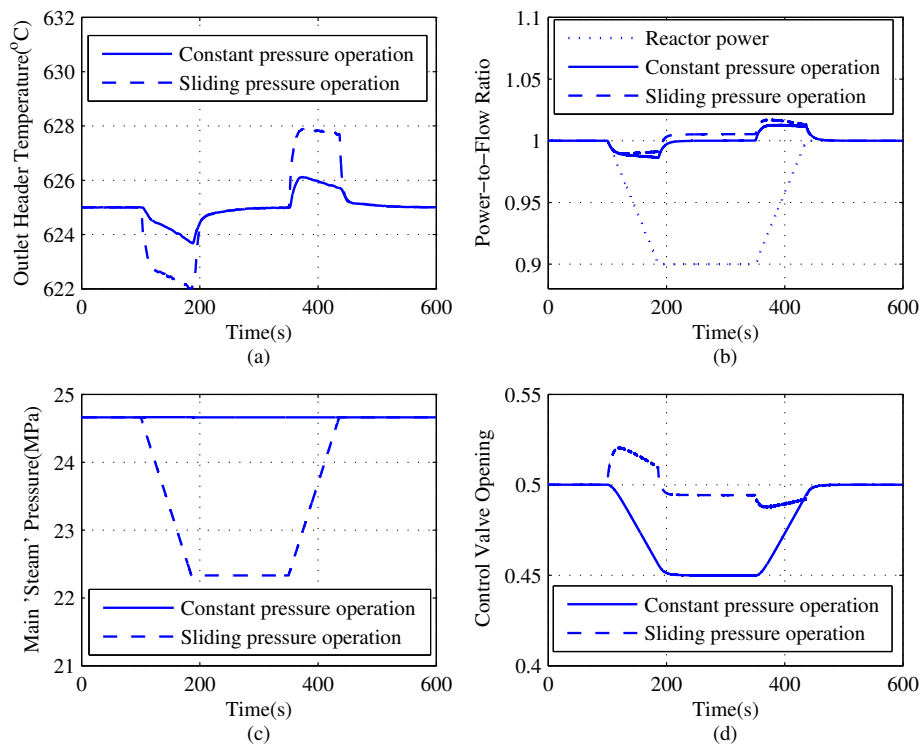
Fig 6.15 Responses of the DM to 7%FP/min load pattern

As shown in Fig 6.15(a), the outlet header temperature decreases (increases) as the reactor power decreases (increases). The outlet header temperature returns to its setpoint when the reactor power is kept constant. The outlet header temperature variation is around 1°C for the constant pressure operation and 3°C for the sliding pressure operation. The temperature variation is within

the limit in both cases. The main reason why the temperature variation for the sliding pressure operation is larger is because the change in the main 'steam' pressure causes disturbances in the feed-water flow rate.

As shown in Fig 6.15(b), the power-to-flow ratio increases as the reactor power increases. In the power-to-flow ratio calculation, the reactor power and the feed-water flow rate are both normalized. For a constant pressure operation, the power-to-flow ratio returns to one when the reactor power is kept constant. But for the sliding pressure operation, it returns to one when the reactor power is kept at 100%FP while it is changed to 1.01 when the reactor power is kept at 90%FP. This phenomena can be explained by Eq. (6.5.2). When the reactor power is kept at 90%FP, the main 'steam' pressure is kept at its corresponding value as shown in Fig 6.15 (c). (h_{out}-h_{in}) has a larger value at a lower supercritical pressure. Thus, M is less than 90% of its original value at 100%FP. Therefore, the power-to-flow ratio is increased. The change of the control valve opening at the sliding pressure operation is larger than that for the constant pressure operation. This is one benefit for adopting sliding pressure operation.

A 3%FP/min load change has beed applied to the Canadian SCWR in the range of 50%-100%FP at the constant pressure operation. The setpoint of the load is regulated as follows: decrease linearly from 100%FP to 50%FP from 100s in 1000 seconds, maintain at 50%FP for 200 seconds, then increase linearly from 50%FP to 100%FP in 1000 seconds and keep at 100%FP to 2500 seconds. The responses of the DM are shown in Fig 6.16.

The largest variation on the 'steam' temperature is approximately 4°C, which is within the limit. There are abrupt changes in the 'steam' temperature at 80%FP and 60%FP as shown in Fig 6.16(a). That is due to the switching of the compensators from one set to another, which affects the power-to-flow ratio as shown in Fig 6.16(d). The temperature fluctuation is larger for 60%FP.

To reduce the effect of controller switching transient, additional operating points can be included in the gain scheduling control strategy, or smoothing functions can be used to trim abrupt changes at the controller outputs.
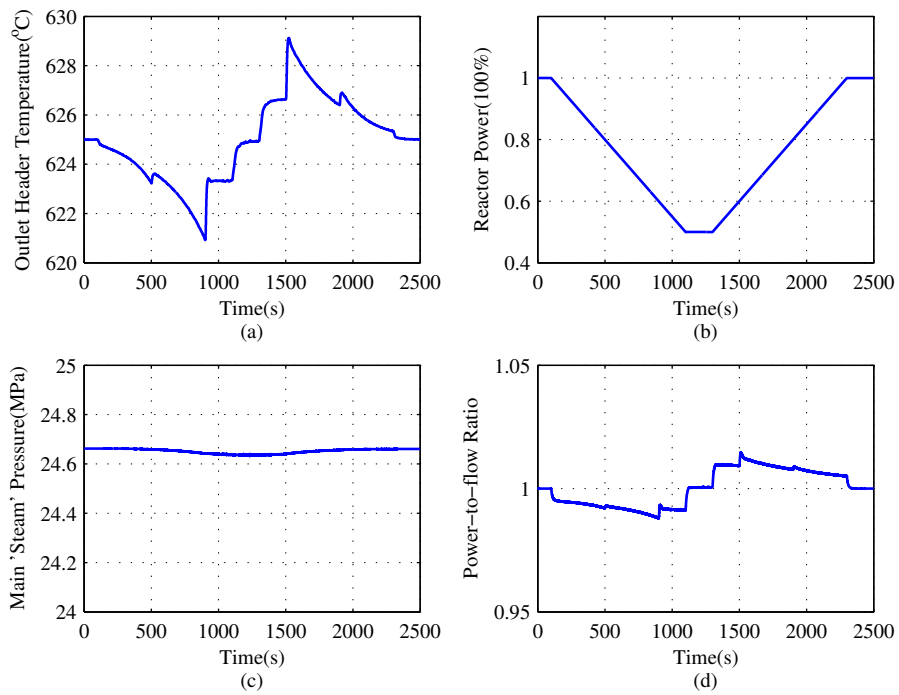
Fig 6.16 Responses of the DM to 3%FP/min load pattern

7   CONCLUSIONS AND FUTURE WORK

The conclusions and future work are presented in this chapter. The conclusions are drawn with reference to the research objectives and the obtained results. However, there are still some improvements and further work to be accomplished. Suggestions on future work are also discussed.

7.1   Conclusions

As mentioned in Chapter 1, the objectives of the study are: establish a suitable dynamic model, construct a linear dynamic model, perform dynamic analysis and design control system of the Canadian SCWR. The conclusions are drawn accordingly as follows:

1.) Dynamic model development of the Canadian SCWR. A dynamic model using moving boundary method is developed. It is verified with CFD code FLUENT and proved to be accurate enough to capture the main dynamics of the Canadian SCWR. The advantages of moving boundary method are derived by comparing with a fixed boundary method: larger time step, wider application range and higher numerical stability. The numerical simulations of the dynamic model show that the steady-state results agree well with the design parameter and the dynamic behaviours can be predicted by the dynamic model. The unique dynamics of the Canadian SCWR are compared with those of ACR as a demonstration of research motivations. The numerical simulations are carried out, and using the simulation data, a set of linear dynamic models are developed using system identification techniques. These models can reasonably predict the dynamic behaviours of the Canadian SCWR around the designed operating point.

2.) Linear dynamic model construction of the Canadian SCWR plant system. A simplified dynamic model of the Canadian SCWR plant system is developed based on mass, energy and momentum conservation equations. A linear dynamic model is obtained through linearization and represented in terms of a transfer function matrix. The linear dynamic model is validated against full order nonlinear models both in time domain and frequency domain. The linearized model can provide sufficient details on the dynamic properties of the Canadian SCWR and is suitable for dynamic analysis and control system studies.

3.) Dynamic analysis of the Canadian SCWR. Steady-state interaction is studied using RGA and dynamic interactions are analyzed based on Nyquist array. It is found that the outlet header temperature can be affected significantly by all three inputs. Due to the high power-to-flow ratio, the outlet header temperature is highly sensitive to the change in the feed-water flow rate or the reactor power. The reactor power is most sensitive to the adjustment of the control rods. The main 'steam' pressure can be influenced by both the feed-water flow rate and the control valve opening, but the latter is more dominant. Thus, the suggested input-output pairing for control system design is as follows: the outlet header temperature should mainly be regulated by the feed-water flow rate, the reactor power by the control rods, and the main 'steam' pressure by the control valve opening. The interactions at different power levels have also been analyzed. At different operating conditions, the steady-state magnitude and the response time of the system are different. This strong nonlinear behaviour can complicate the dynamic analysis and subsequent controller design.

4.) Control system design of the Canadian SCWR. Based on the developed dynamic models, decoupling control via pre-compensator has been used to reduce amount of cross-coupling among system inputs and outputs. It is shown that the pre-compensator can effectively

convert a highly coupled MIMO system into loosely coupled three SISO systems. Subsequently, a SISO controller design approach is used to synthesize three separate controllers for the decoupled loops. The final controller consists of the combination of the pre-compensator and the loop controllers. The variation in 'steam' temperature has been significantly suppressed by using the designed control system. The pre-compensator can adjust the feed-water flow rate to follow the change in the reactor power or pressure to regulate the power-to-flow ratio to a proper value. By doing so, the temperature control system is less affected by the power and pressure control systems. The performance of the designed control system has been evaluated under various operating scenarios using full nonlinear models. The study concludes that the controller designed for one operating condition may not work well under another operating condition. To deal with the nonlinear characteristics, a gain schedule control strategy is developed and the reactor power is selected as the scheduling parameter. Furthermore, the robustness of the controllers designed for different reactor power levels are also analyzed.

7.2 Future Work

Future research work related to the topics presented in this thesis can proceed in several directions:

1.) Dynamic model improvement. The dynamic model of the Canadian SCWR is verified with CFD and system codes, but it is not validated with experimental results. There is no timetable for building an SCWR yet, but the thermal-hydraulic experiments are being performed or to be performed. The thermal-hydraulic model can be corrected and improved against these experimental data. Another issue is the thermal-hydraulic/neutronics coupling of the Canadian SCWR. In the dynamic model, the power distribution is assumed to be a cosine function and

does not change with the thermal-hydraulic conditions. The thermal-hydraulic model supplies the reactivity feedback to the reactor kinetics model, in which only the power magnitude is changed not its distribution. The point reactor kinetics can be replaced by 1D reactor kinetics. Then the thermal-hydraulic/neutronics coupling can be formulated to represent more practical dynamics of the Canadian SCWR.

2.) Limit on the cladding temperature. One design criteria of the Canadian SCWR is that the cladding temperature should be less than 850°C. In the control system design process, the limit on variation of the 'steam' temperature is satisfied. A large variation of the 'steam' temperature may cause thermal stress and fatigue to important components and reduce their useful life. But exceeding the limit of the cladding temperature may cause much severer consequences: radiation leakage. Therefore, a sub-channel model may be introduced to replace the single-channel model and the maximum cladding surface temperature should be evaluated for different transient scenarios. Sufficient operation margin should be guaranteed during normal operation of the Canadian SCWR.

3.) Coordinated control of the Canadian SCWR. There are two basic operation modes in the nuclear power plant: turbine-following-reactor mode and reactor-following-turbine mode. For most nuclear power plants, the dynamics on the reactor side is slow while the dynamics on turbine side is much faster. To protect the expensive nuclear reactor from damages that may be caused by fast and large disturbances from the turbine side, the turbine-following-reactor mode is adopted. But the dynamics of the Canadian SCWR is also fast and the reactor side is coupled with the turbine side. Either of the two basic operation modes alone may not satisfy the performance requirement of the Canadian SCWR. Coordinated control is necessary to integrate the reactor side and the turbine side and consider them as a whole to regulate their parameters.

4.) Startup and shutdown process analysis. The scope of this thesis is limited to the supercritical conditions. The dynamics and operation criteria under subcritical conditions should also be investigated. Especially important part is the process of transition between subcritical and supercritical conditions during startup and shutdown. Having these knowledge, the best startup and shutdown strategies can be developed.

5.) Model predictive control of the Canadian SCWR. Model predictive control is a multivariable control algorithm. It uses the history of past control signals and an optimization cost function to calculate the optimum control signals over the receding prediction horizon. One of important advantages of this control algorithm is its ability to cope with hard constraints on controls and states. Some of the inputs and outputs of the Canadian SCWR are constrained, for example, the maximum rate of control valve stroke is limited to 100%/3.5s and the 'steam' temperature variation is limited to $\pm 5^{o}C$. The nonlinearities of the Canadian SCWR can be incorporated into the nonlinear model predictive control system design.

REFERECES

[1] L. Mez, "Nuclear energy–Any solution for sustainability and climate protection?," *Energy Policy,* vol. 48, pp. 56-63, 2012.

[2] Safety of Nuclear Power Reactors [Online]. Available: http://www.world-nuclear.org/info/inf06.html

[3] "A Technology Roadmap for Generation IV Nuclear Energy Systems," US DOE Nuclear Energy Research Advisory Committe and the Generation IV International Forum GIF-002-00, 2002.

[4] X. Cheng and T. Schulenberg, "Heat Transfer at Supercritical Pressure—Literature Review and Application to an HPLWR," Forschungszentrum Karlsruhe, Germany2001.

[5] I.L. Pioro and R.B. Duffey, *Heat Transfer and Hydraulic Resistance at Supercritical Pressures in Power Engineering Applications*. New York, USA: ASME Press, 2007.

[6] A. Franco and A.R. Diaz, "The future challenges for "clean coal technologies": Joining efficiency increase and pollutant emission control," *Energy,* vol. 34, pp. 348-354, 2009.

[7] Y. Oka and S. Koshizuka, "Supercritical-pressure, once-through cycle light water cooled reactor concept," *Journal of Nuclear Science and Technology,* vol. 38, pp. 1081-1089, 2001.

[8] D. Squarer, T. Schulenberg, D. Struwe, Y. Oka, D. Bittermann, N. Aksan, C. Maraczy, R. Kyrki-Rajamaki, A. Souyri, and P. Dumaz, "High performance light water reactor," *Nuclear Engineering and Design,* vol. 221, pp. 167-180, 2003.

[9] C.K. Chow and H.F. Khartabil, "Conceptual fuel channel designs for CANDU-SCWR," *Nuclear Engineering and Technology,* vol. 40, pp. 139-146, 2008.

[10] M. Yetisir, W. Diamond, L.K.H. Leung, D. Martin, and R.B. Duffey, "Conceptual Mechanical Design for a Pressure-tube Type Supercritical Water-cooled Reactor," in

Proceedings of the 5th International Symposium on Supercritical-Water-Cooled Reactors (ISSCWR5), Vancouver, British Columbia, Canada, March 13-16, 2011.

[11] L.K.H. Leung, "Developing the Canadian SCWR Concept for Addressing GIF Technology Goals," presented at the the 3rd China-Canada Joint Workshop on Supercritical Water-cooled Reactors (CCSC-2012) Xi'an, China, 2012.

[12] G. Harrisson and G. Marleau, "2-D and 3-D Evaluation of Neutronic Properties along a Canadian SCWR Fuel Channel," presented at the the 3rd China-Canada Joint Workshop on Supercritical Water-cooled Reactos (CCSC-2012), Xi'an, China, 2012.

[13] M.H. McDonald, B. Hyland, H. Hamilton, L.K.H. Leung, N. Onder, J. Pencer, and R. Xu, "Pre-conceptual Fuel Design Concepts for the Canadian Supercritical Water-cooled Reactor," in *Proceedings of the 5th International Sympoium on Supercritical Water-cooled Reactors (ISSCWR5)*, Vancouver, British Columbia, Canada, March 13-16, 2011.

[14] D. Novog, G. McGee, D. Rhodes, and M. Yetisir, "Safety Concepts and Systems of the Canadian SCWR," presented at the the 3rd China-Canada Joint Workshop on Supercritical Water-cooled Reactors (CCSC-2012), Xi'an, China, 2012.

[15] E.N. Onder, Y.F. Rao, and J. Pencer, "Assessment of ASSERT Subchannel Code for the Canadian SCWR Bundle at Supercritical Conditions," presented at the the 3rd China-Canada Joint Workshop on Supercritical Water-cooled Reactors (CCSC-2012), Xi'an, China, 2012.

[16] L. Blomeley and J. Pencer, "Uncertainties of In-core Materials with Respect to Nuclear Data for the Canadian SCWR," presented at the the 3rd China-Canada Joint Workshop on Supercritical Water-cooled Reactors (CCSC-2012), Xi'an, China, 2012.

[17] W.G. Cook and R.P. Olive, "Corrosion Product Deposition on Two Possible Fuel Geometries in the Canadian SCWR Concept," presented at the the 3rd China-Canada Workshop on Supercritical Water-cooled Reactors (CCSC-2012), Xi'an, China, 2012.

[18] Q. Xue, K.Y. Zhou, X.H. Xu, and J.Q. Xu, "Dynamic Characteristics of Single-Phase Heated Tubes of Supercritical and Ultra-Supercritical Boilers," *Journal of Power Engineering,* vol. 26, pp. 27-31, 2006.

[19] J.H. Mcfadden, E.D. Hughes, R.E. Narum, and G.C. Gose, "RETRAN02-A Program for Transient Thermal-hydraulic Analysis of Complex Fluid Flow Systems," EPRI NP-1850, May, 1981.

[20] B.N. Hanna, "CATHENA: A thermalhydraulic code for CANDU analysis," *Nuclear Engineering and Design,* vol. 180, pp. 113-131, 1998.

[21] J.X. Zheng, T.K. Chen, X.J. Chen, and D. Yang, "Dynamic Thermal-hydraulic Models for Single-phase Heated Tubes," *Advanced In Mechanics,* vol. 27, pp. 538-548, 1997.

[22] E. Bristol, "On a new measure of interaction for multivariable process control," *IEEE Transactions on Automatic Control,* vol. 11, pp. 133-134, 1966.

[23] J.M. Maciejowski, *Multivariable Feedback Design*. Wokingham, Berkshire, UK: Addison-Wesley Publishing Company, 1989.

[24] J. Yang, Y. Oka, Y. Ishiwatari, J. Liu, and J. Yoo, "Numerical investigation of heat transfer in upward flows of supercritical water in circular tubes and tight fuel rod bundles," *Nuclear Engineering and Design,* vol. 237, pp. 420-430, 2007.

[25] X. Cheng, B. Kuang, and Y.H. Yang, "Numerical analysis of heat transfer in supercritical water cooled flow channels," *Nuclear Engineering and Design,* vol. 237, pp. 240-252, Feb 2007.

[26] Y.N. Zhang, C. Zhang, and J. Jiang, "Numerical simulation of heat transfer of supercritical fluids in circular tubes using different turbulence models," *Journal of Nuclear Science and Technology,* vol. 48, pp. 366-373, 2011.

[27] B. Zhang, J.Q. Shan, and J. Jiang, "Numerical analysis of supercritical water heat transfer in horizontal circular tube," *Progress in Nuclear Energy,* vol. 52, pp. 678-684, 2010.

[28] Q.L. Wen and H.Y. Gu, "Numerical simulation of heat transfer deterioration phenomenon in supercritical water through vertical tube," *Annals of Nuclear Energy,* vol. 37, pp. 1272-1280, 2010.

[29] M.T. Kao, M. Lee, Y.M. Ferng, and C.C. Chieng, "Heat transfer deterioration in a supercritical water channel," *Nuclear Engineering and Design,* vol. 240, pp. 3321-3328, 2010.

[30] A. Kiss and A. Aszodi, "Summary for three different validation cases of coolant flow in supercritical water test sections with the cfd code ansys cfx 11.0," *Nuclear Technology,* vol. 170, pp. 40-53, 2010.

[31] T. Gallaway, S.P. Antal, and M.Z. Podowski, "Multi-dimensional model of fluid flow and heat transfer in Generation-IV Supercritical Water Reactors," *Nuclear Engineering and Design,* vol. 238, pp. 1909-1916, 2008.

[32] M. Sharabi and W. Ambrosini, "Discussion of heat transfer phenomena in fluids at supercritical pressure with the aid of CFD models," *Annals of Nuclear Energy,* vol. 36, pp. 60-71, 2009.

[33] Q.L. Wen and H.Y. Gu, "Numerical investigation of acceleration effect on heat transfer deterioration phenomenon in supercritical water," *Progress in Nuclear Energy,* vol. 53, pp. 480-486, 2011.

[34] S. Mokry, I. Pioro, A. Farah, K. King, S. Gupta, W. Peiman, and P. Kirillov, "Development of supercritical water heat-transfer correlation for vertical bare tubes," *Nuclear Engineering and Design,* vol. 241, pp. 1126-1136, 2011.

[35] B. Zhang, J.Q. Shan, and J. Jiang, "Simulation of heat transfer of supercritical water in obstacle-bearing vertical tube," *Nuclear Science and Techniques,* vol. 21, pp. 241-245, 2010.

[36] Z. Shang and S. Chen, "Numerical investigation of diameter effect on heat transfer of supercritical water flows in horizontal round tubes," *Applied Thermal Engineering,* vol. 31, pp. 573-581, 2011.

[37] Z. Shang, "CFD investigation of vertical rod bundles of supercritical water-cooled nuclear reactor," *Nuclear Engineering and Design,* vol. 239, pp. 2562-2572, 2009.

[38] H.Y. Gu, X. Cheng, and Y.H. Yang, "CFD analysis of thermal-hydraulic behavior of supercritical water in sub-channels," *Nuclear Engineering and Design,* vol. 240, pp. 364-374, 2010.

[39] J.L. Gou, Z. Shang, Y. Ishiwarari, Y. Oka, M. Yamakawa, and S. Ikejiri, "CFD analysis of heat transfer in subchannels of a Super Fast Reactor," *Nuclear Engineering and Design,* vol. 240, pp. 1819-1829, 2010.

[40] J.L. Gou, Y. Ishiwarari, Y. Oka, and M. Yamakawa, "CFD analyses in tight-lattice subchannels and seven-rod bundle geometries of a Super Fast Reactor," *Nuclear Engineering and Design,* vol. 241, pp. 1656-1666, 2011.

[41] H.Y. Gu, X. Cheng, and Y.H. Yang, "CFD analysis of thermal-hydraulic behavior in SCWR typical flow channels," *Nuclear Engineering and Design,* vol. 238, pp. 3348-3359, 2008.

[42] H.Y. Gu, Y.Q. Yu, X. Cheng, and X.J. Liu, "Numerical analysis of thermal-hydraulic behavior of supercritical water in vertical upward/downward flow channels," *Nuclear Science and Techniques,* vol. 19, pp. 178-186, 2008.

[43] Z. Shang and S. Lo, "Numerical investigation of supercritical water-cooled nuclear reactor in horizontal rod bundles," *Nuclear Engineering and Design,* vol. 240, pp. 776-782, 2010.

[44] Z. Shang and S. Lo, "CFD in supercritical water-cooled nuclear reactor (SCWR) with horizontal tube bundles," *Nuclear Engineering and Design,* vol. 241, pp. 4427-4433, 2011.

[45] Y.N. Zhang, C. Zhang, and J. Jiang, "Numerical simulation of fluid flow and heat transfer of supercritical fluids in fuel bundles," *Journal of Nuclear Science and Technology,* vol. 48, pp. 929-935, 2011.

[46] Y.N. Zhang, C. Zhang, and J. Jiang, "Numerical study on the turbulent mixing coefficient for supercritical fluids in subchannels," *Nuclear Technology,* vol. 177, pp. 98-106, 2012.

[47] X.B. Yang, G.H. Su, W.X. Tian, J.Y. Wang, and S.Z. Qiu, "Numerical study on flow and heat transfer characteristics in the rod bundle channels under super critical pressure condition," *Annals of Nuclear Energy,* vol. 37, pp. 1723-1734, 2010.

[48] A. Wank, J. Starflinger, T. Schulenberg, and E. Laurien, "Mixing of cooling water in the mixing chambers of the HPLWR--High Performance Light Water Reactor," *Nuclear Engineering and Design,* vol. 240, pp. 3248-3258, 2010.

[49] J. Yoo, Y. Oka, Y. Ishiwatari, J. Yang, and J. Liu, "Subchannel analysis of supercritical light water-cooled fast reactor assembly," *Nuclear Engineering and Design,* vol. 237, pp. 1096-1105, 2007.

[50] C.Y. Li, J.Q. Shan, and L.K.H. Leung, "Subchannel analysis of CANDU-SCWR fuel," *Progress in Nuclear Energy,* vol. 51, pp. 799-804, 2009.

[51] K. Kitou, K. Nishida, Y. Ishii, K. Fujimura, M. Matsuura, and S. Shiga, "Subchannel analysis to investigate the fuel assembly for the supercritical-water-cooled power reactor," *Journal of Nuclear Science and Technology,* vol. 41, pp. 1075-1082, 2004.

[52] T. Mukohara, S. Koshizuka, and Y. Oka, "Subchannel analysis of a fast reactor cooled by supercritical light water," *Progress in Nuclear Energy,* vol. 37, pp. 197-204, 2000.

[53] J.Q. Shan, B. Zhang, C.Y. Li, and L.K.H. Leung, "SCWR subchannel code ATHAS development and CANDU-SCWR analysis," *Nuclear Engineering and Design,* vol. 239, pp. 1979-1987, 2009.

[54] L. Ammirabile, "Studies on supercritical water reactor fuel assemblies using the sub-channel code COBRA-EN," *Nuclear Engineering and Design,* vol. 240, pp. 3087-3094, 2010.

[55] X. Cheng, T. Schulenberg, D. Bittermann, and P. Rau, "Design analysis of core assemblies for supercritical pressure conditions," *Nuclear Engineering and Design,* vol. 223, pp. 279-294, 2003.

[56] J.Y. Yu, S.T. Wang, and B.S. Jia, "Development of sub-channel analysis code for CANDU-SCWR," *Progress in Nuclear Energy,* vol. 49, pp. 334-350, 2007.

[57] J.Y. Yu, H.Y. Liu, and B.S. Jia, "Sub-channel analysis of CANDU-SCWR and review of heat-transfer correlations," *Progress in Nuclear Energy,* vol. 51, pp. 246-252, 2009.

[58] J.Q. Shan, J.J. Pan, and Y. Jiang, "Thermal consideration of CANDU-SCWR sliding pressure startup through subchannel analysis," *Nuclear Engineering and Design,* vol. 240, pp. 1005-1012, 2010.

[59] J.Q. Shan, W. Chen, B.W. Rhee, and L.K.H. Leung, "Coupled neutronics/thermal-hydraulics analysis of CANDU-SCWR fuel channel," *Annals of Nuclear Energy,* vol. 37, pp. 58-65, 2010.

[60] C. Liangzhi, Y. Oka, Y. Ishiwatari, and S. Zhi, "Fuel, core design and subchannel analysis of a superfast reactor," *Journal of Nuclear Science and Technology,* vol. 45, pp. 138-48, 2008.

[61] X.J. Liu and X. Cheng, "Core and Sub-Channel Evaluation of a Thermal SCWR," *Nuclear Engineering and Technology,* vol. 41, pp. 677-690, 2009.

[62] X.J. Liu and X. Cheng, "Thermal-hydraulic and neutron-physical characteristics of a new SCWR fuel assembly," *Annals of Nuclear Energy,* vol. 36, pp. 28-36, 2009.

[63] X.J. Liu, T. Yang, and X. Cheng, "Core and sub-channel analysis of SCWR with mixed spectrum core," *Annals of Nuclear Energy,* vol. 37, pp. 1674-1682, 2010.

[64] X.J. Liu and X. Cheng, "Coupled thermal-hydraulics and neutron-physics analysis of SCWR with mixed spectrum core," *Progress in Nuclear Energy,* vol. 52, pp. 640-647, 2010.

[65] L. Monti, J. Starflinger, and T. Schulenberg, "Development of a coupled neutronic/thermal-hydraulic tool with multi-scale capabilities and applications to HPLWR core analysis," *Nuclear Engineering and Design,* vol. 241, pp. 1579-1591, 2011.

[66] T. Schulenberg, C. Maráczy, J. Heinecke, and W. Bernnat, "Design and analysis of a thermal core for a high performance light water reactor," *Nuclear Engineering and Design,* vol. 241, pp. 4420-4426, 2011.

[67] B. Vogt, K. Fischer, J. Starflinger, E. Laurien, and T. Schulenberg, "Concept of a pressurized water reactor cooled with supercritical water in the primary loop," *Nuclear Engineering and Design,* vol. 240, pp. 2789-2799, 2010.

[68] J.H. Lee, S. Koshizuka, and Y. Oka, "Development of a LOCA analysis code for the supercritical-pressure light water cooled reactors," *Annals of Nuclear Energy,* vol. 25, pp. 1341-1361, 1998.

[69] Z. Xu, D. Hou, S. Fu, Y. Yang, and X. Cheng, "Loss of flow accident and its mitigation measures for nuclear systems with SCWR-M," *Annals of Nuclear Energy,* vol. 38, pp. 2634-2644, 2011.

[70] Y. Ishiwatari, Y. Oka, S. Koshizuka, and J. Liu, "ATWS characteristics of super LWR with/without alternative action," *Journal of Nuclear Science and Technology,* vol. 44, pp. 572-589, 2007.

[71] Y. Okano, S. Koshizuka, and Y. Oka, "Safety analysis of a supercritical pressure, light water cooled and moderated reactor with double tube water rods," *Annals of Nuclear Energy,* vol. 24, pp. 1447-1456, 1997.

[72] Y. Okano, S. Koshizuka, K. Kitoh, and Y. Oka, "Flow-induced accident and transient analyses of a direct-cycle, light-water-cooled, fast breeder reactor operating at supercritical pressure," *Journal of Nuclear Science and Technology,* vol. 33, pp. 307-315, 1996.

[73] C. Maraczy, A. Kereszturi, I. Trosztel, and G. Hegyi, "Safety analysis of reactivity initiated accidents in a HPLWR reactor by the coupled ATHLET-KIKO3D code," *Progress in Nuclear Energy,* vol. 52, pp. 190-196, 2010.

[74] K. Kitoh, S. Koshizuka, and Y. Oka, "Pressure- and flow-induced accident and transient analyses of a direct-cycle, supercritical-pressure, light-water-cooled fast reactor," *Nuclear Technology,* vol. 123, pp. 233-244, 1998.

[75] Y. Ishiwatari, Y. Oka, and S. Koshizuka, "Safety of the super LWR," *Nuclear Engineering and Technology,* vol. 39, pp. 257-272, 2007.

[76] Y. Ishiwatari, Y. Oka, S. Koshizuka, A. Yamaji, and J. Liu, "Safety of super LWR. II. Safety analysis at supercritical pressure," *Journal of Nuclear Science and Technology,* vol. 42, pp. 935-948, 2005.

[77] Y. Ishiwatari, Y. Oka, S. Koshizuka, and J. Liu, "LOCA analysis of Super LWR," *Journal of Nuclear Science and Technology,* vol. 43, pp. 231-241, 2006.

[78] S. Ikejiri, Y. Ishiwatari, and Y. Oka, "Safety analysis of a supercritical-pressure water-cooled fast reactor under supercritical pressure," *Nuclear Engineering and Design,* vol. 240, pp. 1218-1228, 2010.

[79] S. Ikejiri, C.Y. Han, Y. Ishiwatari, and Y. Oka, "LOCA analysis of super fast reactor," *Journal of Nuclear Science and Technology,* vol. 48, pp. 1289-1299, 2011.

[80] D.H. Zhu, H. Zhao, W.X. Tian, Y.L. Su, K. Saleem Chaudri, G.H. Su, and S.Z. Qiu, "Development of TACOS code for loss of flow accident analysis of SCWR with mixed spectrum core," *Progress in Nuclear Energy,* vol. 54, pp. 150-161, 2012.

[81] S.W. Fu, X.J. Liu, C. Zhou, Z.H. Xu, Y.H. Yang, and X. Cheng, "Modification and application of the system analysis code ATHLET to trans-critical simulations," *Annals of Nuclear Energy,* vol. 44, pp. 40-49, 2012.

[82] A. Vasic and H.F. Khartabil, "Passive Cooling of the CANDU SCWR Fuel at LOCA/LOECC Conditions," presented at the Proceedings of Global, Tsukuba, Japan, 2005.

[83] T. Nakatsuka, Y. Oka, and S. Koshizuka, "Control of a fast reactor cooled by supercritical light water," *Nuclear Technology,* vol. 121, pp. 81-92, 1998.

[84] Y. Ishiwatari, Y. Oka, and S. Koshizuka, "Control of a high temperature Supercritical pressure light water cooled and moderated reactor with water rods," *Journal of Nuclear Science and Technology,* vol. 40, pp. 298-306, 2003.

[85] Y. Ishiwatari, C.H. Peng, S. Ikejiri, and Y. Oka, "Improvements of feedwater controller for the super fast reactor," *Journal of Nuclear Science and Technology,* vol. 47, pp. 1155-1164, 2010.

[86] W.J. Yi, C.S. Li, and R.J. Wei, "Comparison of Fixed and Movable Boundary Models for OTSG," *Chinese Journal of Nuclear Science and Engineering,* vol. 22, pp. 314-317, 2002.

[87] L.C. Burmeister, *Convective Heat Transfer*, Second Edition ed. New York, USA: John Wiley & Sons, Inc., 2007.

[88] D.C. Arwood and T.W. Kerlin, "A mathematical model for an integral economizer U-tube steam generator," *Nuclear Technology,* vol. 35, pp. 12-32, 1977.

[89] D. Gal, D. Saphier, and E. Elias, "A DSNP Movable Boundary U-Tube Steam-Generator Model," *Nuclear Technology,* vol. 95, pp. 64-76, 1991.

[90] G. Berry, "Model of a once-through steam generator with moving boundaries and a variable number of nodes," presented at the ASME winter annual meeting, Boston, MA, USA, 1983.

[91] M.A. Abdalla, "A 4-Region, Moving-Boundary Model of a Once-through, Helical-Coil Steam-Generator," *Annals of Nuclear Energy,* vol. 21, pp. 541-562, 1994.

[92] C.P. Tzanos, "A Movable Boundary Model for Once-through Steam-Generator Analysis," *Nuclear Technology,* vol. 82, pp. 5-17, 1988.

[93] J.Y. Yoon, J.P. Kim, H.Y. Kim, D.J. Lee, and M.H. Chang, "Development of a Computer Code, ONCESG, for the Thermal-Hydraulic Design of a Once-Through Steam Generator," *Journal of Nuclear Science and Technology,* vol. 37, pp. 445-454, 2000.

[94] F. Ahnert, J.F. Kikstra, and P. Colonna, "Modeling of a Large Scale Evaporator with Moving Phase Boundaries," in *Seventh International Conference on Computational*

Modelling of Free and Moving Boundary Problems, Santa Fe, NM, United States, 2004, pp. 315-324.

[95] W. Zhang, X.Q. Bian, and G.Q. Xia, "Simulation analysis of static and dynamic characteristics of once-through steam generator in concentric annuli tube," *Journal of Marine Science and Application,* vol. 5, pp. 36-40, 2006.

[96] H.P. Li, X.J. Huang, and L.J. Zhang, "A lumped parameter dynamic model of the helical coiled once-through steam generator with movable boundaries," *Nuclear Engineering and Design,* vol. 238, pp. 1657-1663, 2008.

[97] G.Y. Han and T.P. Stanley, "Thermal-hydraulic transient analysis of light water reactors using moving boundaries," *Annals of Nuclear Energy,* vol. 26, pp. 301-326, 1999.

[98] G.Y. Han, T.P. Stanley, and P.A. Secker, "Thermal-hydraulic modeling and transient analysis of pressurized water reactors," *International Communications in Heat and Mass Transfer,* vol. 26, pp. 909-918, 1999.

[99] V.B. Garea, D.A. Drew, and R.T. Lahey Jr, "A moving-boundary nodal model for the analysis of the stability of boiling channels," *International Journal of Heat and Mass Transfer,* vol. 42, pp. 3575-3584, 1999.

[100] Y.S. Fan, Z.G. Xu, and L.J. Chen, "Modelling and simulation study on a supercritical once-through boiler steam generator," *Proceedings of the Chinese Society of Electrical Engineering,* vol. 18, pp. 246-253, 1998.

[101] Y.S. Fan, Z.G. Xu, and L.J. Chen, "Modelling and simulation study on a supercritical once-through boiler steam generator," *Chinese Journal of Lasers,* vol. 25, pp. 350-356, 1998.

[102] Y.Q. Li and T.J. Ren, "Moving Boundary Modeling Study on Supercritical Boiler Evaporator: By Using Enthalpy to Track Moving Boundary Location," in *2009 Asia-Pacific Power and Energy Engineering Conference*, Wuhan, China, 2009, pp. 1-4.

[103] J.Y. Zhao, P. Saha, and M.S. Kazimi, "Hot-channel stability of supercritical water-cooled reactors I: Steady state and sliding pressure startup," *Nuclear Technology,* vol. 158, pp. 158-173, 2007.

[104] M. Pandey and M.A. Kumar, "Analysis of Coupled Neutronic-Thermohydraulic Instabilities in Supercritical Water-Cooled Reactor by Lumped Parameter Modeling," in *Proceedings of the 16th International Conference on Nuclear Engineering (ICONE16)*, Orlando, Florida, USA, 2008, pp. 357-366.

[105] J. Buongiorno and P.E. MacDonald, "Supercrtical Water Reactor: Progress Report for the FY-03 Generation-IV R&D Activities for the Develoment of the SCWR in the U.S.," INEEL/EXT-03-01210, September 30, 2003.

[106] N. Roy, S. Mensah, and J. Boisvert, "Design of a multivariable controller for a CANDU 600 MWe nuclear power plant using the INA method," Chalk River Nuclear Laboratories, Chalk River, Ontario, Canada, April, 1994.

[107] H. Pan, M.R. Fei, L. Wang, and K. Li, "A Frequency Domain Approach to PID Controllers Design in Boiler-Turbine Units," in *Life System Modeling and Intelligent Computing*. vol. 98, K. Li*, et al.*, Eds., ed: Springer Berlin Heidelberg, 2010, pp. 73-81.

[108] W. Tan, J.Z. Liu, F. Fang, and Y.Q. Chen, "Tuning of PID controllers for boiler-turbine units," *ISA Transactions,* vol. 43, pp. 571-583, 2004.

[109] I.L. Pioro, H.F. Khartabil, and R.B. Duffey, "Heat transfer to supercritical fluids flowing in channels--empirical correlations (survey)," *Nuclear Engineering and Design,* vol. 230, pp. 69-91, 2004.

[110] I.L. Pioro and R.B. Duffey, "Experimental heat transfer in supercritical water flowing inside channels (survey)," *Nuclear Engineering and Design,* vol. 235, pp. 2407-2430, 2005.

[111] R.B. Duffey and I.L. Pioro, "Experimental heat transfer of supercritical carbon dioxide flowing inside channels (survey)," *Nuclear Engineering and Design,* vol. 235, pp. 913-24, 2005.

[112] K. Yamagata, K. Nishikawa, S. Hasegawa, T. Fujii, and S. Yoshida, "Forced convective heat transfer to supercritical water flowing in tubes," *International Journal of Heat and Mass Transfer,* vol. 15, pp. 2575-2593, 1972.

[113] J.K. Fink, "Thermophysical properties of uranium dioxide," *Journal of Nuclear Materials,* vol. 279, pp. 1-18, 2000.

[114] W. Wulff, H.S. Cheng, and A.N. Mallen, "Analytical modeling techniques for efficient heat transfer simulation in nuclear power plant transients," presented at the National Heat Transfer Conference, Denver, CO, USA, 1985.

[115] W. Wagner, J.R. Cooper, A. Dittmann, J. Kijima, H.J. Kretzschmar, A. Kruse, R. Mares, K. Oguchi, H. Sato, I. Stocker, O. Sifner, Y. Takaishi, I. Tanishita, J. Trubenbach, and T. Willkommen, "The IAPWS Industrial Formulation 1997 for the Thermodynamic Properties of Water and Steam," *Journal of Engineering for Gas Turbines and Power,* vol. 122, pp. 150-184, 2000.

[116] W.M. Stacey, *Nuclear Reactor Physics*. New York, USA: John Wiley & Sons, Inc., 2001.

[117] C. Fazekas, G. Szederkenyi, and K.M. Hangos, "A simple dynamic model of the primary circuit in VVER plants for controller design purposes," *Nuclear Engineering and Design,* vol. 237, pp. 1071-1087, 2007.

[118] T. Kato, *Perturbation Theory for Linear Operations*. Berlin, Germany: Springer, 1995.

[119] H.P. Li, X.J. Huang, and L.J. Zhang, "A simplified mathematical dynamic model of the HTR-10 high temperature gas-cooled reactor with control system design purposes," *Annals of Nuclear Energy,* vol. 35, pp. 1642-1651, 2008.

[120] P.W. Sun, J. Jiang, and J.Q. Shan, "Construction of dynamic model of CANDU-SCWR using moving boundary method," *Nuclear Engineering and Design,* vol. 241, pp. 1701-1714, 2011.

[121] R.D. Paranjape, "Modeling and Control of a Supercritical Coal Fired Boiler," Doctor of Philosophy, Chemical Engineering, Texas Tech University, Lubbock, Texas, USA, 1996.

[122] K.M. Zhou and J.C. Doyle, *Essentials of Robust Control*. Upper Saddle River, New Jersey, USA: Prentice Hall, 1998.

[123] C.Y. Du and H.J. Ling, "Generalized predictive control algorithm applied to thermal power units based on PID neural network," in *2010 2nd International Conference on Advanced Computer Control (ICACC)*, 2010, pp. 38-42.

[124] H.H. Rosenbrock, *Computer-aided Control System Design*. London, UK: Academic Press, 1974.

[125] I. Postlethwaite and A.G.J. MacFarlane, *A Complex Variable Approach to the Analysis of Linear Multivariable Feedback Systems*. Berlin, Germany: Springer-Verlag, 1979.

[126] J.A.G. MacFarlane, *Complex Variable Methods for Linear Multivariable Feedback Systems*. London, UK: Taylor and Francis, 1980.

[127] P.K. Sinha, *Multivariable Control: An Introduction*. New York, USA: Marcel Dekker, Inc., 1984.

[128] M. Hovd, R.D. Braatz, and S. Skogestad, "SVD controllers for H2−, H∞− and μ-optimal control," *Automatica,* vol. 33, pp. 433-439, 1997.

[129] Y.S. Hung and A.G.J. MacFarlane, *Multivariable Feedback: A Quasi-Classical Approach* vol. 40 of Lectures Notes in Control and Information Sciences. Berlin: Springer-Verlag, 1982.

[130] E. Bristol, "On a new measure of interaction for multivariable process control," *Automatic Control, IEEE Transactions on,* vol. 11, pp. 133-134, 1966.

[131] S. Skogestad and I. Postlethwaite, *Multivariable Feedback Control: Analysis and Design*, Second Edition ed.: John Wiley & Sons, Ltd, 2005.

[132] N. Jensen, D.G. Fisher, and S.L. Shah, "Interaction analysis in multivariable control systems," *Aiche Journal,* vol. 32, pp. 959-970, 1986.

[133] D. Flynn, *Thermal Power Plant Simulation and Control*. London, UK: Institution of Electrical Engineers, 2003.

[134] R. Viswanathan, J. Henry, J. Tanzosh, G. Stanko, J. Shingledecker, B. Vitalis, and R. Purgert, "U.S. program on materials technology for ultra-supercritical coal power plants," *Journal of Materials Engineering and Performance,* vol. 14, pp. 281-292, 2005.

[135] M.P. Ford and K.C. Daly, "Dominance improvement by pseudodecoupling," *Proceedings of the Institution of Electrical Engineers,* vol. 126, pp. 1316-1320, 1979.

[136] W.J. Rugh and J.S. Shamma, "Research on gain scheduling," *Automatica,* vol. 36, pp. 1401-1425, 2000.

[137] A. Dehghani, M.C. Rotkowitz, B.D.O. Anderson, and S.H. Cha, "Simplified Rapid Switching Gain Scheduling for a Class of LPV Sstems," *IEEE Transactions on Automatic Control,* vol. 57, pp. 2633-2639, 2012.

[138] K.Y. Lee, J.S. Heo, J.A. Hoffman, S.H. Kim, and W.H. Jung, "Neural Network-Based Modeling for A Large-Scale Power Plant," in *IEEE Power Engineering Society General Meeting*, 2007, pp. 1-8.

APPENDIX A

The input-output relationship of the Canadian SCWR at 100%FP can be described by

$$
Y = \begin{bmatrix} y_1(s) \\ y_2(s) \\ y_3(s) \end{bmatrix} = P(s)U(s) = \begin{bmatrix} p_{11}(s) & p_{12}(s) & p_{13}(s) \\ p_{21}(s) & p_{22}(s) & p_{23}(s) \\ p_{31}(s) & p_{32}(s) & p_{33}(s) \end{bmatrix} \begin{bmatrix} u_1(s) \\ u_2(s) \\ u_3(s) \end{bmatrix}
$$

where $u_1(s)$, $u_2(s)$ and $u_3(s)$ are the Laplace Transforms of the inputs, i.e. the feed-water flow rate, control rod reactivity and control valve opening, respectively. $y_1(s)$, $y_2(s)$ and $y_3(s)$ are the Laplace Transform of the outputs, i.e. the outlet header temperature, reactor power and main 'steam' pressure, respectively. The elements of the transfer function matrix $P(s)$ are as follows:

$$
p_{11}(s) = \frac{\begin{matrix} 3.10(s+4.98)(s-5.96)(s+0.29)(s+0.13)(s+2.51*10^{-2}) \\ (s+5.64*10^{-4})(s^2+0.13s+4.45*10^{-3})(s^2+0.31s+3.14*10^{-2}) \end{matrix}}{\begin{matrix} (s+7.17)(s+5.26)(s+4.68)(s+2.38)(s+0.69)(s+0.30)(s+0.15)(s+7.18*10^{-2}) \\ (s+6.84*10^{-2})(s+2.83*10^{-2})(s+5.84*10^{-4})(s^2+0.25s+2.45*10^{-2}) \end{matrix}}
$$

$$
p_{12}(s) = \frac{\begin{matrix} -3.62*10^6(s-5.29)(s+3.79)(s+1.39)(s+0.70)(s+0.32)(s+0.26)(s+0.12) \\ (s+7.18*10^{-2})(s+6.57*10^{-2})(s+3.16*10^{-2})(s+6.12*10^{-4})(s^2+3.12s+2.92) \end{matrix}}{\begin{matrix} (s+18.13)(s+6.68)(s+5.46)(s+4.71)(s+3.64)(s+2.36)(s+1.65) \\ (s+1.20)(s+0.30)(s+0.15)(s+7.40*10^{-2})(s+6.60*10^{-2})(s+2.86*10^{-2}) \\ (s+5.86*10^{-4})(s^2+0.25s+2.57*10^{-2})(s^2+0.79s+0.32) \end{matrix}}
$$

$$
p_{13}(s) = \frac{\begin{matrix} 4.22*10^3(s+4.98)(s+0.70)(s+0.29)(s+0.13)(s+2.54*10^{-2}) \\ (s-5.97)(s+5.65*10^{-4})(s^2+0.13s+4.80*10^{-3})(s^2+0.31s+3.14*10^{-2}) \end{matrix}}{\begin{matrix} (s+6.68)(s+5.46)(s+4.71)(s+2.36)(s+1.65)(s+0.30)(s+0.15)(s+7.40*10^{-2}) \\ (s+6.60*10^{-2})(s+2.86*10^{-2})(s+5.86*10^{-4})(s^2+0.25s+2.57*10^{-2})(s^2+0.79s+0.32) \end{matrix}}
$$

$$p_{21}(s) = \frac{\begin{array}{c}1.37*10^{-3}(s+3.79)(s+1.39)(s+0.57)(s+0.32)\\(s+0.12)(s+6.57*10^{-2})(s+3.16*10^{-2})(s+6.12*10^{-4})\end{array}}{\begin{array}{c}(s+18.13)(s+3.64)(s+1.89)(s+1.20)(s+0.15)(s+7.18*10^{-2})\\(s+2.83*10^{-2})(s+5.84*10^{-4})(s^2+0.25s+2.46*10^{-2})\end{array}}$$

$$p_{22}(s) = \frac{\begin{array}{c}3.03*10^3(s+3.79)(s+1.66)(s+1.39)(s+0.32)(s+0.12)(s+7.18*10^{-2})\\(s+6.61*10^{-2})(s+6.57*10^{-2})(s+3.16*10^{-2})(s+6.12*10^{-4})(s^2+0.80s+0.33)\end{array}}{\begin{array}{c}(s+18.13)(s+3.64)(s+1.65)(s+1.20)(s+0.15)(s+7.40*10^{-2})(s+6.60*10^{-2})\\(s+2.86*10^{-2})(s+5.86*10^{-4})(s^2+0.25s+2.57*10^{-2})(s^2+0.79s+0.32)\end{array}}$$

$$p_{23}(s) = \frac{\begin{array}{c}1.88(s+7.17)(s+5.26)(s+4.68)(s+3.78)(s+2.38)(s+1.39)(s+0.70)(s+0.69)(s+0.57)\\(s+0.32)(s+0.30)(s+0.12)(s+6.84*10^{-2})(s+6.57*10^{-2})(s+3.16*10^{-2})(s+6.12*10^{-4})\end{array}}{\begin{array}{c}(s+18.13)(s+6.68)(s+5.46)(s+4.71)(s+3.64)(s+2.36)(s+1.89)(s+1.65)\\(s+1.20)(s+0.30)(s+0.15)(s+7.40*10^{-2})(s+6.60*10^{-2})(s+2.86*10^{-2})\\(s+5.86*10^{-4})(s^2+0.25s+2.57*10^{-2})(s^2+0.79s+0.32)\end{array}}$$

$$p_{31}(s) = \frac{\begin{array}{c}5.90*10^{-2}(s+4.92)(s+4.48)(s+3.65)(s+2.31)(s+0.29)(s+0.15)(s+0.10)(s+7.59*10^{-2})\\(s+6.44*10^{-2})(s+2.91*10^{-2})(s+5.89*10^{-4})(s^2+0.26s+2.73*10^{-2})(s^2+0.46s+0.63)\end{array}}{\begin{array}{c}(s+7.17)(s+5.26)(s+4.68)(s+3.64)(s+2.38)(s+0.70)(s+0.698)(s+0.69)(s+0.30)\\(s+0.15)(s+7.18*10^{-2})(s+6.84*10^{-2})(s+2.83*10^{-2})(s+5.84*10^{-4})(s^2+0.25s+2.45*10^{-2})\end{array}}$$

$$p_{32}(s) = \frac{\begin{array}{c}-3.27*10^4(s-5.29)(s+4.58)(s+3.79)(s+2.34)(s+1.89)(s+1.43)(s+1.39)(s+0.32)\\(s+0.26)(s+0.12)(s+0.11)(s+7.18*10^{-2})(s+6.57*10^{-2})(s+3.16*10^{-2})(s+6.12*10^{-4})\end{array}}{\begin{array}{c}(s+18.13)(s+6.68)(s+5.46)(s+4.71)(s+3.64)(s+2.36)(s+1.89)(s+1.65)\\(s+1.20)(s+0.30)(s+0.15)(s+7.40*10^{-2})(s+6.60*10^{-2})(s+2.86*10^{-2})\\(s+5.86*10^{-4})(s^2+0.25s+2.57*10^{-2})(s^2+0.79s+0.32)\end{array}}$$

$$p_{33}(s) = \frac{\begin{array}{c}-34.45(s+7.30)(s+5.24)(s+4.68)(s+2.34)(s+0.71)(s+0.70)(s+0.15)(s+7.16*10^{-2})\\(s+6.85*10^{-2})(s+2.83*10^{-2})(s+5.84*10^{-4})(s^2+0.25s+2.46*10^{-2})\end{array}}{\begin{array}{c}(s+6.68)(s+5.46)(s+4.71)(s+2.36)(s+1.65)(s+0.15)(s+7.40*10^{-2})(s+6.60*10^{-2})\\(s+2.86*10^{-2})(s+5.86*10^{-4})(s^2+0.25s+2.57*10^{-2})(s^2+0.79s+0.32)\end{array}}$$

The pre-compensator designed at 100%FP is

$$K(s) = \begin{bmatrix} 1.0 & \dfrac{0.53}{1.95s + 0.24} & \dfrac{-1.23s - 0.21}{1.24s^2 + 1.16s + 0.23} \\ 0.0 & 1.0 & \dfrac{6.00 * 10^{-3}}{1.24s^2 + 1.16s + 0.23} \\ 0.0 & \dfrac{0.47}{1.95s + 0.24} & 1.0 \end{bmatrix}$$

The loop compensator designed at 100%FP is

$$C(s) = \begin{bmatrix} -\dfrac{0.85s + 0.5}{s} & 0.0 & 0.0 \\ 0.0 & 0.004\dfrac{0.1s + 1.0}{s} & 0.0 \\ 0.0 & 0.0 & -4.0\dfrac{s + 1.0}{20.0s + 1.0} \end{bmatrix}$$

APPENDIX B

The input-output relationship of the Canadian SCWR at 80%FP can be described by

$$Y = \begin{bmatrix} y_1(s) \\ y_2(s) \\ y_3(s) \end{bmatrix} = P(s)U(s) = \begin{bmatrix} p_{11}(s) & p_{12}(s) & p_{13}(s) \\ p_{21}(s) & p_{22}(s) & p_{23}(s) \\ p_{31}(s) & p_{32}(s) & p_{33}(s) \end{bmatrix} \begin{bmatrix} u_1(s) \\ u_2(s) \\ u_3(s) \end{bmatrix}$$

where $u_1(s)$, $u_2(s)$ and $u_3(s)$ are the Laplace Transforms of the inputs, i.e. the feed-water flow rate, control rod reactivity and control valve opening, respectively. $y_1(s)$, $y_2(s)$ and $y_3(s)$ are the Laplace Transform of the outputs, i.e. the outlet header temperature, reactor power and main 'steam' pressure, respectively. The elements of the transfer function matrix $P(s)$ are as follows:

$$p_{11}(s) = \frac{\begin{array}{c} 1.80(s-4.87)(s+4.12)(s+3.64)(s+1.31)(s+1.20)(s+2.61*10^{-2}) \\ (s+5.71*10^{-4})(s^2+0.31s+3.16*10^{-2})(s^2+0.13s+4.50*10^{-3}) \end{array}}{\begin{array}{c} (s+6.02)(s+4.52)(s+3.74)(s+3.63)(s+1.90)(s+1.31)(s+1.20)(s+0.55) \\ (s+6.78*10^{-2})(s+6.12*10^{-2})(s+2.87*10^{-2})(s+5.87*10^{-4})(s^2+0.27s+2.65*10^{-2}) \end{array}}$$

$$p_{12}(s) = \frac{\begin{array}{c} -1.50*10^6(s-4.14)(s+3.79)(s+1.39)(s+1.31)(s+0.56)(s+0.32)(s+0.24) \\ (s+0.12)(s+6.78*10^{-2})(s+6.39*10^{-2})(s+3.16*10^{-2})(s+6.12*10^{-4})(s^2+2.48s+1.86) \end{array}}{\begin{array}{c} (s+14.60)(s+5.42)(s+4.85)(s+3.76)(s+3.63)(s+1.85)(s+1.19)(s+0.27)(s+0.15) \\ (s+6.85*10^{-2})(s+6.01*10^{-2})(s+2.90*10^{-2})(s+5.88*10^{-4})(s^2+2.65s+1.75) \\ (s^2+0.65s+0.21)(s^2+0.26s+2.81*10^{-2}) \end{array}}$$

$$p_{13}(s) = \frac{\begin{array}{c} 2.16*10^3(s+14.60)(s-4.87)(s+4.11)(s+3.64)(s+1.31)(s+1.20)(s+0.56) \\ (s+0.13)(s+2.61*10^{-2})(s+5.71*10^{-4})(s^2+0.31s+3.16*10^{-2})(s^2+0.13s+4.50*10^{-3}) \end{array}}{\begin{array}{c} (s+14.60)(s+5.42)(s+4.85)(s+3.76)(s+3.63)(s+1.85)(s+1.19)(s+0.15)(s+6.85*10^{-2}) \\ (s+6.01*10^{-2})(s+2.90*10^{-2})(s+5.88*10^{-4})(s^2+2.65s+1.75)(s^2+0.26s+2.81*10^{-2}) \end{array}}$$

$$p_{21}(s) = \frac{\begin{array}{c} 1.00*10^{-3}(s+3.79)(s+1.39)(s+0.47)(s+0.32)(s+0.12) \\ (s+0.10)(s+6.39*10^{-2})(s+3.16*10^{-2})(s+6.12*10^{-4}) \end{array}}{\begin{array}{c} (s+14.6)(s+3.63)(s+1.31)(s+1.20)(s+0.15)(s+0.10) \\ (s+6.78*10^{-2})(s+2.87*10^{-2})(s+5.87*10^{-4})(s^2+0.25s+2.65*10^{-2}) \end{array}}$$

$$p_{22}(s) = \frac{\begin{array}{c}2.42*10^3(s+3.79)(s+1.39)(s+1.33)(s+1.31)(s+0.32)(s+0.12)(s+6.78*10^{-2})\\(s+6.39*10^{-2})(s+5.91*10^{-2})(s+3.16*10^{-2})(s+6.12*10^{-4})(s^2+0.66s+0.21)\end{array}}{\begin{array}{c}(s+14.60)(s+3.63)(s+1.19)(s+0.15)(s+6.85*10^{-2})(s+6.01*10^{-2})(s+2.90*10^{-2})\\(s+5.88*10^{-4})(s^2+2.65s+1.75)(s^2+0.65s+0.21)(s^2+0.26s+2.81*10^{-2})\end{array}}$$

$$p_{23}(s) = \frac{\begin{array}{c}1.25(s+6.02)(s+4.52)(s+3.79)(s+3.74)(s+1.90)(s+1.39)(s+0.56)(s+0.55)(s+0.47)\\(s+0.32)(s+0.27)(s+0.12)(s+6.39*10^{-2})(s+6.12*10^{-2})(s+3.16*10^{-2})(s+6.12*10^{-4})\end{array}}{\begin{array}{c}(s+14.60)(s+5.42)(s+4.85)(s+3.76)(s+3.63)(s+1.85)(s+1.19)(s+0.27)(s+0.15)\\(s+6.85*10^{-2})(s+6.01*10^{-2})(s+2.90*10^{-2})(s+5.88*10^{-4})(s^2+2.65s+1.75)\\(s^2+0.65s+0.21)(s^2+0.26s+2.81*10^{-2})\end{array}}$$

$$p_{31}(s) = \frac{\begin{array}{c}4.29*10^{-2}(s+4.02)(s+3.54)(s+2.05)(s+0.14)(s+0.10)(s+6.92*10^{-2})(s+5.88*10^{-2})\\(s+2.94*10^{-2})(s+5.91*10^{-4})(s^2+0.45s+0.39)(s^2+0.27s+3.01*10^{-2})\end{array}}{\begin{array}{c}(s+6.02)(s+4.52)(s+3.74)(s+1.90)(s+0.56)(s+0.56)(s+0.55)(s+0.15)(s+0.10)\\(s+6.78*10^{-2})(s+6.12*10^{-2})(s+2.87*10^{-2})(s+5.87*10^{-4})(s^2+0.25s+2.65*10^{-2})\end{array}}$$

$$p_{32}(s) = \frac{\begin{array}{c}-1.69*10^4(s-4.14)(s+3.79)(s+3.66)(s+1.92)(s+1.39)(s+1.31)(s+1.12)(s+0.32)(s+0.24)\\(s+0.12)(s+9.29*10^{-2})(s+6.78*10^{-2})(s+6.39*10^{-2})(s+3.16*10^{-2})(s+6.12*10^{-4})\end{array}}{\begin{array}{c}(s+14.60)(s+5.42)(s+4.85)(s+3.76)(s+3.63)(s+1.85)(s+1.19)(s+0.27)(s+0.15)\\(s+6.85*10^{-2})(s+6.01*10^{-2})(s+2.90*10^{-2})(s+5.88*10^{-4})(s^2+2.65s+1.75)\\(s^2+0.65s+0.21)(s^2+0.26s+2.81*10^{-2})\end{array}}$$

$$p_{33}(s) = \frac{\begin{array}{c}-34.45(s+6.02)(s+4.52)(s+3.74)(s+3.63)(s+1.92)(s+1.31)(s+1.20)(s+0.56)(s+0.55)\\(s+0.15)(s+6.78*10^{-2})(s+6.12*10^{-2})(s+2.87*10^{-2})(s+5.87*10^{-4})(s^2+0.25s+2.65*10^{-2})\end{array}}{\begin{array}{c}(s+5.42)(s+4.85)(s+3.76)(s+3.63)(s+1.85)(s+1.19)(s+0.15)(s+6.85*10^{-2})(s+6.01*10^{-2})\\(s+2.90*10^{-2})(s+5.88*10^{-4})(s^2+2.65s+1.75)(s^2+0.65s+0.21)(s^2+0.26s+2.81*10^{-2})\end{array}}$$

The pre-compensator designed at 80%FP is

$$K(s) = \begin{bmatrix} 1.0 & \dfrac{0.40}{2.02s+0.29} & \dfrac{-0.99s-0.15}{1.24s^2+0.98s+0.17} \\[3mm] 0.0 & 1.0 & \dfrac{2.00*10^{-3}}{1.24s^2+0.98s+0.17} \\[3mm] 0.0 & \dfrac{0.43}{2.02s+0.29} & 1.0 \end{bmatrix}$$

The loop compensator designed at 80%FP is

$$C(s) = \begin{bmatrix} -\dfrac{0.6s + 0.3}{s} & 0.0 & 0.0 \\ 0.0 & 0.004\dfrac{0.1s + 1.0}{s} & 0.0 \\ 0.0 & 0.0 & -3.5\dfrac{s + 1.0}{20.0s + 1.0} \end{bmatrix}$$

APPENDIX C

The input-output relationship of the Canadian SCWR at 60%FP can be described by

$$Y = \begin{bmatrix} y_1(s) \\ y_2(s) \\ y_3(s) \end{bmatrix} = P(s)U(s) = \begin{bmatrix} p_{11}(s) & p_{12}(s) & p_{13}(s) \\ p_{21}(s) & p_{22}(s) & p_{23}(s) \\ p_{31}(s) & p_{32}(s) & p_{33}(s) \end{bmatrix} \begin{bmatrix} u_1(s) \\ u_2(s) \\ u_3(s) \end{bmatrix}$$

where $u_1(s)$, $u_2(s)$ and $u_3(s)$ are the Laplace Transforms of the inputs, i.e. the feed-water flow rate, control rod reactivity and control valve opening, respectively. $y_1(s)$, $y_2(s)$ and $y_3(s)$ are the Laplace Transform of the outputs, i.e. the outlet header temperature, reactor power and main 'steam' pressure, respectively. The elements of the transfer function matrix $P(s)$ are as follows:

$$p_{11}(s) = \frac{\begin{array}{c} 1.01(s-3.60)(s+3.61)(s+3.23)(s+0.50)(s+0.13)(s+2.64*10^{-2}) \\ (s+5.74*10^{-4})(s^2+0.30s+3.21*10^{-2})(s^2+0.12s+3.80*10^{-3}) \end{array}}{\begin{array}{c} (s+4.82)(s+3.76)(s+3.62)(s+2.81)(s+1.40)(s+0.49)(s+0.41)(s+0.14) \\ (s+6.50*10^{-2})(s+5.23*10^{-2})(s+2.90*10^{-2})(s+5.88*10^{-4})(s^2+0.26s+2.81*10^{-2}) \end{array}}$$

$$p_{12}(s) = \frac{\begin{array}{c} -4.76*10^5(s+3.79)(s-2.94)(s+1.39)(s+0.49)(s+0.42)(s+0.32)(s+0.23)(s+0.12) \\ (s+6.50*10^{-2})(s+6.21*10^{-2})(s+3.16*10^{-2})(s+6.12*10^{-4})(s^2+1.83s+1.02) \end{array}}{\begin{array}{c} (s+11.08)(s+3.62)(s+2.82)(s+1.20)(s+0.50)(s+0.24)(s+0.14)(s+6.50*10^{-2})(s+5.16*10^{-2}) \\ (s+2.92*10^{-2})(s+5.90*10^{-4})(s^2+8.44s+17.80)(s^2+2.26s+1.29)(s^2+0.52s+8.05*10^{-2}) \end{array}}$$

$$p_{13}(s) = \frac{\begin{array}{c} 9.12*10^2(s-3.65)(s+3.23)(s+1.19)(s+0.42)(s+0.13)(s+2.69*10^{-2}) \\ (s+5.76*10^{-4})(s^2+0.30s+3.18*10^{-2})(s^2+0.13s+4.30*10^{-3}) \end{array}}{\begin{array}{c} (s+2.82)(s+1.20)(s+0.14)(s+6.50*10^{-2})(s+5.16*10^{-2})(s+2.92*10^{-2}) \\ (s+5.90*10^{-4})(s^2+8.44s+17.80)(s^2+2.26s+1.29)(s^2+0.52s+8.05*10^{-2}) \end{array}}$$

$$p_{21}(s) = \frac{\begin{array}{c} 5.73*10^{-4}(s+3.79)(s+1.39)(s+0.32)(s+0.30)(s+0.12) \\ (s+6.21*10^{-2})(s+3.16*10^{-2})(s+6.12*10^{-4}) \end{array}}{\begin{array}{c} (s+11.08)(s+3.62)(s+1.19)(s+0.49)(s+0.14)(s+6.50*10^{-2}) \\ (s+2.90*10^{-2})(s+5.88*10^{-4})(s^2+0.26s+2.81*10^{-2}) \end{array}}$$

$$p_{22}(s) = \frac{\begin{matrix} 1.82*10^3(s+3.79)(s+2.82)(s+1.39)(s+0.49)(s+0.32)(s+0.24)(s+0.12) \\ (s+6.50*10^{-2})(s+6.21*10^{-2})(s+5.08*10^{-2})(s+3.16*10^{-2})(s+6.12*10^{-4}) \end{matrix}}{\begin{matrix} (s+11.08)(s+3.62)(s+2.82)(s+1.20)(s+0.50)(s+0.24)(s+0.14)(s+6.50*10^{-2}) \\ (s+5.16*10^{-2})(s+2.92*10^{-2})(s+5.90*10^{-4})(s^2+2.26s+1.29)(s^2+0.52s+8.05*10^{-2}) \end{matrix}}$$

$$p_{23}(s) = \frac{\begin{matrix} 0.52(s+4.82)(s+3.79)(s+3.76)(s+2.81)(s+1.40)(s+1.39)(s+0.42)(s+0.41) \\ (s+0.30)(s+0.12)(s+6.21*10^{-2})(s+5.23*10^{-2})(s+3.16*10^{-2})(s+6.12*10^{-4}) \end{matrix}}{\begin{matrix} (s+11.08)(s+3.62)(s+2.82)(s+1.20)(s+0.50)(s+0.14)(s+6.50*10^{-2})(s+5.16*10^{-2}) \\ (s+2.92*10^{-2})(s+5.90*10^{-4})(s^2+8.44s+17.80)(s^2+2.26s+1.29)(s^2+0.52s+8.05*10^{-2}) \end{matrix}}$$

$$p_{31}(s) = \frac{\begin{matrix} 3.19*10^{-2}(s+3.06)(s+2.51)(s+1.93)(s+0.50)(s+6.51*10^{-2}) \\ (s+5.13*10^{-2})(s+2.95*10^{-2})(s+5.92*10^{-4})(s^2+0.44s+0.21) \end{matrix}}{\begin{matrix} (s+4.82)(s+3.76)(s+2.81)(s+1.40)(s+0.49)(s+0.42)(s+0.42)(s+0.41) \\ (s+6.50*10^{-2})(s+5.23*10^{-2})(s+2.90*10^{-2})(s+5.88*10^{-4})(s^2+0.26s+2.81*10^{-2}) \end{matrix}}$$

$$p_{32}(s) = \frac{\begin{matrix} -7.16*10^3(s+3.79)(s-2.94)(s+2.74)(s+1.41)(s+1.39)(s+0.84)(s+0.49)(s+0.32) \\ (s+0.23)(s+0.12)(s+6.98*10^{-2})(s+6.50*10^{-2})(s+6.21*10^{-2})(s+3.16*10^{-2})(s+6.12*10^{-4}) \end{matrix}}{\begin{matrix} (s+11.08)(s+3.62)(s+2.82)(s+1.20)(s+0.50)(s+0.24)(s+0.14)(s+6.50*10^{-2})(s+5.16*10^{-2}) \\ (s+2.92*10^{-2})(s+5.90*10^{-4})(s^2+8.44s+17.80)(s^2+2.26s+1.29)(s^2+0.52s+8.05*10^{-2}) \end{matrix}}$$

$$p_{33}(s) = \frac{\begin{matrix} -34.45(s+4.82)(s+3.77)(s+2.81)(s+1.41)(s+1.19)(s+0.49)(s+0.42)(s+0.41) \\ (s+6.50*10^{-2})(s+5.23*10^{-2})(s+2.90*10^{-2})(s+5.88*10^{-4})(s^2+0.26s+2.81*10^{-2}) \end{matrix}}{\begin{matrix} (s+2.82)(s+1.20)(s+0.50)(s+6.50*10^{-2})(s+5.16*10^{-2})(s+2.92*10^{-2})(s+5.90*10^{-4}) \\ (s^2+8.44s+17.80)(s^2+2.26s+1.29)(s^2+0.52s+8.05*10^{-2})(s^2+0.27s+3.05*10^{-2}) \end{matrix}}$$

The pre-compensator designed at 60%FP is

$$K(s) = \begin{bmatrix} 1.0 & \dfrac{0.30}{2.15s+0.32} & \dfrac{-0.77s-6.20*10^{-2}}{1.24s^2+0.72s+6.70*10^{-2}} \\ 0.0 & 1.0 & \dfrac{5.00*10^{-3}}{1.24s^2+0.72s+6.70*10^{-2}} \\ 0.0 & \dfrac{0.34}{2.15s+0.32} & 1.0 \end{bmatrix}$$

The loop compensator designed at 60%FP is

$$C(s) = \begin{bmatrix} -\dfrac{0.5s + 0.2}{s} & 0.0 & 0.0 \\[3mm] 0.0 & 0.003\dfrac{0.1s + 1.0}{s} & 0.0 \\[3mm] 0.0 & 0.0 & -3.0\dfrac{s + 1.0}{20.0s + 1.0} \end{bmatrix}$$

APPENDIX D

Copyright Permission

Supplier	Elsevier Limited
	The Boulevard, Langford Lane
	Kidlington,Oxford,OX5 1GB,UK
Registered Company Number	1982084
Customer name	Peiwei Sun
License number	3005390817359
License date	Oct 10, 2012
Licensed content publisher	Elsevier
Licensed content publication	Nuclear Engineering and Design
Licensed content title	Construction of dynamic model of CANDU-SCWR using

moving boundary method

Licensed content author	Peiwei Sun, Jin Jiang, Jianqiang Shan
Licensed content date	May 2011
Licensed content volume number	241
Licensed content issue number	5
Number of pages	14
Start Page	1701
End Page	1714
Type of Use	reuse in a thesis/dissertation
Portion	full article
Format	both print and electronic
Are you the author of this Elsevier article?	Yes
Will you be translating?	No
Order reference number	
Title of your thesis/dissertation	Dynamic Model Construction and Control System Design for Canadian Supercritical Water-cooled Reactors
Expected completion date	Oct 2012
Estimated size (number of pages)	218

Elsevier VAT number   GB 494 6272 12

Permissions price   0.00 USD

VAT/Local Sales Tax   0.0 USD / 0.0 GBP

Total   0.00 USD

Terms and Conditions

CURRICULUM VIATE

Name:	Peiwei Sun
Place of Birth:	Rizhao, Shandong, China
Year of Birth:	1981
Post Secondary	Bachelor of Engineering Science, Nuclear Engineering and Technology
Education and	Xi'an Jiaotong University
Degrees:	Xi'an, Shaanxi, China
	2000-2004
	Master of Engineering Science, Nuclear Science and Technology
	Xi'an Jiaotong University
	Xi'an, Shaanxi, China
	2004-2007
	Doctor of Philosophy
	The University of Western Ontario
	London, Ontario, Canada
	2007-2012
Honors and	Excellent Graduate of Xi'an Jiaotong University
Awards:	Xi'an Jiaotong University, 2004
	Excellent Graduate of Xi'an Jiaotong University

Xi'an Jiaotong University, 2007

Western Engineering Scholarship

The University of Western Ontario, 2007-2011

Publications:

Journal papers

1. Peiwei Sun, Jin Jiang and Jianqiang Shan, "Construction of Dynamic Model of CANDU-SCWR Using Moving Boundary Method," *Nuclear Engineering and Design*, vol. 241, pp. 1701-1714, 2011.

2. Peiwei Sun and Jin Jiang, "Construction and Analysis of a Dynamic Model for a Canadian Direct-cycle SCWR for Control System Studies," *Nuclear Technology* (accepted).

3. Peiwei Sun and Jin Jiang, "Decoupling Control of Canadian Supercritical Water-cooled Reactors," *Nuclear Technology* (submitted).

Conference papers

1. Peiwei Sun and Jin Jiang, "Modelling and Simulation of Dynamic Characteristics of CANDU-SCWR," *2nd Canada-China Joint Workshop on Supercritical Water-cooled Reactors (CCSC-2010)*, Toronto, Ontario, Canada, April 25-28, 2010.

2. Peiwei Sun and Jin Jiang, "Thermal-hydraulic Modeling of CANDU-SCWR and Linear Dynamic Model Development," *18th International Conference on Nuclear Engineering (ICONE 18)*, Xi'an, Shaanxi, China, May 17-21, 2010.

3. Peiwei Sun, Chao Zhang and Jin Jiang, "Analysis of Dynamic Cross-coupling and Design of Decoupling Controller for Canadian SCWR," *3rd China-Canada Joint Workshop on*

Supercritical Water-cooled Reactors (CCSC-2012), Xi'an, Shaanxi, China, April 18-20, 2012.

4. Peiwei Sun, Jin Jiang and Jianmin Zhang, "Modeling, Analysis of Nonlinearities of Canadian SCWR and their Gain Scheduling Control," *the 6th International Symposium on Supercritical Water-cooled Reactors (ISSCWR-6)*, Shenzhen, Guangdong, China, March 3-7, 2013 (accepted).